

CHEMICAL ANALYSIS OF TATTOO INKS TO AID IN THE IDENTIFICATION OF HIGHLY DECOMPOSED  
REMAINS

By

Trevor Curtis

A THESIS

Submitted to  
Michigan State University  
in partial fulfillment of the requirements  
for the degree of

Forensic Science - Master of Science

2017

## ABSTRACT

### CHEMICAL ANALYSIS OF TATTOO INKS TO AID IN THE IDENTIFICATION OF HIGHLY DECOMPOSED REMAINS

By

Trevor Curtis

Tattooing has existed for thousands of years and has recently risen in popularity. This has led to an increase in the potential use of tattoos to identify highly decomposed remains. Current tattoo visualization methods can be inhibited by discoloration of the skin during decomposition. Although the ink is no longer visible, the components of the tattoo ink still remain within the skin and therefore can be used to determine the color and position of tattoos on decomposed remains.

In this study, 30 tattoo inks were analyzed to determine organic and inorganic composition. This included the use of x-ray fluorescence (XRF) spectroscopy, attenuated total reflectance-Fourier transform infrared (ATR-FTIR) spectroscopy, and scanning electron microscopy-energy dispersive spectroscopy (SEM-EDS). XRF and ATR-FTIR spectroscopy data were analyzed using multivariate statistical analyses which determined the differentiation of ink colors was possible through composition including the separation of mixtures of inks.

Finally, porcine tissue samples tattooed with dark red ink were allowed to decompose for 19 days and were analyzed using SEM-EDS and compared to pure ink samples. In the analysis of tissue samples throughout 19 days of decomposition, iron, silicon, and magnesium were observed in both the tattooed tissue sample and the pure ink sample, but not in porcine tissue which had not been tattooed. This serves as a proof of concept in the application of the analysis of tattoo ink composition to aid in the identification of highly decomposed remains.

## ACKNOWLEDGEMENTS

First, I would like to thank my research advisor and committee member Dr. Ruth Smith without whom this research would not have been possible. This project was an idea that I had when I was in my undergraduate career. Was it not for Dr. Smith's encouragement, guidance, and drive; it would have remained just that, an idea. She has been a wonderful advisor and I truly feel honored to have worked for her. Next, I would like to thank Dr. Sheila Maxwell and Amy Albin for agreeing to serve on my committee and to bear with me through this process. I couldn't have performed the SEM-EDS analysis without Amy Albin as well as the other members of the Center for Advanced microscopy at MSU. Their patient instruction on the use of the SEM-EDS, the aid in the development of the method for processing the tissue samples, and their enthusiasm for my research project have been very much appreciated. I would also like to thank Dr. Kathy Severin and Dr. Joseph Ward for the use of their instruments throughout my research and for their aid during unexpected turns.

I am very grateful to my fellow forensic master's students, both past and present, who have both aided me and challenged me to do better throughout the last few years. I especially would like to thank Fanny Chu who has read almost every chapter of this thesis and has supported me throughout every bit of the writing process. Finally, I would like to thank my family for supporting me, especially my sister Tracy.

P.S. Bu, I am so sorry for everything I put you through. Thank you for being there when I needed you and not breaking down on me.

## TABLE OF CONTENTS

LIST OF TABLES.....	vi
LIST OF FIGURES.....	vii
Chapter 1 Introduction .....	1
1.1 Identification of Human Remains with Tattoos .....	1
1.2 Chemical Composition of Tattoo Inks .....	2
1.3 Comparison of ICP-MS, XRF, and EDS for the Analysis of Tattoo inks .....	6
1.4 Comparison of Raman and IR Spectroscopy of Tattoo inks .....	8
1.5 Investigation of Tattoos in Skin .....	9
1.6 Applications of Multivariate Statistical Analysis .....	12
1.7 Research Objectives .....	14
REFERENCES .....	16
Chapter 2 Theory .....	20
2.1 Attenuated Total Reflectance-Fourier Transform Infrared (ATR-FTIR) Spectroscopy ...	20
2.2 X-ray Fluorescence (XRF) Spectroscopy .....	24
2.3 Scanning Electron Microscopy -Energy Dispersive Spectroscopy (SEM-EDS).....	29
2.4 Multivariate Statistical Analysis .....	33
2.4.1 Principal Components Analysis.....	33
2.4.2 Hierarchical Cluster Analysis .....	38
REFERENCES .....	43
Chapter 3 Materials and Method .....	45
3.1 Tattoo Ink Sample Preparation .....	45
3.2 Tattoo Ink Sample Analysis .....	47
3.2.1 ATR-FTIR Spectroscopy Analysis .....	47
3.2.2 XRF Spectroscopy Analysis .....	48
3.2.3 Data Analysis.....	49
3.2.4 SEM-EDS Analysis .....	49
3.3 Tissue Sample Preparation.....	50
3.4 SEM-EDS Analysis of Tissue Samples.....	52
Chapter 4 Statistical Differentiation of Tattoo Inks Based on Organic and Inorganic Content ..	53
4.1 X-ray Fluorescence Spectroscopy Analysis of Tattoo Inks .....	53
4.2 IR analysis of Tattoo Inks.....	59
4.3 Multivariate Statistical Analysis of Tattoo Ink Spectra .....	62
4.3.1 XRF and IR Feature Selection for Statistical Analysis .....	62
4.3.2 Principal Components Analysis of the Reduced Variable Dataset .....	66
4.3.3 Hierarchical Cluster Analysis.....	74

4.4 Conclusion .....	76
APPENDICES.....	78
Appendix 4.1 Representative X-ray Fluorescence Spectra of Tattoo Ink samples.....	79
Appendix 4.2 Representative Infrared Spectra of Tattoo Ink samples.....	91
REFERENCES .....	105
Chapter 5 Mixed Inks and Tissue Sample Results and Discussion .....	107
5.1 XRF analysis of Ink Mixtures.....	107
5.2 IR analysis of Mixed Ink Samples .....	116
5.3 Multivariate Statistical Analysis of Reduced Variable Mixed Inks .....	125
5.3.1 PCA analysis of Mixed Inks.....	125
5.3.2 HCA analysis of Mixed Inks .....	130
5.4 Summary of Multivariate Statistical Analysis of Mixed Ink Samples .....	134
5.5 SEM-EDS Analysis of Tattoo Inks.....	134
5.6 Analysis of Tattoo Ink within Decomposed Tissue via SEM-EDS .....	138
5.7 SEM-EDS Analysis of Tattoo Inks.....	144
APPENDIX.....	146
REFERENCES.....	150
Chapter 6 Conclusions and Future Directions .....	152
6.1 Conclusions.....	152
6.2 Future Directions.....	154
REFERENCES.....	157

## LIST OF TABLES

<b>Table 1.1:</b> Ink components based on literature (13, 15-17).....	4
<b>Table 3.1:</b> Table of ink names, colors, manufacturers, lot numbers, and sample set designation. .....	46
<b>Table 3.2:</b> XRF spectroscopy scan parameters. ....	49

## LIST OF FIGURES

<b>Figure 2.1:</b> Diagram of a Michelson interferometer. ....	21
<b>Figure 2.2:</b> Diagram of attenuated total reflectance (ATR) attachment .....	22
<b>Figure 2.3:</b> Diagram of XRF instrument .....	25
<b>Figure 2.4:</b> Diagram exhibiting examples of electron transitions from the excited state to the ground state resulting in x-ray fluorescence. ....	28
<b>Figure 2.5:</b> Diagram of SEM-EDS instrument.....	30
<b>Figure 2.6:</b> Diagram of A) a two-variable dataset, B) two principal components applied to the two-variable dataset with the loadings for variable 1 on PC 1 calculated, and C) the scores plot resulting from the PCA.....	34
<b>Figure 2.7:</b> Example scree plot showing how the percent variance changes from PC to PC. ....	36
<b>Figure 2.8:</b> Demonstration of the differences of complete (red lines), single (blue lines), and group average (green lines) linkage methods. A) The initial clustering of the samples with the shortest Euclidean distance which is not dependent on the linkage method B) the second cluster which forms in which all linkage methods produce the same result C) the third cluster to form in which the type of linkage method used causes a difference in clustering.....	39
<b>Figure 2.9:</b> Dendrogram representing data from Figure 2.8 with the complete linkage method. ....	41
<b>Figure 3.1:</b> Positioning of tattoos and blanks on porcine sample .....	51
<b>Figure 4.1:</b> Representative XRF spectra of True Blue and Sky Blue inks. The specific transition and element are labeled for each major peak in each spectrum.....	54
<b>Figure 4.2:</b> Representative XRF spectra of Lipstick Red, Lining Black, and Dark Red inks. The specific transition and element are labeled for each major peak in each spectrum. ....	55
<b>Figure 4.3:</b> (A) Representative XRF spectra of Lime Green, Caramel, Lightning Yellow, and Canary Yellow inks. The specific transition and element are labeled for each major peak in each spectrum. The inlayed graph (B) shows a magnified spectrum of Lightning Yellow and Canary Yellow between 2 and 6 keV and 0 and 200,000 counts.....	58

<b>Figure 4.4:</b> (A) Overlay of representative absorbance IR spectra of True Blue and Sky Blue inks. The specific wavenumber is labeled for structurally indicative peaks in each spectrum. (B) Sky Blue IR with the absorbance scale set between 0.005 and 0.025. ....	59
<b>Figure 4.5:</b> (A) Overlaid IR spectra of Lining Black, Lipstick Red, and Dark Red inks. The specific wavenumber is labeled for structurally indicative peaks in each spectrum. ....	61
<b>Figure 4.6:</b> Principal components analysis of tattoo inks based on IR and XRF spectra. (A) Scores plots for first two principal components (PCs) and (B) corresponding loadings plots for first two PCs.....	63
<b>Figure 4.7:</b> Raw IR spectra of a Lining Black ink (Top Left) and Lipstick Red ink (Bottom Left) compared to the SNV-normalized spectra (Top and Bottom Right respectively) .....	64
<b>Figure 4.8:</b> Scree plot describing the variance of each PC in the PCA analyzed feature selected IR and XRF spectral data .....	67
<b>Figure 4.9:</b> Loadings plot for PCs 1-6 of the PCA of the reduced variable IR and XRF spectra ....	67
<b>Figure 4.10:</b> PCA scores plots for (A) PC 1 vs PC 2, (B) PC 1 vs PC 3, (C) PC 2 vs PC 3 and (D) PC 3 vs PC 4 of the feature selected IR and XRF spectra .....	70
<b>Figure 4.11:</b> Projected PCA scores plots for (A) PC 1 vs PC 2, (B) PC 1 vs PC 3, (C) PC 2 vs PC 3 and (D) PC 3 vs PC 4 of feature selected IR and XRF spectra.....	73
<b>Figure 4.12:</b> Projected HCA dendrogram for truncated IR and XRF spectral datasets for PCs 1-4. The dashed line marks 86.0% similarity.....	77
<b>Figure A 4.1:</b> Representative XRF spectra of blank filter paper. The specific transition and element are labeled for each major peak in the spectrum. ....	80
<b>Figure A 4.2:</b> Representative XRF spectra of Triple Black. The specific transition and element are labeled for each major peak in the spectrum.....	80
<b>Figure A 4.3:</b> Representative XRF spectra of Black Outliner. The specific transition and element are labeled for each major peak in the spectrum. ....	81
<b>Figure A 4.4:</b> Representative XRF spectra of Deep Red. The specific transition and element are labeled for each major peak in the spectrum.....	81
<b>Figure A 4.5:</b> Representative XRF spectra of Crimson Red. The specific transition and element are labeled for each major peak in the spectrum. ....	82



<b>Figure A 4.6:</b> Representative XRF spectra of Light Red. The specific transition and element are labeled for each major peak in the spectrum.....	82
<b>Figure A 4.7:</b> Representative XRF spectra of Scarlet Red. The specific transition and element are labeled for each major peak in the spectrum.....	83
<b>Figure A 4.8:</b> Representative XRF spectra of Orange. The specific transition and element are labeled for each major peak in the spectrum.....	83
<b>Figure A 4.9:</b> Representative XRF spectra of Bright Orange. The specific transition and element are labeled for each major peak in the spectrum. ....	84
<b>Figure A 4.10:</b> Representative XRF spectra of Golden Yellow. The specific transition and element are labeled for each major peak in the spectrum. ....	84
<b>Figure A 4.11:</b> Representative XRF spectra of Bright Yellow. The specific transition and element are labeled for each major peak in the spectrum. ....	85
<b>Figure A 4.12:</b> Representative XRF spectra of Graffiti Green. The specific transition and element are labeled for each major peak in the spectrum. ....	85
<b>Figure A 4.13:</b> Representative XRF spectra of Nuclear Green. The specific transition and element are labeled for each major peak in the spectrum. ....	86
<b>Figure A 4.14:</b> Representative XRF spectra of Mint Green. The specific transition and element are labeled for each major peak in the spectrum. ....	86
<b>Figure A 4.15:</b> Representative XRF spectra of Deep Turquoise. The specific transition and element are labeled for each major peak in the spectrum. ....	87
<b>Figure A 4.16:</b> Representative XRF spectra of Dark Purple. The specific transition and element are labeled for each major peak in the spectrum. ....	87
<b>Figure A 4.17:</b> Representative XRF spectra of Light Purple. The specific transition and element are labeled for each major peak in the spectrum. ....	88
<b>Figure A 4.18:</b> Representative XRF spectra of Light Magenta. The specific transition and element are labeled for each major peak in the spectrum. ....	88
<b>Figure A 4.19:</b> Representative XRF spectra of Hot Pink. The specific transition and element are labeled for each major peak in the spectrum.....	89
<b>Figure A 4.20:</b> Representative XRF spectra of Pink. The specific transition and element are labeled for each major peak in the spectrum.....	89

<b>Figure A 4.21:</b> Representative XRF spectra of White. The specific transition and element are labeled for each major peak in the spectrum.....	90
<b>Figure A 4.22:</b> Representative XRF spectra of Brite White. The specific transition and element are labeled for each major peak in the spectrum. ....	90
<b>Figure A 4.23:</b> Representative IR spectrum of Blank Filter Paper. The specific wavenumber is labeled for structurally indicative peaks in the spectrum. ....	92
<b>Figure A 4.24:</b> Representative IR spectrum of Black Outliner ink. The specific wavenumber is labeled for structurally indicative peaks in the spectrum. ....	92
<b>Figure A 4.25:</b> Representative IR spectrum of Triple Black ink. The specific wavenumber is labeled for structurally indicative peaks in the spectrum. ....	93
<b>Figure A 4.26:</b> Representative IR spectrum of Deep Red ink. The specific wavenumber is labeled for structurally indicative peaks in the spectrum. ....	93
<b>Figure A 4.27:</b> Representative IR spectrum of Crimson Red ink. The specific wavenumber is labeled for structurally indicative peaks in the spectrum .....	94
<b>Figure A 4.28:</b> Representative IR spectrum of Light Red ink. The specific wavenumber is labeled for structurally indicative peaks in the spectrum .....	94
<b>Figure A 4.29:</b> Representative IR spectrum of Scarlet Red ink. The specific wavenumber is labeled for structurally indicative peaks in the spectrum .....	95
<b>Figure A 4.30:</b> Representative IR spectrum of Orange ink. The specific wavenumber is labeled for structurally indicative peaks in the spectrum. ....	95
<b>Figure A 4.31:</b> Representative IR spectrum of Bright Orange ink. The specific wavenumber is labeled for structurally indicative peaks in the spectrum. ....	96
<b>Figure A 4.32:</b> Representative IR spectrum of Caramel ink. The specific wavenumber is labeled for structurally indicative peaks in the spectrum. ....	96
<b>Figure A 4.33:</b> Representative IR spectrum of Golden Yellow ink. The specific wavenumber is labeled for structurally indicative peaks in the spectrum .....	97
<b>Figure A 4.34:</b> Representative IR spectrum of Lightning Yellow ink. The specific wavenumber is labeled for structurally indicative peaks in the spectrum .....	97
<b>Figure A 4.35:</b> Representative IR spectrum of Bright Yellow ink. The specific wavenumber is labeled for structurally indicative peaks in the spectrum .....	98

<b>Figure A 4.36:</b> Representative IR spectrum of Canary Yellow ink. The specific wavenumber is labeled for structurally indicative peaks in the spectrum .....	98
<b>Figure A 4.37:</b> Representative IR spectrum of Graffiti Green ink. The specific wavenumber is labeled for structurally indicative peaks in the spectrum .....	99
<b>Figure A 4.38:</b> Representative IR spectrum of Nuclear Green ink. The specific wavenumber is labeled for structurally indicative peaks in the spectrum .....	99
<b>Figure A 4.39:</b> Representative IR spectrum of Lime Green ink. The specific wavenumber is labeled for structurally indicative peaks in the spectrum .....	100
<b>Figure A 4.40:</b> Representative IR spectrum of Mint Green ink. The specific wavenumber is labeled for structurally indicative peaks in the spectrum .....	100
<b>Figure A 4.41:</b> Representative IR spectrum of Deep Turquoise ink. The specific wavenumber is labeled for structurally indicative peaks in the spectrum. ....	101
<b>Figure A 4.42:</b> Representative IR spectrum of Dark Purple ink. The specific wavenumber is labeled for structurally indicative peaks in the spectrum .....	101
<b>Figure A 4.43:</b> Representative IR spectrum of Light Purple. The specific wavenumber is labeled for structurally indicative peaks in the spectrum. ....	102
<b>Figure A 4.44:</b> Representative IR spectrum of Light Magenta. The specific wavenumber is labeled for structurally indicative peaks in the spectrum. ....	102
<b>Figure A 4.45:</b> Representative IR spectrum of Hot Pink. The specific wavenumber is labeled for structurally indicative peaks in the spectrum.....	103
<b>Figure A 4.46:</b> Representative IR spectrum of Pink. The specific wavenumber is labeled for structurally indicative peaks in the spectrum.....	103
<b>Figure A 4.47:</b> Representative IR spectrum of White ink. The specific wavenumber is labeled for structurally indicative peaks in the spectrum.....	104
<b>Figure A 4.48:</b> Representative IR spectrum of Brite White ink. The specific wavenumber is labeled for structurally indicative peaks in the spectrum. ....	104
<b>Figure 5.1:</b> A) Representative XRF spectra of Lipstick Red and True Blue as well as 25/75, 50/50 and 75/25 v/v mixtures of these inks and B) Representative XRF spectrum of Dark Purple ink	109

**Figure 5.2:** A) Representative XRF spectra of Lighting Yellow and True Blue as well as 25/75, 50/50 and 75/25 mixtures of these inks and B) Representative XRF spectra of Deep Turquoise and Lime Green ..... 111

**Figure 5.3:** Representative XRF spectra of Lining Black and True Blue as well as 25/75, 50/50 and 75/25 mixtures of these inks ..... 114

**Figure 5.4:** A) Representative XRF spectra of Lining Black and Lipstick Red as well as 25/75, 50/50 and 75/25 mixtures of these inks and B) Representative XRF spectra of Dark Red and Deep Red ..... 115

**Figure 5.5:** A) Representative IR spectra of Lipstick Red and True Blue as well as 25/75, 50/50 and 75/25 v/v mixtures of these inks and B) Representative IR spectrum of Dark Purple ..... 118

**Figure 5.6:** A) Representative IR spectra of Lightning Yellow and True Blue as well as 25/75, 50/50 and 75/25 mixtures of these inks and B) Representative IR spectra of Deep Turquoise and Lime Green ..... 120

**Figure 5.7:** A) Representative IR spectra of Lining Black and True Blue as well as 25/75, 50/50 and 75/25 mixtures of these inks ..... 123

**Figure 5.8:** A) Representative IR spectra of Lining Black and Lipstick Red as well as 25/75, 50/50 and 75/25 mixtures of these inks and B) Representative IR spectrum of Dark Red and Deep Red ..... 124

**Figure 5.9:** Projected PCA scores plots showing mixed inks for (A) PC 1 vs PC 2, (B) PC 1 vs PC 2 with the area near the red inks enlarged, (C) PC 1 vs PC 2 with the area near the blue inks enlarged and (D) PC 1 vs PC 2 with the area near the yellow inks enlarged of feature selected IR and XRF ..... 127

**Figure 5.10:** Scores plot of PC2 vs PC 4 of feature selected XRF and IR data with mixed inks projected ..... 128

**Figure 5.11:** HCA dendrogram of ink mixtures. **Group 1:** 25/75 Lipstick Red/True Blue, two 75/25 and two 50/50 Lining Black/True Blue v/v mixtures, and all True Blue replicates, **Group 2:** one 75/25 Lining Black/True Blue v/v mixture, **Group 3:** all 25/75 Lining Black/True Blue v/v mixtures, **Group 4:** one 50/50 Lining Black/True Blue v/v mixture, **Group 5:** all 75/25 and 50/50 Lipstick Red/True Blue v/v mixtures, **Group 6:** all 75/25 Lightning Yellow/True Blue v/v mixtures, **Group 7:** all 50/50 and 25/75 Lightning Yellow/True Blue v/v mixtures, **Group 8:** all 75/25 Lining Black /Lipstick Red mixtures, **Group 9:** all 50/50 Lining Black/ Lipstick Red v/v mixtures, and **Group 10:** all 25/75 Lining Black/Lipstick Red mixtures ..... 133

**Figure 5.12:** SEM images (500x magnification, Working Distance 10 mm, 15 keV) in backscatter mode with EDS spectra of (A) True Blue, (B) Lining Black, and (C) Lipstick Red tattoo inks ..... 135

**Figure 5.13:** (A) Picture of Pig after 1 day of decomposition (B) SEM-EDS layered map image of pig skin without ink 1500x with corresponding EDS spectrum (C) SEM-EDS layered map image of porcine tissue with Dark Red ink 1500X with corresponding EDS spectrum. .... 141

**Figure 5.14:** (A) Picture of Pig after 19 days of decomposition (B) SEM-EDS layered map image of pig skin without ink 1500X with corresponding EDS spectrum (C) SEM-EDS layered map image of porcine tissue with Dark Red ink 1500X with corresponding EDS spectrum. .... 143

**Figure A 5.1:** (A) Picture of Pig after 3 days of decomposition (B) SEM-EDS layered map image of pig skin without ink 1500X with corresponding EDS spectrum (C) SEM-EDS layered map image of porcine tissue with Dark Red ink 1500X with corresponding EDS spectrum. .... 147

**Figure A 5.2:** (A) Picture of Pig after 6 days of decomposition (B) SEM-EDS layered map image of pig skin without ink 1500X with corresponding EDS spectrum (C) SEM-EDS layered map image of porcine tissue with Dark Red ink 1500X with corresponding EDS spectrum. .... 148

**Figure A 5.3:** (A) Picture of Pig after 13 days of decomposition (B) SEM-EDS layered map image of pig skin without ink 1500X with corresponding EDS spectrum (C) SEM-EDS layered map image of porcine tissue with Dark Red ink 1500X with corresponding EDS spectrum. .... 149

## Chapter 1 Introduction

### 1.1 Identification of Human Remains with Tattoos

Tattoos have existed for thousands of years and have been used for identification purposes throughout history. Tattoos were used to aid in the identification of bodies in both the attack on the World Trade Center in 2001 (1) and the 2004 Indian Ocean Tsunami (2). Up to 10% of the global and 25% of the United States population are tattooed (3-5). This number has even been shown to be as high as 40% in cases of death requiring a forensic investigation (4, 6, 7).

The use of tattoos as an identification tool is due to their relative permanence in tissue. Tattoo ink is injected between 0.400 and 2.00 mm into the skin (3, 8, 9). Damage to the skin usually occurs in the upper layers of the dermis which, on average, reaches a depth of 0.1 mm (10). When the ink is injected into the skin, the body reacts to it as a foreign substance. Macrophages engulf ink particles; some bring the particles to the lymph nodes while others hold it at the site of injection (9). The depth of the ink injection along with the macrophages, which remain at the site of injection, result in the perpetuity of the tattoo. Due to their permanence, increasing popularity, and relevance to forensic cases, tattoos have the potential to aid in the identification of highly decomposed remains. However, visual inspection of the tattoos can be distorted as tattoos can be covered by discoloration of the skin during decomposition. Owing to this, the use of the chemical composition of the ink to aid in identification of highly decomposed remains is the focus of this study as the components of the ink remain in the skin even after decomposition has obscured the tattoo site.

## 1.2 Chemical Composition of Tattoo Inks

Tattoo inks typically consist of a pigment suspended in a solvent such as water or ethanol. The pigments consist of a variety of substances that are organic (compounds containing C, H, O, and N) or inorganic (compounds containing elements other than C, H, O, and N) in nature and that determine the color of the ink. Additional components such as preservatives, which increase shelf life, and thixotropic agents, which affect the flow of the ink out of the tattoo machine during the injection, also aid in the identification of tattoo ink in the skin as these components contain elements such as silicon (Si), titanium (Ti), and aluminum (Al) which are not typically observed in high concentrations in tissue (11, 12).

As tattoo culture has existed since prehistoric times, regulation of tattoo inks has been difficult as guidelines are retroactively placed. For example, the United States Food and Drug Administration's regulation of tattoo inks is post-market; action can only be taken after a product being sold is found to be misbranded or adulterated (13). Further, many ink manufacturers do not report ink components in material safety datasheets, listing the components as proprietary. In 2003, the European Council attempted to regulate the concentration of metallic components in tattoo inks, especially metals such as chromium (Cr) which can cause allergic reactions. However, these are guidelines and not requirements (12). This has caused the composition of many tattoo inks to not be widely reported. Research has been done into the composition of tattoo inks. However, research has either been focused on a few select brands such as in the case of Forte *et al.* which focused on the composition of StarBrite™ inks or the papers containing the composition of the inks have removed the

identifiers so that it is not possible to relate the results of the research back to a particular brand such as in the study done by Danish Environmental Protection Agency (12, 14).

In research done by previous analysts, iron (Fe), copper (Cu), chlorine (Cl), Ti, Al, Si, and magnesium (Mg) are the most common elements in the tattoo inks observed (12, 14-16). The elements present indicate the color of the ink. For example, Fe is often present in black and red inks and likely originates from iron oxides (Table 1.1). Copper and Cl are often observed in blue and green inks and likely originate from copper phthalocyanine and its chlorinated forms (Table 1.1). The presence of Cl was also observed in several other inks including red, yellow, and purple inks (12, 15). These inks likely contain chlorine-containing azo compounds; example structures are shown in Table 1.1. Titanium was primarily present in blue inks (12, 15) but was also observed in some hues of every other ink color. Titanium likely comes from titanium dioxide, which is a whitening agent and opacifier (Table 1.1) that is added to make the inks a lighter shade (12, 14-16). The presence of Al, Si, and Mg in inks is likely due to thixotropic agents which usually consists of aluminum silicates or magnesium aluminum silicates (12).

Other elements detected in tattoo inks include barium (Ba), sulfur (S), and Cr, although they are not as common as the elements listed above (12, 14, 16, 17). Barium and S likely originate from barium sulfate, a whitening and thixotropic agent (Table 1.1). Chromium was often observed in shades blue and green in older studies (17).



**Table 1.1:** Ink components based on literature (13, 15-17)

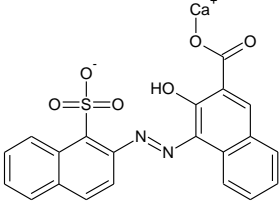
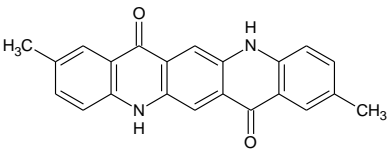
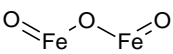
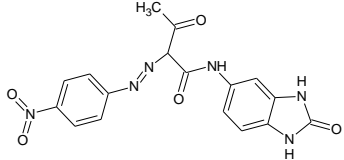
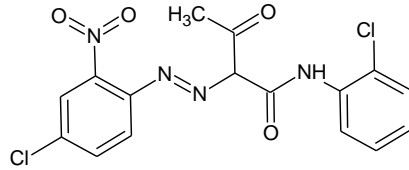
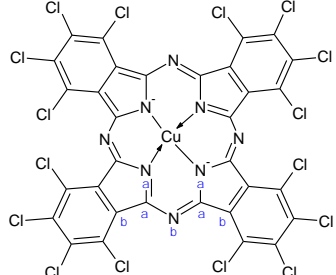
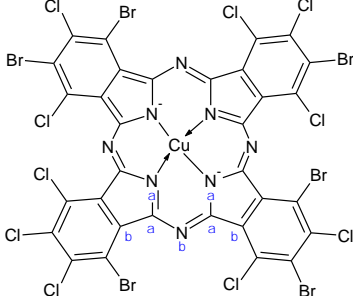
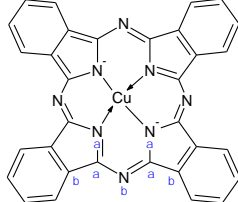
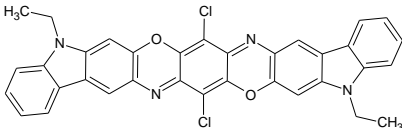
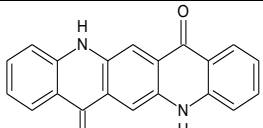
Color	Ink Component Examples	
Red	 Pigment Red 63.1	 Pigment Red 122   Ferric Oxide
Orange	 Pigment Orange 62	
Yellow	 Pigment Yellow 3	
Green	 Phthalocyanine green	 Pigment Green 36
Blue	 Copper phthalocyanine	
Purple	 Pigment Violet 23	 Pigment Violet 19

Table 1.1 (cont'd)

Color	Ink Component Examples	
White	$\text{Ba}^{2+} \text{O}^- \text{S} \begin{array}{c} \text{O} \\ \parallel \\ \text{O}^- \end{array}$ Barium sulfate	$\text{O}=\text{Ti}=\text{O}$ Titanium dioxide
Black	Carbon	$\text{O}=\text{Fe}-\text{O}-\text{Fe}=\text{O}$ Ferric Oxide
Other	$\begin{array}{c} \text{O}^- \\   \\ \text{O}^- \text{Si} \text{O}^- \\   \\ \text{O}^- \end{array} \text{Al}^{3+} \begin{array}{c} \text{O}^- \\   \\ \text{O}^- \text{Si} \text{O}^- \\   \\ \text{O}^- \end{array}$ Aluminum Silicate	$\begin{array}{c} \text{O}^- \\   \\ \text{O}^- \text{Si} \text{O}^- \\   \\ \text{O}^- \end{array} \text{Al}^{3+} \begin{array}{c} \text{O}^- \\   \\ \text{O}^- \text{Si} \text{O}^- \\   \\ \text{O}^- \end{array} \text{Mg}^{2+}$ Magnesium Aluminum Silicate

Several components contribute to the organic composition of tattoo inks (12, 15).

However, most of the pigments fall into one of four classes; phthalocyanines (15, 18), azo-pigments (15, 18), quinacridones, and carbon black pigments. Phthalocyanines often contain a metallic core which determines the color of the pigment. In tattoo inks, this core is usually Cu, which creates either a blue or green pigment. These organic molecules are characterized by the presence of isoindole groups. Examples of phthalocyanines are copper phthalocyanine, phthalocyanine green, and Pigment Green 36 (Table 1.1).

Azo-pigments are defined as any pigment that contains an azo (N=N) bond. These pigments are used to synthesize a wide variety of colors including reds, oranges, and yellows (15).

Examples of these are Pigments Red 63.1, Red 146, Orange 62, Yellow 3 (Table 1.1).

Quinacridones are characterized by five connected ring structures of which rings 2 and 4 contain a N atom in the ring and a para ketone structure. These types of pigments have been

observed in both red and purple inks (15) and are in Pigments Red 122 and Violet 19 (Table 1.1).

The last type of pigment, which does not fit into any of the above categories, is carbon black, the main pigment in many black tattoo inks (12, 15). This pigment is difficult to detect due to a lack of distinguishing elements or bonds. Previous studies indicate that it is present in black ink through thermogravimetric analysis; however, the Raman or IR spectra were not provided (12, 15). Carbon black is typically associated with S compounds due to the burning process involved in its creation.

As elements such as Cu are associated with specific colors such as blue and bonds such as azo bonds can be associated with colors such as red, orange, and yellow, these components can be used to detect not only the presence of tattoo ink within tissue, but also the color. In order to detect these ink components, instrumentation must be selected that is able to differentiate the tattoo ink components from components present in tissue. Additionally, the use of instrumentation currently used in forensic labs would be preferable as this would allow implementation into current forensic labs.

### 1.3 Comparison of ICP-MS, XRF, and EDS for the Analysis of Tattoo inks

To determine the inorganic composition of tattoo ink, inductively coupled plasma-mass spectrometry (ICP-MS), x-ray fluorescence (XRF) spectroscopy, and energy dispersive spectroscopy (EDS) have been used in previous studies (12, 14, 15). Inductively coupled plasma-mass spectrometry (ICP-MS) is a sensitive, multi-element technique that can detect elements with masses between 6 and 250 amu (12, 14). However, for an analysis to be performed via ICP-MS, the tattoo ink needs to be completely digested to have an accurate representation of the

elements the ink contains. Digestion of tattoo ink for ICP-MS analysis requires the use of nitric, hydrochloric, sulfuric, or hydrofluoric acid (12, 14). A study by the Danish Environmental Protection Agency used ICP-MS to analyze 61 tattoo inks, determining the concentration of elements present. In this research, nitric acid was used to digest the inks. Although the concentrations of Ti and Al, two prevalent components in tattoo inks, were reported in this study, the researchers acknowledged that the results were an underestimation due to incomplete digestion of these elements. Additionally, the concentrations of Br, Cl, and S, which aid in the identification of some tattoo inks, were not reported as a result of interferences caused by the digestion method.

Hydrofluoric acid is capable of digesting Al and Ti and was used in a study by Forte *et al.* of 56 inks from 4 different brands with a range of colors including red, orange, yellow, green, blue, purple, brown, black, and white. The aim of the research was to determine whether the inks analyzed exceeded the safe allergological limit of 1 µg/g. The inks were digested in a mixture of nitric acid, hydrofluoric acid, and hydrogen peroxide. However, the concentration of Ti was not reported for any of the inks. This is likely due to an incomplete digestion of the ink as in the study done by the Danish Environmental Protection agency. Further, hydrofluoric acid is highly dangerous to work with as it is corrosive to glass as well as many metals and causes severe, delayed burns(19). Its use is not advised as it has the potential to damage the ICP-MS instrument if not properly diluted before analysis. However, dilution can also cause inaccurate analysis of the elements within the samples, as trace elements that are present within the ink have the potential to be diluted below the limit of detection for ICP-MS analysis.

In a forensic analysis, it is advantageous for analysts to use as few destructive techniques as possible to preserve evidence for future analyses. In both XRF and EDS analyses, the sample is not destroyed, but scanned by applying energy to the sample in either the form of x-rays or a beam of electrons which excite electrons within the sample. When the electrons within the sample release the energy, the energy is released in the form of x-rays which are unique to the element they originate from. This allows the analyst to detect elements without damaging the sample. Further, the two techniques are advantageous for the analysis of solid samples; most can be directly scanned without elaborate preparation, and in the case of EDS analysis, location-specific identification of elements in a tattoo sample is possible. Further, the XRF and EDS are currently more frequently available in forensic science labs than ICP-MS. Due to these advantages, XRF and SEM-EDS were chosen for investigation in this study. However, these instruments are unable to detect organic components and therefore investigation of other instruments was necessary.

#### 1.4 Comparison of Raman and IR Spectroscopy of Tattoo inks

Techniques that have been employed to determine the organic components of tattoo ink include Raman spectroscopy and infrared (IR) spectroscopy (15). Both Raman and IR spectroscopy are rapid and non-destructive techniques that are used to determine organic functional groups present within a sample. Raman and IR spectroscopy are complementary techniques. IR spectroscopy measures the light absorbed by the bonds between functional groups in a molecule based on changes in dipole moment while Raman spectroscopy measures scattered light from changes in polarizability of a molecule. Typically, if a bond is Raman active (i.e. it is able to be observed by Raman spectroscopy) it will be IR inactive and vice versa. A

study done by Miranda compared the analysis of tattoo inks with Raman spectroscopy and IR spectroscopy (15). Raman spectroscopy was able to be used with less consideration of the sample size being analyzed (15). Miranda also reported that in normal Raman spectroscopy, some inks were not able to be observed due to fluorescence within the sample. In Raman spectroscopy, scattered light from the sample is detected at a 90-degree angle from the light source to ensure that light from the light source does not affect detection. However, fluorescent light is emitted from the sample and is omnidirectional causing it to be detected by the Raman detector. Furthermore, the scattered light detected in Raman spectroscopy is orders of magnitude less intense than the transmitted light detected in IR spectroscopy, causing fluorescence to have more of an effect on Raman spectroscopy than IR. Due to the limitations of Raman, IR was used in this work.

### 1.5 Investigation of Tattoos in Skin

Currently, tattoos found on human remains are most often identified by a visual inspection of the body by a forensic pathologist. However, the tattoo can be masked by skin surface modifications such as discoloration during decomposition. Techniques such as IR cameras, x-ray radiography, and microscopy have been explored to aid in the visualization of tattoos in tissue with limited results (20, 21).

Starkie *et al.* photographed a tattooed pig which had gone through decomposition as well as 30 tattooed human participants (20). A digital SLR camera both with and without an infrared attachment, as well as a digital video camera in IR mode, were used. Infrared photography allowed the visualization of tattoos that had been masked due to skin discoloration. However, tattoos which had red pigments in both the pig sample and the 30 participants were not visible

in the IR mode (11). Similar results were observed in a later study by Clarkson and Birch in which IR spectral cameras were used to visualize tattoos that had either been covered by other tattoos or had been removed using lasers (21).

Clarkson and Birch also used X-ray radiography to visualize tattoos on a pig's thigh through a body bag (21). This was done to determine if X-ray radiographs could be used to quickly analyze bodies for the presence of tattoos in mass disaster scenarios. The study found that to visualize tattoos with X-ray radiographs, the X-ray system used an exposure time of over seven minutes and used energy levels that were more intense than in typical hospital X-ray radiographs. Clarkson and Birch reported that this technique was only useful in tattoos containing inks with high metallic content and that the images were hard to interpret unless the analyst was specifically targeting tattoos.

Previous studies on tattoos in skin also include microscopic analyses that aimed to identify allergens from tattoo ink and differentiate between lymph nodes swollen with tattoo ink and melanomas (22-24). In these case studies, where only 1-4 cases were analyzed, lymph node dissections were performed and the tissues were then analyzed via microscopy. Most analysts noted that the tattoo ink can be visually differentiated from the surrounding tissue based on the color of the pigments; however, the lymph node and skin biopsies were taken either from living participants or before decomposition had begun (22-24). Although these pigments are visible in fresh tissue, the pigments may be harder to differentiate in tissue which has undergone decomposition or other damage.

The IR camera, X-ray radiography, and microscopy studies show that the enhanced visualization of tattoo inks in skin is possible, but the results are subjective and open to

analysts' interpretations. These studies also highlight differences in the composition of tattoo inks, with some inks being more metallic-based than others.

Some efforts have been made to determine the composition of tattoo inks in skin; however, these efforts have mainly focused on the metallic composition of inks due to the potential for these components to cause allergic reactions. In a study by Taffe *et al.*, scanning electron microscopy-energy dispersive spectroscopy (SEM-EDS) was used to analyze skin biopsies from four patients suffering from allergic reactions to tattoo sites. The analysts specifically focused on analyzing the tissue for mercury as it was thought that mercuric chloride was causing the allergic reactions; however, mercury was only detected in one of the skin biopsies. The analysts had received pigments from tattoo sources which contained Ti, Al, Cl, Si, calcium, and zinc (25). However, since these results were observed in 1978, they may not apply to modern tattoo inks.

Two studies have been done to determine the organic components of tattoo ink within skin. These were done by Miranda and by Poon *et al.* (15, 18). In the study by Miranda, a sample of pig tissue was tattooed with seven ink colors: red, orange, yellow, green, blue, purple, and white. Each ink was tattooed twice onto the tissue and was then sectioned and preserved, either by freezing the tissue or submerging in formalin without decomposition occurring. The sections of tattooed tissue were then analyzed by Raman spectroscopy and compared to pure ink samples analyzed on the same instrument. Spectral peaks from the analysis of tattooed tissue samples had similar wavelengths and intensity patterns as those of their corresponding tattoo ink for all tissue samples. Similarly, Poon *et al.* compared five tattooed sections of pig tissue containing red, yellow, green, blue, and black inks to their pure



ink equivalents via Raman spectroscopy; the tissue samples had similar wavelengths and intensity patterns as their corresponding original inks with the exception of the black ink which had large deviations in its spectra.

These studies have clearly demonstrated it is possible to correlate tattooed tissue samples with the original tattoo inks by comparing their chemical compositions; however, one thing of note is that tissue decomposition studies of this nature have not been performed. As the majority of human identification using tattoos is performed on decomposed remains where tattoos may be obscured, the potential for linking the tattooed decomposed tissue samples to the original inks through tattoo chemical compositions needs to be investigated.

#### 1.6 Applications of Multivariate Statistical Analysis

Previous studies have shown that differentiation of tattoo inks colors is possible based on their chemical composition (12, 14, 15, 18). However, the analytical techniques used can lead to datasets with 1000 – 4000 variables per tattoo ink. The comparison of similarities and differences among tattoo inks that yield several thousand measurements per sample is challenging. Further, no previous study mentioned above investigated the possibility of differentiating ink mixtures, which would be important in the analysis of a tattoo that is composed of multiple tattoo inks. Multivariate statistical analysis approaches such as principal components analysis (PCA) and hierarchical cluster analysis (HCA), which have not been previously applied in the differentiation of tattoo inks, can aid in data interpretation and differentiation of mixed and non-mixed inks.

Principal components analysis is an unsupervised statistical procedure that has been widely applied in forensic applications including the dating of ballpoint pen inks, the differentiation of

paint samples, and differentiation of heroin samples (26-28). Principal components analysis is used to reduce the number of variables into a few principal components that highlight the most variation within the dataset. Samples are displayed on a scores plot in which samples that are chemically similar are positioned closely to one another and samples that are chemically different are positioned farther apart. Principal components analysis has been used previously to differentiate inks for determining the authenticity of documents (29), for differentiation between blue ballpoint pen inks, and for determining the effect of time between when the ink was applied to a document and the analysis of the ink (26).

While PCA is a powerful multivariate statistical technique used widely for data reduction and comparison of samples across many variables, a drawback to the technique is the visual evaluation of a scores plot as part of data interpretation. This leads to subjectivity in the data analysis. To make data analysis less subjective, a complementary technique such as HCA can be used in tandem with PCA. In HCA, the distance between two samples is calculated in multidimensional space. Samples that have the shortest distances between them are grouped together first, proceeded by samples that have longer distances between them. A similarity level of between 0 and 1 among each of the samples is then calculated based on the largest distance found within the dataset where the samples that have the largest distance between them have a similarity level of 0. Hierarchical cluster analysis has previously been used to determine the similarity in chemical composition between layers of paint chips (30) and also has been used in tandem with PCA to differentiate spray paint colors based on their chemical composition (31). Overall, PCA and HCA allow for easy visualization of results which are less

subjective than non-statistical approaches and were used for differentiation of the inks in this study.

### 1.7 Research Objectives

In many of the studies previously mentioned, the researchers either focused on one or two brands of ink or did not report any identifying information about the inks analyzed. In order to add to the knowledge of the composition of tattoo inks, the first goal of this study is to determine the composition of a wide range of tattoo inks from popular brands currently used. This was done by purchasing two sets of inks from popular brands. The inks were then analyzed by IR spectroscopy, XRF spectroscopy, and SEM-EDS. These techniques were selected as they would provide both organic and inorganic information on each ink and are widely available in forensic laboratories.

Secondly, as the differentiation of tattoo inks based on their organic and inorganic composition has not been previously accomplished, the potential for differentiation and association of tattoo ink colors by their organic and inorganic composition through the application of PCA and HCA was investigated. Further testing of the ability to differentiate inks by PCA and HCA was done through mixing inks to determine if the mixed inks could be differentiated from manufactured inks of similar colors as well as the inks from which they originate.

The last objective of this research was to determine if decomposition of the surrounding tissue affects the association of tattoo ink within the tissue with the pure tattoo ink as this has not been previously investigated. This was done through the analysis of tattooed decomposed tissue with SEM-EDS which was chosen as it is widely available in forensic labs as well as having

the ability to provide inorganic and organic information. As the association of tattoo ink in decomposed tissue with the tattoo ink source has not been previously studied, this study provides a new aid in the identification of highly decomposed remains.

## REFERENCES

## REFERENCES

1. World Trade Center Operational Statistics. New York City: New York City Office of the Chief Medical Examiner; 2015
2. Wright K, Mundorff A, Janet C, Forrest A, Maquire C, Crane DI. A new disaster victim identification management strategy targeting “near identification-threshold” cases: Experiences from the Boxing Day tsunami Forensic Science International. 2015;250:91-7.
3. Tsokos M, Cains G, Byard R. The Forensic and Cultural Implications of Tattooing. Forensic Pathology Reviews. 2008;5:197-218.
4. Laumann A, Derick A. Tattoos and body piercings in the United States: A national data set. American Academy of Dermatology. 2006:1-9.
5. Mayers L, Chiffriller S. Body Art (Body Piercing and Tattooing) among Undergraduate University Students: “Then and Now” Journal of Adolescent Health. 2008;42:201-3.
6. Armstrong ML, Murphy KP. Tattooing: Another Adolescent Risk Behavior Warranting Health Education. Applied Nursing Research. 1997;10(4):181-9.
7. Blackburn J, Cleveland J, Griffin R, Davis G, Lienert J, McGwin G. Tattoo Frequency and Types Among Homicides and Other Deaths, 2007-2008. Am J Forensic Med Pathol. 2012;33(3):202-5.
8. Kossida T, Rigopoulos D, Katsambas A, Anderson RR. Optimal tattoo removal in a single laser session based on the method of repeated exposures Journal of the American Academy of Dermatology. 2011;66(2):271-7.
9. Sperry K. Tattoos and Tattooing Part II; Gross Pathology, Histopathology, Medical Complications, and Applications. The American Journal of Forensic Medicine and Pathology. 1992;13(1):7-17.
10. Sandby-Møller J, Poulsen T, Wulf HC. Epidermal Thickness at Different Body Sites: Relationship to Age, Gender, Pigmentation, Blood Content, Skin Type, and Smoking Habits. Acta Derm Venereol. 2003;83:410-3
11. Laux P, Tralau T, Tentschert J, Blume A, Dahouk S, Baulmer W, et al. A medical-toxicological view of tattooing. The Lancet. 2015;387(10016):395-402.
12. Chemical Substances in Tattoo Ink Survey of chemical substances in consumer products Copenhagen, DK: Miljøstyrelsen; 2012;155.

13. Katz L, editor. Regulation of Tattoo Inks in the US. First International Conference on Tattoo Safety 2013 June 6-7; Free University of Berlin. Bundesinstitut fur Risikobewertung.
14. Forte G, Petrucci F, Cristuado A, Bocca B. Market survey on toxic metals contained in tattoo inks. *Science of the Total Environment*. 2009;407:5997-6002.
15. Miranda MD. *Forensic Analysis of Tattoos and Tattoo Inks*. 1 ed. Boca Rotan, Fl: CRC Press, 2016.
16. Timko A, Miller C, Johnson F, Ross V. In Vitro Quantitative Chemical Analysis of Tattoo Pigments. *Arch Dermatol*. 2001;137:143-7.
17. Lea P, Pawlowski M. Human Tattoo: Electron Microscopic Assessment of Epidermis, Epidermal-Dermal Junction, and Dermis *International Journal of Dermatology*. 1987;26(7):453-8.
18. Poon K, Dadour I, McKinley A. In situ chemical analysis of modern organic tattooing inks and pigments by micro-Raman spectroscopy *Journal of Raman Spectroscopy*. 2008;39:1227-37.
19. Scientific F. Material Safety Data Sheet Hydrofluoric Acid (47-51%). 2007 [updated 2007; cited 2017 January 17, 2017]; 15:[Available from: <https://fscimage.fishersci.com/msds/11171.htm>].
20. Starkie A, Birch W, Ferllini R, Thompson TJU. Investigation into the Merits of Infrared Imaging in the Investigation of Tattoos Postmortem *Journal of Forensic Sciences*. 2011;56(6):1569-73.
21. Clarkson H, Birch W. Tattoos and Human Identification: Investigation into the Use of X-Ray and Infrared Radiation in the Visualization of Tattoos 2013;58(5):1264-72.
22. Kluger N, Cohen-Valensi R, Nezri M. Black lymph nodes—and a colourful skin. *Lancet*. 2008;371:1214.
23. Bordea C, Latifaj B, Jaffe W. Delayed presentation of tattoo lymphadenopathy mimicking malignant melanoma lymphadenopathy *Journal of Plastic, Reconstructive, & Aesthetic Surgery*. 2009;62:e283-e5.
24. Cabalag M, Christie M, Miller J. Pigmented lymphadenopathy secondary to tattoo ink: A potential masquerader *Surgery*. 2015;157:959-60.
25. Taafe A, Knight AG, Marks R. Lichenoid tattoo hypersensitivity. *British Medical Journal*. 1978;1:616-8.

26. Senior S, Hamed E, Masoud M, Shehata E. Characterization and Dating of Blue Ballpoint Pen Inks Using Principal Component Analysis of UV–Vis Absorption Spectra, IR Spectroscopy, and HPTLC. *Journal of Forensic Sciences*. 2012;57(4):1087-93.
27. Lambert D, Muehlethaler C, Essieva P, Massonnet G. Combining spectroscopic data in the forensic analysis of paint: Application of a multiblock technique as chemometric tool. *Forensic Science International*. 2016;263:39-47.
28. Klemenc S. In common batch searching of illicit heroin samples — evaluation of data by chemometrics methods. *Forensic Science International*. 2001;115(1-2):43-52.
29. Hoehse M, Paul A, Gornushkin I, Panne U. Multivariate classification of pigments and inks using combined Raman spectroscopy and LIBS Anal Bioanal Chem. 2012;402:1443-50.
30. Flynn K, O'Leary R, Lennard C, Roux C, Reedy B. Forensic Applications of Infrared Chemical Imaging: Multi-Layered Paint Chips *Journal of Forensic Science*. 2005;50(4):1-10.
31. Muehlethaler C, Massonnet G, Esseiva P. Discrimination and classification of FTIR spectra of red, blue and green spray paints using a multivariate statistical approach. *Forensic Science International*. 2014;244:170-8.



## Chapter 2 Theory

As tattoo inks can consist of both organic and inorganic materials, both are needed to have a complete comprehension of ink composition. To do this, three instruments are used in this study; attenuated total reflectance- Fourier transform infrared (ATR-FTIR) spectroscopy, x-ray fluorescence (XRF) spectroscopy, and scanning electron microscopy-energy dispersive spectroscopy (SEM-EDS). All of these techniques are considered rapid, non-destructive, and are commonly used in forensic laboratories.

### 2.1 Attenuated Total Reflectance-Fourier Transform Infrared (ATR-FTIR) Spectroscopy

ATR-FTIR is a technique in which wavelengths of infrared (IR) light excite vibrational motions within a sample. Vibrations of functional groups within a molecule absorb characteristic wavelengths of light. This allows for functional groups within the sample to be identified based on the wavelengths of light that reach the instrument's detector.

The ATR-FTIR combines two techniques used in IR spectroscopy to produce a spectrum. The first is the Fourier-transform spectrometer and the other is the total internal reflection within a crystal provided by the ATR attachment. Fourier-transform spectroscopy is a technique used in spectroscopy to achieve faster run times, better signal-to-noise ratio, and better resolving power than dispersive IR spectrometers (1). This is achieved with a Michelson interferometer (Figure 2.1).

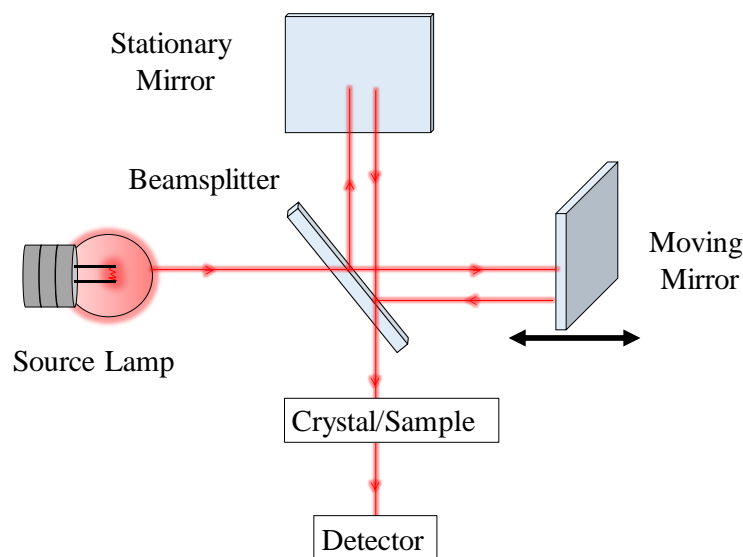


**Figure 2.1:** Diagram of a Michelson interferometer.

The Michelson interferometer scans through many frequencies of light within a period of time allowing for what is known as time-domain spectroscopy. In this, a beam of light from the source lamp is aimed at a partially transparent mirror known as the beamsplitter. Part of the light passes through the mirror to a moving mirror while the rest of the beam is reflected towards a stationary mirror. These mirrors reflect their respective beams of light back towards the beamsplitter where they are recombined. While the sample is scanned, the moving mirror traverses back and forth in a transverse movement. This movement results in pathlength differences between the beam of light reflecting from the moving mirror to the beamsplitter and that from the stationary mirror to the beamsplitter. Because of these pathlength differences, both constructive and destructive interference occur at the beamsplitter when the beams of light recombine. This produces what is known as an interferogram (1).

In an interferogram, the center of the spectrum is where the most constructive interference occurs, and thus has the highest amplitude wave; this point is known as the centerburst. Complete constructive interference occurs when the moving mirror is the same

distance from the beamsplitter as the stationary mirror. This distance is known as the zero path distance (ZPD) and is used by the instrument to align spectra for signal averaging.

The second part of the instrument is the attenuated total reflectance (ATR) attachment (Figure 2.2). Once the beam from the source lamp passes through the interferometer, the beam is reflected by a series of mirrors into a crystal, with the sample of interest above the crystal. The mirrors are used to aim the beam into the crystal at an angle which will cause total internal reflectance at the interface between the crystal and air, where the sample contacts the crystal. Total internal reflection is achieved when the angle of incidence is greater than the critical angle required for reflection and when the medium at the other side of the interface has a smaller reflective index than that of the medium in which the beam of light is traveling (1). At the interface between the air and the crystal, an evanescent wave is produced which penetrates the sample on the order of microns.

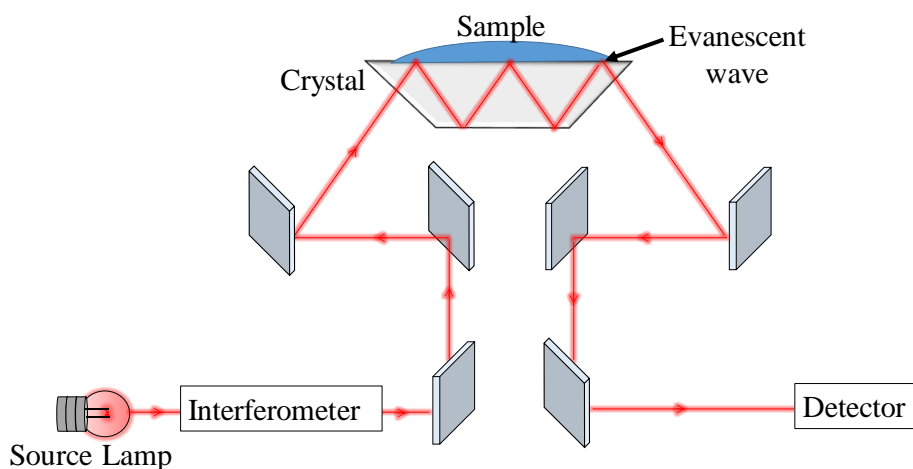


**Figure 2.2:** Diagram of attenuated total reflectance (ATR) attachment

The distance which the evanescent wave penetrates the sample depends on the type of ATR crystal used. Several types of ATR crystal are manufactured depending on what is needed for the analysis. Some examples of ATR crystals are diamond and zinc selenide (ZnSe) crystals,

which have low refractive indices that cause the depth of penetration of their evanescent waves to be 1.66  $\mu\text{m}$ , as well as germanium (Ge), which has a high refractive index causing a smaller depth of penetration of 0.65  $\mu\text{m}$ . Diamond and ZnSe crystals can be combined to form a robust crystal that can be used for general analysis. To ensure that the IR light penetrates the sample, contact between the crystal and the sample must be maintained. This is achieved with a pressure arm which applies force to the sample.

As the beam penetrates the sample, the bonds in the molecules within a sample absorb energy from the IR beam. This energy is then dissipated throughout all the bonds within a molecule. Vibrational motion occurs when the frequency of the vibrational motion is equal to the energy imparted onto the molecule and occurs to dissipate the energy imparted. The remaining energy not absorbed is then transmitted to the detector. The amount of IR light absorbed at a given wavelength is dependent on the concentration of the sample which is expressed through Beer's Law (Equation 1).

$$A = \epsilon bc \quad \text{Equation 1.}$$

In Beer's law, A is absorbance,  $\epsilon$  is the molar absorptivity of the sample, b is the distance the IR beam travels, and c is the concentration or amount of the sample which the beam passes through. As the molar absorptivity is a constant to the molecule, the only factor which can be altered to improve absorption of the sample is the pathlength. This is controlled through the number of bounces the beam takes through the crystal. With a larger number of bounces through the crystal, the pathlength increases and more absorption from the same concentration of analyte will occur. However, the increased number of interactions with the sample also increases the amount of light scattering, which causes the signal-to-noise ratio to

decrease. Therefore, a balance must be found when choosing the number of bounces during an analysis.

Although IR spectroscopy provides valuable structural information about a sample through a non-destructive analysis, it is only capable of providing organic information. To obtain inorganic information, a different instrument must be used.

## 2.2 X-ray Fluorescence (XRF) Spectroscopy

X-ray fluorescence spectroscopy is a non-destructive technique in which samples can be directly analyzed with no sample preparation. X-ray fluorescence spectroscopy uses x-ray photons to excite electrons within the sample. When the electrons relax to their ground states, they release energy in the form of fluorescence, which is unique to the elements within the sample. This allows for elements within the sample to be identified based on the energy of the fluorescence that reaches the instrument's detector. In XRF spectroscopy, photons used to excite the sample are produced by an x-ray tube by creating a potential difference between a heated cathode and an anode. This potential difference is also known as the accelerating voltage and can be as high as 100 kV. The anode usually consists of a heavy element such as tungsten or palladium. As the electrons collide with the anode, the beam is partially converted into x-ray photons. This conversion from the energy to x-ray photons is expressed in the Duane-Hunt Law (Equation 2):

$$\frac{hc}{\lambda_0} = Ve \quad \text{Equation 2.}$$

where  $h$  is Planck's constant,  $c$  is the speed of light,  $\lambda_0$  is the maximum wavelength in angstroms of x-ray photons which can be produced,  $V$  is the accelerating voltage used, and  $e$  is the charge of an electron. The accelerating voltage is inversely proportional to the maximum possible

wavelength; thus, as the accelerating voltage increases, the maximum wavelength produced decreases (1). This necessitates either the use of varying accelerating voltages or the use of filters within the XRF spectrometer to achieve wavelengths of x-ray photons with energy higher than the excitation energy sample electrons.

X-ray photons released from the source irradiate the sample in the sample holder (Figure 2.3). As the x-ray photons penetrate the sample, the photons interact with the atoms in the sample in several ways. As x-ray photons are a form of energy, they are either transmitted, reflected, or absorbed when they interact with the sample. The interactions that occur between the photons and the atoms in the sample are dependent on the energy of the x-ray, the excitation energy of electrons within the element that the x-ray interacts with, and the uniformity of the atomic structure. Transmittance occurs when the x-ray does not contact any of the atoms within the sample and passes through the sample. Diffraction occurs as a product of scattering within the material. For diffraction to occur, the spacing between layers of atoms in the sample must be similar to the wavelength of the photon. Scattering centers within the sample must also be arranged in a consistent pattern (1).

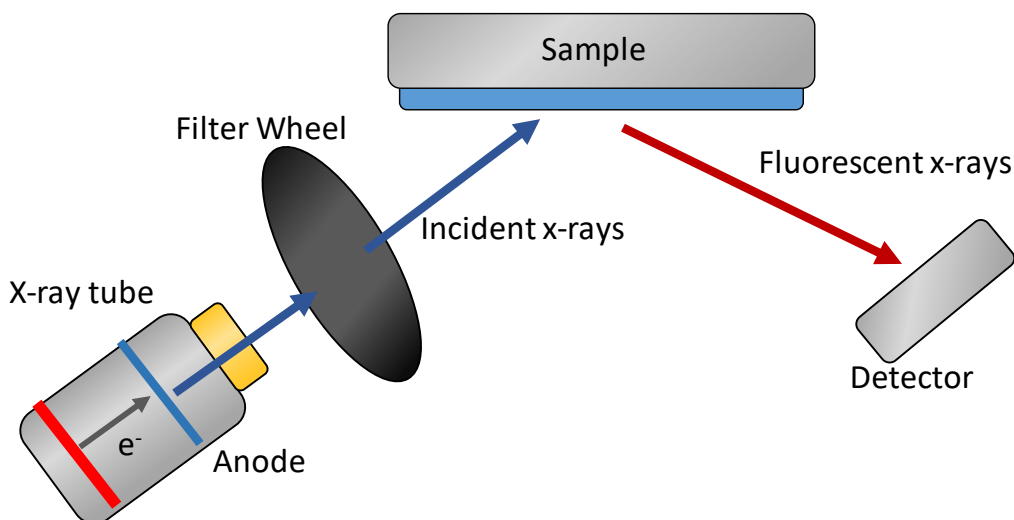


**Figure 2.3:** Diagram of XRF instrument

Absorbance occurs when the energy required for the excitation of an electron is lower than the energy of the x-ray that interacts with the electron. When an electron absorbs energy, it enters an excited state.

When an electron enters an excited singlet state in which it maintains the spin pair between itself and the electron in the pair it originates from, the electron can release energy in the form of x-ray photons to return to its ground state. However, this only occurs when it is kinetically favorable compared to other deactivation processes. This process is called fluorescence. The fluoresced x-ray photons then travel to the detector.

The detector is orthogonal to the x-ray source and sample; this placement of the detector allows for reduced interference so that the detector detects x-rays fluoresced from the sample rather than those emitted from the source (Figure 2.3). Several types of x-ray detectors exist for XRF spectrometers, including gas-filled transducers and silicon photodiode transducers. Gas-filled transducers consist of an inert gas-filled chamber which contains both an anode and a cathode. The x-ray photons collide with electrons in the inert gas. When the energy of the x-ray photons is higher than the binding energy of the electron, ionization of the gas in the tube occurs which causes the electrons to accumulate near the anode and cations to accumulate near the cathode (1). This accumulation causes a change in the conduction of the gas that is then detected as a signal. Silicon photodiode transducers work similarly to a transducer; a cathode and an anode are on either side of a silicon disc. When photons collide with the silicon detector, the electrons within the silicon are excited into a conduction band. The electrons then accumulate at the anode, creating a current which is detected as a signal (1). The primary advantage of silicon photodiode transducers is the reduced dead time compared to

that in photodiode transducers. However, silicon detectors typically have a lower resolution at wavelengths longer than one angstrom (1).

In XRF spectroscopic analysis, the energy of the fluorescence produced is characteristic of the element and is a result of the transition from the electron's excited state to its ground state during relaxation. The transition is named based on the ground state orbital from which the electron originates and electron's transition during relaxation. Typically, the x-rays observed in an XRF spectroscopic analysis originate from the K, L, and M orbitals of an atom with the K orbital being the innermost orbital. The orbital transitions are labeled with Greek letters  $\alpha$ ,  $\beta$ ,  $\gamma$ , etc., with  $\alpha$  representing the transition from one orbital higher than the ground state,  $\beta$  representing the transition from an excited state that is located two orbitals above the ground state, and the other Greek letters representing transitions from higher orbitals (Figure 2.4). Transitions can additionally be labeled with an Arabic numeral subscript, which represents the subshell from which the excited electron originates; however, the XRF used in this study does not have enough resolution to distinguish among these subshells (1, 2).



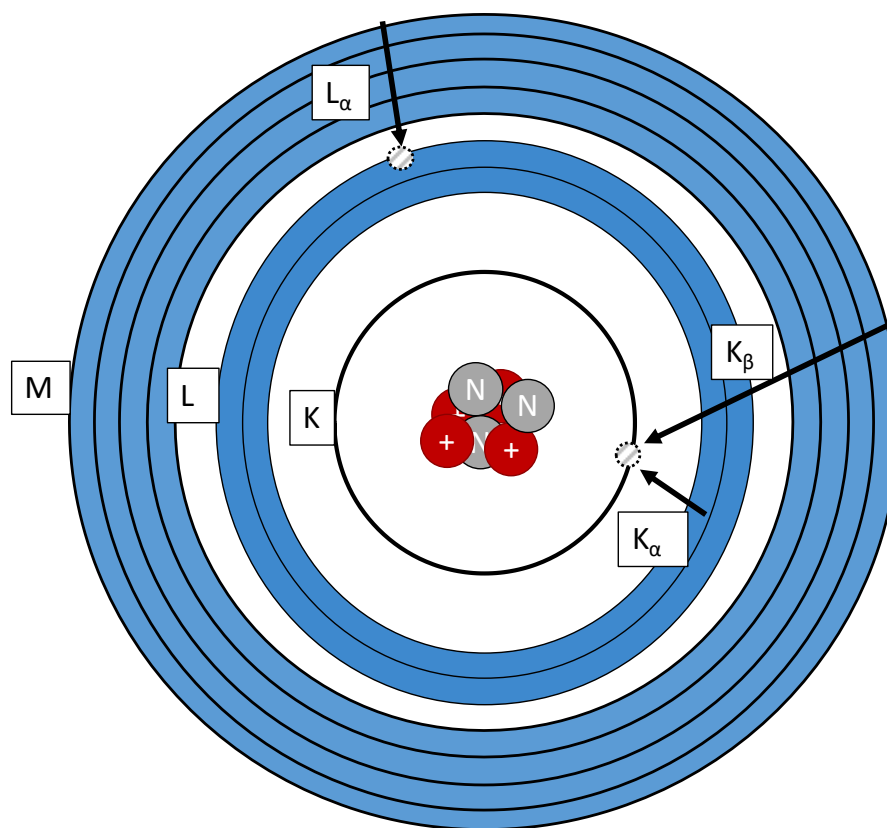


**Figure 2.4:** Diagram exhibiting examples of electron transitions from the excited state to the ground state resulting in x-ray fluorescence.

Despite the robustness and non-destructive nature of an XRF spectroscopic analysis, limitations of the technique exist. One such limitation is that the detection of x-rays fluoresced by the sample is dependent on the composition of the sample. When a sample produces x-rays through fluorescence, not only do atoms near the surface of the sample fluoresce, but atoms within the matrix of the sample fluoresce as well due to the penetration of the x-rays. The depth of penetration of x-rays into the sample matrix and the quantity of x-rays fluoresced by the sample are dependent on the energy of the source x-rays and the mass absorption coefficient of the sample. The mass absorption coefficient of the sample, in turn, is dependent on the absorption coefficients of all elements within the sample. Therefore, quantitative analysis of elements by XRF spectroscopy is challenging, as many factors not related to the

elemental concentration may affect the number of x-rays that reach the detector. Quantitative analysis is typically performed by computer software which accounts for these variables. Nonetheless, for such programs to reliably measure inorganic content within a sample, suitable calibrants that mimic the composition of the sample matrix must be used or pre-existing knowledge of the sample must be input by the user into the program. However, semi-quantitative analysis of samples is possible using Equation 3, where  $I_x$  is the intensity in counts of the element of interest present in the sample,  $I_u$  is the intensity in counts of the element of interest assuming unity, and  $W_x$  is the weight percent of the element of interest in the sample.

$$\frac{I_x}{I_u} = W_x \quad \text{Equation 3.}$$

For Equation 3 to be implemented, the intensity of the pure element must be known for each element within the sample (1). As the composition of tattoo inks is not well characterized and the elements that are incorporated into the ink are not known, it is impractical to identify all of the pure element standards required for analysis to obtain a reliable semi-quantitative analysis of each tattoo ink. Therefore, a qualitative analysis was performed in this study.

### 2.3 Scanning Electron Microscopy -Energy Dispersive Spectroscopy (SEM-EDS)

Scanning electron microscopy-energy dispersive spectroscopy (SEM-EDS) operates in a similar manner as XRF spectroscopy. However, the irradiation of samples occurs with a beam of electrons in SEM-EDS rather than with x-rays. An electron beam is first emitted by the electron gun at the top of the instrument (Figure 2.5). These electrons are produced by a potential difference between a cathode and an anode which is typically a tungsten wire (2). The potential difference is known as the accelerating voltage and is usually between 5 and 30 kV. The electrons are condensed into a beam by a ring-shaped electromagnetic lens known as the

condenser lens. The condenser lens aids in determining the spot size of the beam which can be between 1 and 99 nm. The beam then passes through the objective lens, which further focuses the beam, the scan coils, which are another set of electromagnets that allow the beam to be rastered across the sample, and the final aperture, which acts as a filter to limit the number of electrons that contact the sample. The final aperture allows for control of the brightness and contrast of the image produced (2).

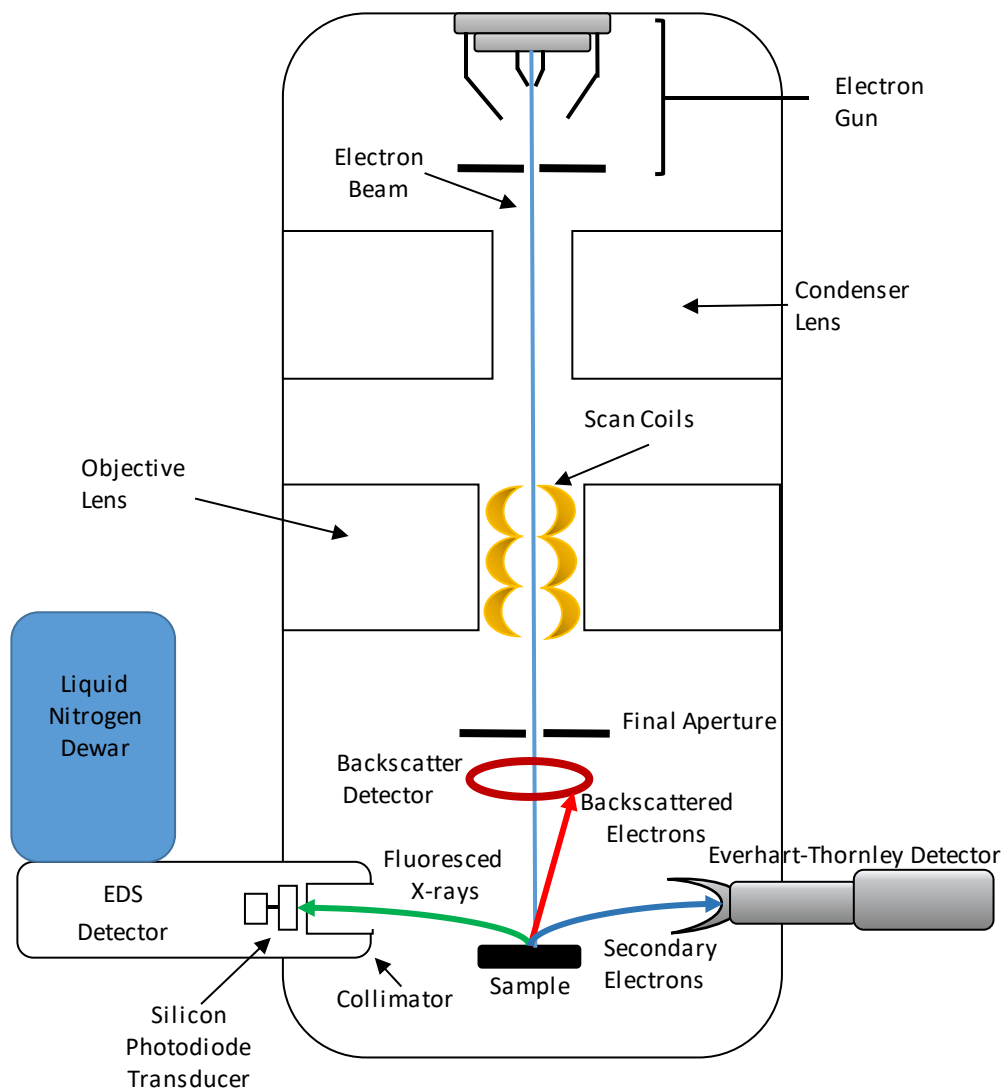


**Figure 2.5:** Diagram of SEM-EDS instrument

For the beam of electrons to reach the sample, the electrons must have as few interactions with atoms that are not a part of the sample as possible. When such interactions occur, noise is produced causing a decrease in resolution of the SEM image. Thus, to reduce the noise and produce an SEM image of high resolution, the entire apparatus must be under vacuum (2). There are two vacuum settings which can be selected: high vacuum and low vacuum. When high vacuum is used, the sample must be dried and then fixed or coated. The purpose of this sample preparation step is to prevent the release of volatile compounds when the sample is exposed to the vacuum, as this is likely to decrease the resolution and damage the filaments of the instrument. In low vacuum mode, the vacuum is not sufficiently high to volatilize some compounds. What will be volatilized can be determined by the component's vapor pressure. This allows for some samples to be directly analyzed with little sample preparation, such as applying the sample to the appropriate stub. However, the resolution of the SEM image is greatly diminished compared to high-vacuum mode. In either vacuum mode, tissue samples that contain lipids and proteins must undergo a fixation process as these compounds can be volatile in either vacuum mode. Typically, tissue samples undergo a glutaraldehyde fixation, which fixes the proteins within the sample, and an osmium tetroxide fixation to fix the lipids (2). A compromise between resolution and sample preparation time is needed to generate SEM images of sufficiently high resolution appropriate for the application.

Once the sample is prepared, the beam of electrons is focused onto and penetrates the sample in an area known as the interaction volume of the beam. The shape and size of the interaction volume are dependent on the density of the material; high-density materials produce a shallower and smaller interaction volume than low-density materials. When the

beam of electrons contacts the sample, electrons can either have inelastic or elastic interactions with the atoms within the sample. These interactions, in turn, produce either secondary electrons from the sample via inelastic interactions with a sample electron or are backscattered via elastic interaction with a nucleus. Typical SEM analysis produces images based on the production and subsequent detection of secondary electrons via an Everhart-Thornley detector; however, as this type of imaging is not used in this study, the principles behind secondary electron production and detection will not be discussed further.

Backscattered electrons are beam electrons that have undergone an elastic collision with the sample and are then reflected back towards the electron beam. Ten to fifty percent of beam electrons undergo this process and are reflected back towards the electron beam. These backscattered electrons maintain up to 80% of their original beam energy. Due to this high energy, backscatter electrons can be produced and escape from deep within the sample interaction volume (2). The maximum escape depth and width inversely depends on the atomic number of the elements within the sample. This allows backscattered images to produce more information in the form of the elemental composition of the sample; yet, the resolution of backscattered images is lower than normal SEM images due to the electrons originating from deeper in the sample and covering a wider area than secondary electrons (2).

As the elemental composition of tattoo inks is a focus of this study, backscattered images of tattoo inks and tissue samples were obtained. Additionally, x-rays produced through fluorescence caused by incident electrons displacing inner-shell electrons can also be detected when an EDS detector is coupled to the SEM; this process and subsequent detection of x-rays

aid in the identification of elements within the sample. The production and detection of these x-rays is the same as previously discussed in section 2.3.

## 2.4 Multivariate Statistical Analysis

Multivariate data is any dataset that consists of multiple variables per sample (3). All previously discussed instruments create this type of dataset in an analysis. Data interpretation of spectra generated with the aforementioned techniques becomes highly complex and difficult with a large sample set, given the sheer number of measurements generated for each variable per sample. For example, IR spectra in this work contained 3551 variables whereas, XRF spectra contained 1570 variables. The use of multivariate statistical analysis is necessary for large datasets to allow simultaneous consideration of all variables in all samples, to identify variables that contribute to sample differences, and to group similar samples. In this study, two complementary unsupervised multivariate statistical techniques are used: principal components analysis (PCA) and hierarchical cluster analysis (HCA).

### 2.4.1 Principal Components Analysis

Principal components analysis attempts to group variables together which are positioned similarly in multidimensional space. This is done to represent the variation among the samples with as few factors as possible. In PCA, the variation within the samples is represented as linear combinations of the variables which describe each sample. These linear representations are known as principal components (PCs). As it is difficult to visualize multidimensional space, a simplified example of PCs is shown in Figure 2.6 using two variables.

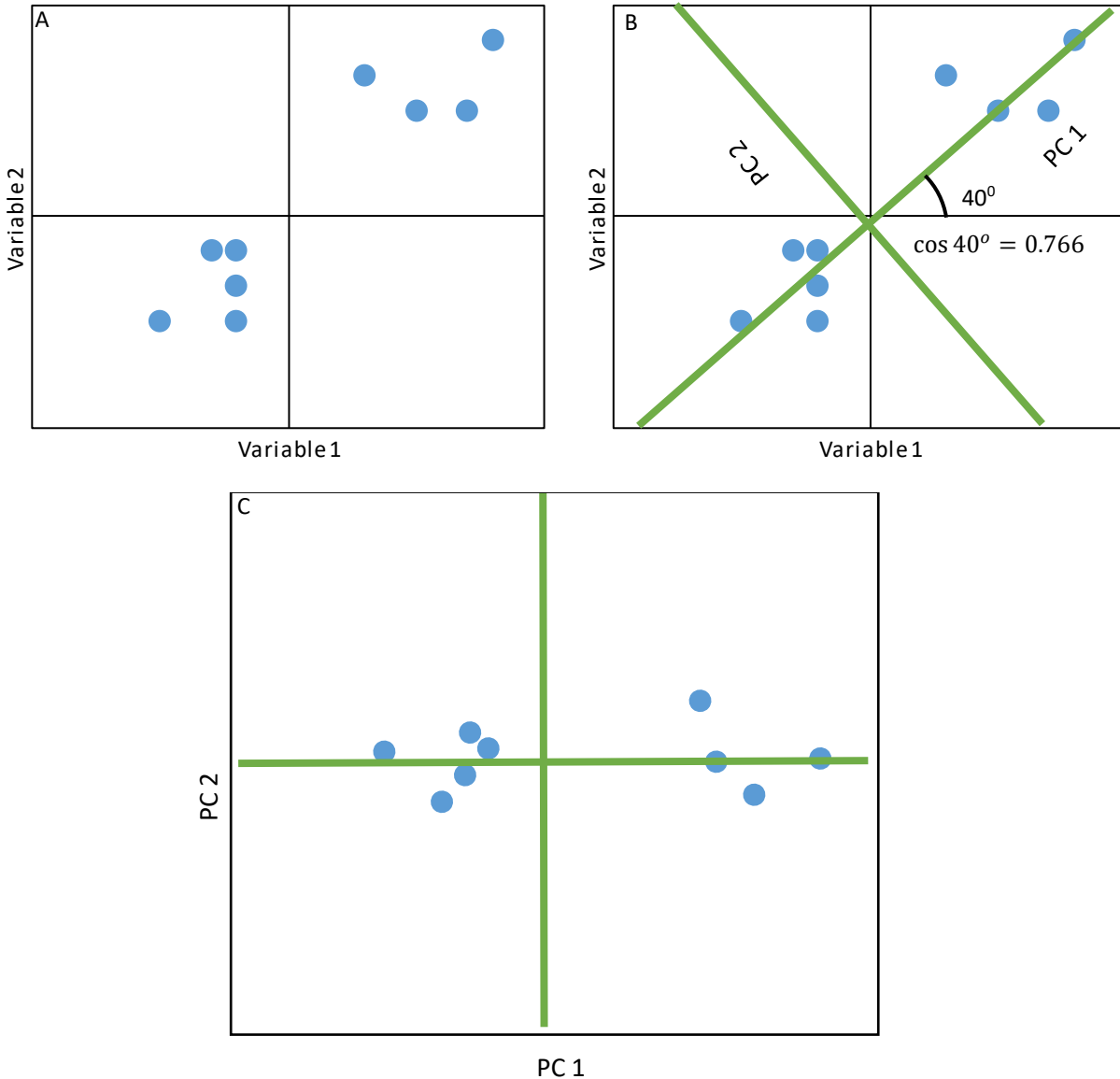


**Figure 2.6:** Diagram of A) a two-variable dataset, B) two principal components applied to the two-variable dataset with the loadings for variable 1 on PC 1 calculated, and C) the scores plot resulting from the PCA.

PC 1 describes the most variation within the dataset (Figure 2.6). PC 2 describes the second most variation within the dataset and lies orthogonal to PC 1. This pattern of variation follows to the higher PCs; thus higher PCs consist of lower signal to noise ratios. This is due to some PCs describing minute differences among samples which are non-sample in origin such as

instrument noise. Higher PCs can potentially describe some of the same variation as lower PCs. These reasons can lead to the exclusion of some higher PCs. This allows for a reduction in the number of variables within the dataset and for fewer variables to represent a large amount of variation. When the original samples of the dataset are plotted against the PCs, this results in a plot known as a scores plot (Figure 2.6C). Principal components analysis allows the analyst to interpret association and discrimination of samples based on their positioning in the scores plot(3, 4). For instance, in Figure 2.6C, two distinct groups are observed.

When PCA is performed, several figures can be plotted which allow the user to interpret the quality of the PCA. One of these figures is the scree plot. Scree plots can be generated by determining what percent of the total variance each PC contributes to the PCA. This is done by dividing the eigenvalue of the PC by the sum of the eigenvalues of all the PCs and multiplying by 100 to express as a percent. The percent of the total variance is then plotted against the PC number to form the scree plot (Figure 2.7). This plot allows the analyst to eliminate PC's from the analysis as the variance they describe is not large enough to account for variance in samples and likely can be attributed to variations in instrument noise and other factors which don't attribute to the variation within the samples. In Figure 2.7, such PCs would include PCs 5-9.



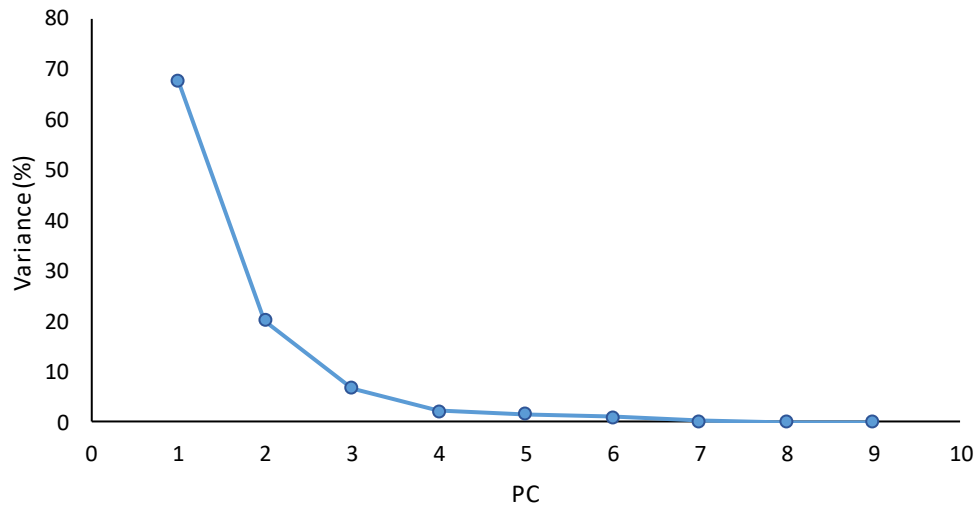


**Figure 2.7:** Example scree plot showing how the percent variance changes from PC to PC.

Another one of these figures is the loadings plot, which describes the contribution of each of the variables to each PC. This contribution is determined by the cosine of the angle between the variable axis and the PC referred to as the loadings (Figure 2.6B). When the angle between the variable axis and the PC is 0, i.e. the axes are the same direction, the cosine is 1. When the variable axis and the PC are orthogonal to each other, the cosine is 0 meaning they have no variables in common. When the axis has the opposite directionality, the cosine is -1 (3). The loadings plot allows for the visualization of the contribution of each variable to each PC and allows the analyst to relate the position of the samples in the scores plot back to the original data. Loadings plots can also be used to determine if a small set of components are dominating a PC. This is observed when a set of variables has a large absolute value on a PC in the loadings plot while the other variables plot near zero on the PC. The large contribution of a portion of the variables in a dataset is usually due to variables having different magnitudes, thus the variables that have higher magnitude are the variables that have a greater contribution. To

correct for this, scaling can be applied. Several types of scaling exist and the use depends on the type of data being analyzed. Examples of scaling are Pareto scaling and autoscaling (5).

$$\tilde{x}_{vs} = \frac{x_{vs} - \bar{x}_s}{s_s} \quad \text{Equation 4.}$$

Variables are autoscaled (Equation 4) by subtracting the average of the variable across all samples ( $\bar{x}_s$ ) and dividing by the standard deviation of the variable across the samples ( $s_s$ ). This must be done for all variables across all samples of the dataset ( $x_{vs}$ ) (3). For example, in an IR spectroscopic dataset,  $\bar{x}_s$  is the average intensity of one wavenumber across all samples and  $s_s$  is the associated standard deviation. This is performed for all variables across all samples, thus generating a scaling vector and a deviation vector for the dataset. The difference between an individual measurement and the scaling vector is then obtained and normalized to the deviation vector. The advantage of autoscaling is the normalization of the variables to a standard deviation of 1 and a mean of zero; all variables equally contribute to the PCA. However, one disadvantage of autoscaling is that it causes inflation of low-intensity data that is near the limit of detection. Autoscaling also does not retain the original data structure as the standard deviation is set to 1. Other scaling methods, such as Pareto scaling, which normalizes to the square root of the standard deviation, better retain the general data structure; however, differences in the intensity of two datasets still cause variation within the PCA (5). Therefore, autoscaling is more advantageous when comparing two datasets on vastly different intensity scales as in this study.

Additionally, non-sample dependent variation can occur which affects the PCA. One example of this is the amount of sample applied to the ATR-FTIR crystal. Absorbance is directly proportional to the amount of sample being analyzed (Equation 1). In ATR-FTIR spectroscopic

analysis, it is difficult to control the amount of solid sample applied to the crystal. This causes variation in the sample spectrum that is not due to the components within the sample. To correct for this, standard normal variate (SNV) normalization can be used (Equation 5)(6).

$$\tilde{x}_{vs} = \frac{x_{vs} - \bar{x}_v}{s_v} \quad \text{Equation 5.}$$

In SNV normalization,  $\tilde{x}_{vs}$  is the normalized measurement,  $x_{vs}$  is the unnormalized measurement,  $\bar{x}_v$  is the average measurement of all variables of a sample, and  $s_v$  is the standard deviation of the measurements of a sample across all variables. This centers the slope of the baseline of the IR data to the mean baseline slope of the IR data (6). With these corrections, PCA can visually represent the data accurately. However, PCA consists of a purely visual interpretation of the scores and loading plots by the analyst. To obtain more quantitative information of the dataset, hierarchical cluster analysis can be applied.

#### 2.4.2 Hierarchical Cluster Analysis

Hierarchical cluster analysis is a data processing technique in which samples form clusters based on similarity in multidimensional space. In agglomerative HCA, which is used in this study, each sample is treated as a cluster and clusters which are closest together in multidimensional space are joined to form one cluster. This is repeated until only one cluster describing the entire dataset remains. The results are then visualized in a plot known as a dendrogram which displays the hierarchy of cluster formation (6).

The process of HCA can be observed in Figure 2.8, which displays five samples represented by two variables in two-dimensional space. To start, each sample is considered a member of an individual cluster. First, the distances between clusters are calculated. There are

numerous distance metrics that can be applied; the metric used in this study is Euclidean distance (Equation 6):

$$d = \sqrt{\sum_{i=1}^n (M_i - N_i)^2} \quad \text{Equation 6.}$$

where  $d$  is Euclidean distance in  $n^{\text{th}}$  space,  $M$  is one sample or cluster,  $N$  is the sample or cluster  $M$  is being compared to, and  $i$  represents the variable in  $n^{\text{th}}$  space used in the calculation (7).

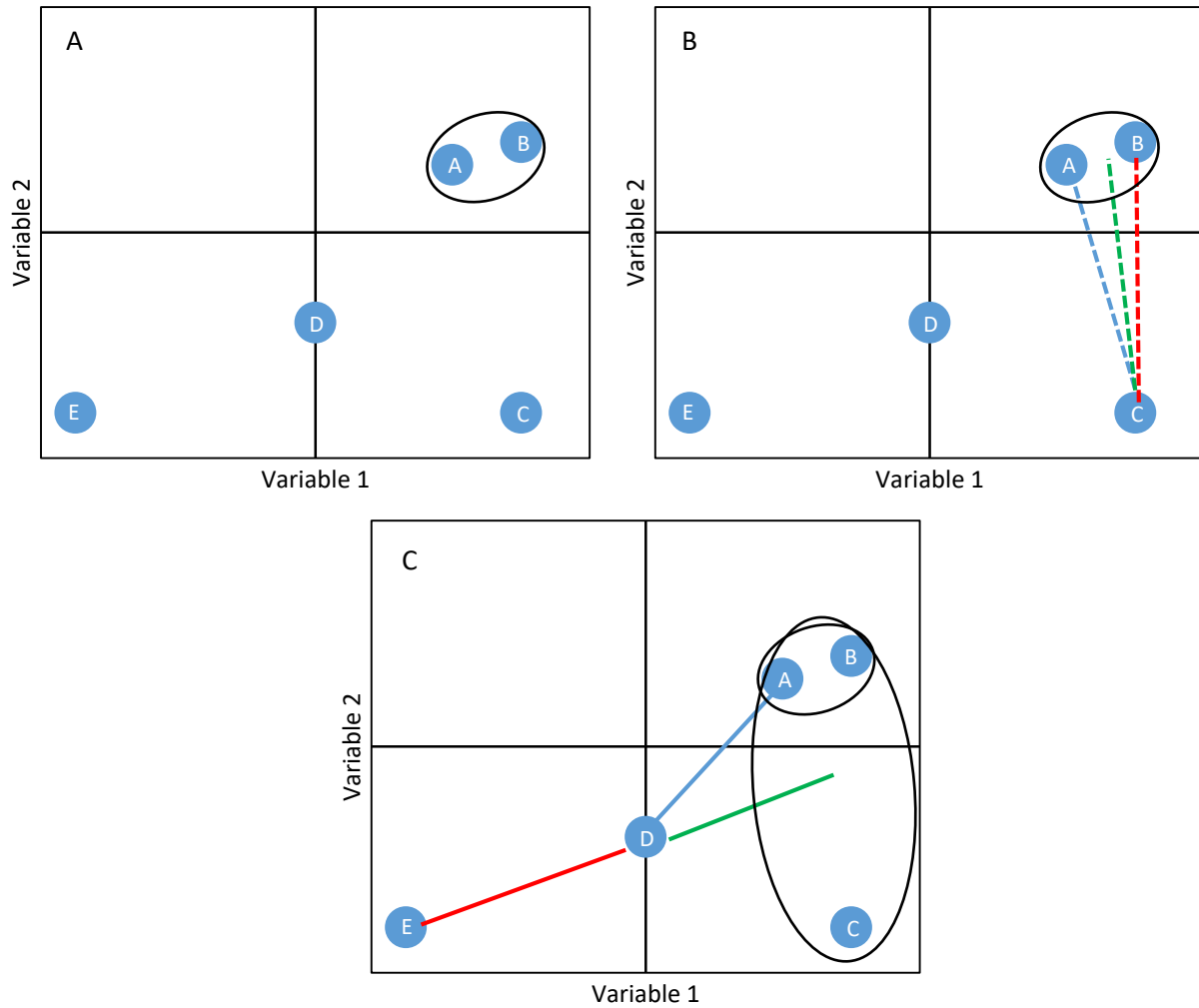


**Figure 2.8:** Demonstration of the differences of complete (red lines), single (blue lines), and group average (green lines) linkage methods. A) The initial clustering of the samples with the shortest Euclidean distance which is not dependent on the linkage method B) the second cluster which forms in which all linkage methods produce the same result C) the third cluster to form in which the type of linkage method used causes a difference in clustering

After this, the samples that have the shortest Euclidean distance between them cluster together, forming a new cluster that now contains two samples (Figure 2.8A). Once more than one sample is in a cluster, it is necessary to define the linkage method used to determine clusters for subsequent grouping. In each linkage method, the clusters with the shortest Euclidean distance from one another cluster first. However, the linkage method determines which samples or positions in clusters the distance is measured from.

One such linkage method is complete linkage; samples with the maximum distance between clusters are measured (Figure 2.8B and C). In complete linkage, the shortest maximum distance exists first between samples C and B causing the cluster of A and B to cluster to sample C first. This is followed by the distance between samples D and E as the distance between D and B, the sample with the maximum distance from D in the A-B-C cluster, is a larger distance. This is a conservative linkage method and more often groups outliers in the correct cluster; however, these outliers can then affect subsequent clustering due to their proximity to unrelated clusters. This can cause the cluster they are positioned in to incorrectly cluster.

Another linkage method is single linkage; samples with the minimum distance between clusters are measured (Figure 2.8B and C). In single linkage, the shortest minimum distance exists first between samples C and B causing the cluster of A and B to cluster to sample C first. This is followed by the distance between samples D and A, the sample with the minimum distance from D in the A-B-C cluster, as the distance between D and E is a larger distance. This causes the opposite problem of the complete linkage method in which outliers may not cluster to the correct groups.

A compromise between these two methods is the group average linkage; the average among all members of a cluster is measured (Figure 2.8B and C). (4, 8). In group average linkage, the shortest minimum distance exists first between cluster A-B and sample C causing the cluster of A and B to cluster to sample C first. This is followed by the distance between sample D and the average position of all members of cluster A-B-C as the distance between D and E is a larger distance.

This shows the importance of the linkage method chosen. However, this leads to one of the disadvantages of HCA. Typically, the method for determining which linkage method to use is trial and error and is determined by which the analyst believes best suits the data. After the linkage method is chosen, similarity levels of each cluster are then calculated using Equation 7:

$$S = 1 - \frac{D_i}{D_M} \quad \text{Equation 7.}$$

where S is the similarity level,  $D_i$  is the distance between two clusters, and  $D_M$  is the maximum distance among all clusters in the dataset. The similarity levels are then visualized in a dendrogram (Figure 2.9). The dendrogram in Figure 2.9 displays the complete linkage method for the data shown in Figure 2.8.

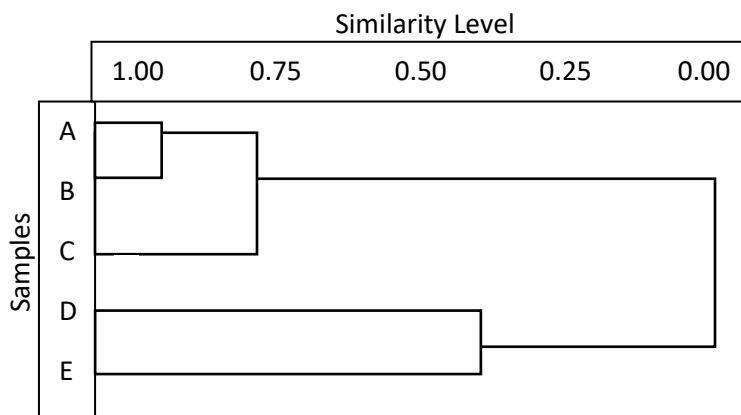


**Figure 2.9:** Dendrogram representing data from Figure 2.8 with the complete linkage method.

PCA provides chemical information on the samples within a dataset and how those variables affect the similarity between samples while HCA provides a numerical value to assess the similarity of samples. Overall, PCA and HCA are complementary procedures that allow for a fuller understanding of multivariate data.

## REFERENCES



## REFERENCES

1. Skoog D, Holler FJ, Crouch S. Principles of Instrumental Analysis. 6th ed. Belmont, CA: David Harris, Thomson Higher Education, 2007.
2. Flegler S, Heckman J, Klomparens K. Scanning and Transmission Electron Microscopy, An Introduction. New York: Oxford University Press, 1993.
3. Beebe K, Pell R, Seacholtz MB. Chemometrics: A Practical Guide New York: John Wiley and Sons, Inc., 1998.
4. Varmuza K, Filzmoser P. Introduction to Multivariate Statistical Analysis in Chemometrics. Boca Raton, FL: CRC Press, 2009.
5. van den Berg R, Hoefsloot H, Westerhuis J, Smilde A, van der Werf M. Centering, scaling, and transformations: improving the biological information content of metabolomics data BMC Genomics. 2006; 7.
6. Barnes RJ, Dhanoa MS, Lister SJ. Standard Normal Variate Transformation and De-trending of Near-Infrared Diffuse Reflectance Spectra Applied Spectroscopy. 1989;43(5).
7. Deza M, Deza E. Metrics of Normed Structures. Encyclopedia of Distances. Second ed. Heidelberg, Germany: Springer; 2013;89-99.
8. Manning C, Raghavan P, Schutze H. Introduction to Information Retrieval. Online: Cambridge University Press, 2008.

## Chapter 3 Materials and Method

### 3.1 Tattoo Ink Sample Preparation

A total of 30 tattoo inks were purchased for this study: 25 from Eternal Ink (Brighton, MI) and five from StarBrite (Tommy's Tattoo Supplies, Sommers, CT) (Table 3.1). Pure tattoo ink samples were prepared for analysis by infrared (IR) spectroscopy, x-ray fluorescence (XRF) spectroscopy, and scanning electron microscopy-energy dispersive spectroscopy (SEM-EDS). For each pure ink sample, five drops of tattoo ink were applied to a 2 cm x 2 cm piece of filter paper (Whatman, Lot# 1001 110, Cardiff, UK). Of the five drops of ink, four were applied directly from the original bottle to each of the four corners of the filter paper, and the last drop was applied to the middle of the filter paper. These drops were then spread over the matrix until the surface of the filter paper was covered with tattoo ink. This filter paper was then dried in a desiccator for 24 hours prior to analysis to eliminate the interference from water in the IR spectroscopic analysis. Additionally, seven tattoo inks comprising a range of colors were selected for sample preparation method validation; the inks were prepared on filter paper 10 times and subsequently analyzed via IR and XRD spectroscopy to evaluate the consistency of the preparation method (Table 3.1).

**Table 3.1:** Table of ink names, colors, manufacturers, lot numbers, and sample set designation.

<b>Ink</b>	<b>Manufacturer</b>	<b>Lot #</b>	<b>Set</b>
Blank Filter	Whatman	1001 110	Training/Validation
Triple Black	Eternal Ink	125	Training
Lining Black	Eternal Ink	125	Training/Validation
Black Outliner	StarBrite	S0312308	Test
Lipstick Red	Eternal Ink	125	Training/Test
Crimson Red	Eternal Ink	125	Training
Dark Red	Eternal Ink	125	Training/ Validation
Deep Red	Eternal Ink	125	Test
Light Red	Eternal Ink	125	Test
Scarlet Red	StarBrite	SR*	Test
Caramel	Eternal Ink	125	Training/Validation
Orange	Eternal Ink	125	Training
Bright Orange	Eternal Ink	125	Test
Lightning Yellow	Eternal Ink	125	Training
Golden Yellow	Eternal Ink	125	Training/Test
Bright Yellow	Eternal Ink	125	Training
Canary Yellow	StarBrite	CY363291	Training/Validation
Graffiti Green	Eternal Ink	125	Training
Lime Green	Eternal Ink	125	Training/Validation
Mint Green	Eternal Ink	125	Test
Nuclear Gree	Eternal Ink	125	Test
True Blue	Eternal Ink	125	Training
Sky Blue	Eternal Ink	125	Training
Deep Turquoise	StarBrite	DT*	Test
Light Magenta	Eternal Ink	125	Training
Dark Purple	Eternal Ink	125	Training/Validation
Hot Pink	Eternal Ink	125	Training
Pink	Eternal Ink	125	Training
Light Purple	Eternal Ink	125	Test
White	Eternal Ink	125	Training/Validation
Brite White	StarBrite	BW249270	Test

\*Label was damaged upon delivery

### 3.2 Tattoo Ink Sample Analysis

The tattoo inks were separated into two groups, a training set to develop the PCA model and a test set used to validate the model (Table 3.1). These sets were chosen by randomly drawing the tattoo ink samples out of the desiccator for analysis by IR and XRF spectroscopy.

#### 3.2.1 ATR-FTIR Spectroscopy Analysis

Samples were analyzed using a Perkin Elmer Spectra 2 Fourier transform IR spectrometer with an attenuated total reflectance (ATR) accessory (Perkin Elmer, Waltham, MA). The crystal was a Diamond Zn/Se one bounce crystal. Four scans between 4000 and 450  $\text{cm}^{-1}$  in transmittance mode were averaged to obtain a spectrum. The pressure arm was set to 70 units of pressure for each scan. Ethanol was used to clean the crystal after each sample was analyzed. Before each data collection, a set of system suitability checks were performed to ensure the proper functionality of the ATR-FTIR spectrometer, including contamination checks and noise assessments. Background scans were performed at the beginning of the analysis and after every sixth analysis. For samples with low IR absorption and whose spectra were more affected by the background, background scans were performed more frequently. Tattoo ink samples not selected for the sample preparation validation study were analyzed in triplicate to determine differences in absorption intensity and wavenumber due to instrument variation. To test for cross-contamination, blank filter paper samples were analyzed between each sample on the ATR-FTIR.

After data acquisition, raw spectra were first converted to absorbance mode through the instrument software (Spectrum v.10.4.4, Perkin Elmer, Waltham, MA). Baseline correction was performed through the Spectrum software; a baseline region was defined by the first

derivative plot, and a quadratic equation was then fit to the baseline region and subsequently subtracted from all regions of the spectrum. The baseline-corrected spectra were then smoothed using a Savitsky-Golay algorithm over 5 points.

### 3.2.2 XRF Spectroscopy Analysis

The tattoo ink samples analyzed via ATR-FTIR spectroscopy were also analyzed by a Bruker S2 XRF spectrometer (Bruker, Billerica, MA). Before each XRF spectroscopic analysis, the spectrometer was automatically calibrated with a Cu disc using the instrument software. The calibration was then assessed with a silicon disc using the quality check function of the instrument. This assessment compared the percent composition of the glass disc to the known percent composition programmed into the instrument. The glass disc consisted of silicon (Si), calcium (Ca), manganese (Mn), molybdenum (Mo), antimony (Sb), and arsenic (As). If the concentration varied more than 3.20% for Si, 0.49% for Ca, 0.12% for Mn, 0.01% for Mo, 0.18% for Sb, or 0.006% for As, a warning would be shown and another calibration with the glass disc was performed. This was followed by the Cu disc and an assessment with the glass disc.

Once the assessment was completed and accepted, the samples were analyzed in a similar order as in the IR spectroscopy analysis: the blank filter paper sample was analyzed following each sample set consisting of one tattoo ink color and all its replicates to prevent cross-contamination between different tattoo ink samples. Each sample was analyzed using the Equa\_Oxides method from the instrument, which designated four scan parameters with different accelerating voltages (Table 3.2). Each scan had a range of 0.6-32.0 keV. Raw data from each scan were obtained from the XRF spectrometer; however, only scan 4 was selected

for later analysis as all elements identified in the other scan ranges and the most intense spectral peaks were observed in scan 4.

**Table 3.2:** XRF spectroscopy scan parameters.

Parameter	Scan 1	Scan 2	Scan 3	Scan 4
Dead Time (%)	16.024	32.587	30.197	30.572
Filter	Cu, 250 $\mu$ m	Al, 500 $\mu$ m	None	None
keV	50	40	10	20
Pressure (Pa)	2.722032	2.495196	2.948868	2.722032

### 3.2.3 Data Analysis

Prior to multivariate statistical analysis, both the IR and XRF spectroscopic data were standard normal variate (SNV) normalized, truncated, and autoscaled using Microsoft Excel 2016 (Microsoft, Redmond, WA). The data were then analyzed using principal components analysis (PCA) in MatLab R2016a (Mathworks, Natick, MA) and hierarchical cluster analysis (HCA) using Pirouette v.4.0 (Infometrix, Bothell, WA). All output data were exported to Microsoft Excel for further processing.

### 3.2.4 SEM-EDS Analysis

As SEM-EDS provides elemental composition information similar to that obtained via XRF spectroscopy, only red, blue, and black ink samples were analyzed by SEM-EDS (Jeol 6610LV SEM/ JED-2300 EDS, Jeol, Tokyo, Japan). The output data were then compared to those obtained by XRF spectroscopy. The same tattoo ink samples prepared for IR and XRF spectroscopic analyses were modified for SEM-EDS analysis. Each tattoo ink sample prepared on filter paper was cut to a smaller size to fit on a 9 mm diameter stub. The tattoo ink samples and blank filter paper samples were fixed to the stub using a 9 mm diameter carbon conductive tab so that the inked surface was visible. The samples were analyzed with SEM-EDS in low

vacuum mode, with a vacuum of 60 Pa. Scanning electron microscope images were gathered in backscatter mode with a working distance of between 10 and 12 mm, a spot size between 57 and 59 nm, and a magnification of 500X. These same parameters were used in the EDS analysis. EDS was operated through the AZtec Software (version 3.1, Oxford Instruments, Abingdon, UK) in Acquisition mode with a process time was set to 6 (This corresponds to the Jeol 6610LV SEM/JED-2300 EDS, Jeol, Tokyo, Japan instrument) and a dead time of 30%. The resulting raw spectra and calculated percent compositions were used to determine the elemental compositions of tattoo inks.

### 3.3 Tissue Sample Preparation

In August of 2016, an 180 lbs. pig was tattooed with Deep Red (Eternal Ink) and Triple Black (Eternal Ink) tattoo ink. The tattoos were 2 cm x 2 cm squares arranged in five rows of three. Additional squares were marked but not tattooed; five rows adjacent to the inked squares were designated for SEM-EDS sample preparation method development (“test” rows), and five rows adjacent to the “test” rows were designated as blanks (Figure 3.1). Five sampling dates were chosen between Aug. 14<sup>th</sup> and Aug. 31<sup>st</sup> based on the appearance of decomposition and the visibility of the tattoo inks. The tissue samples were removed using scalpels and stored at -20 °C until sample preparation for SEM-EDS analysis was performed.

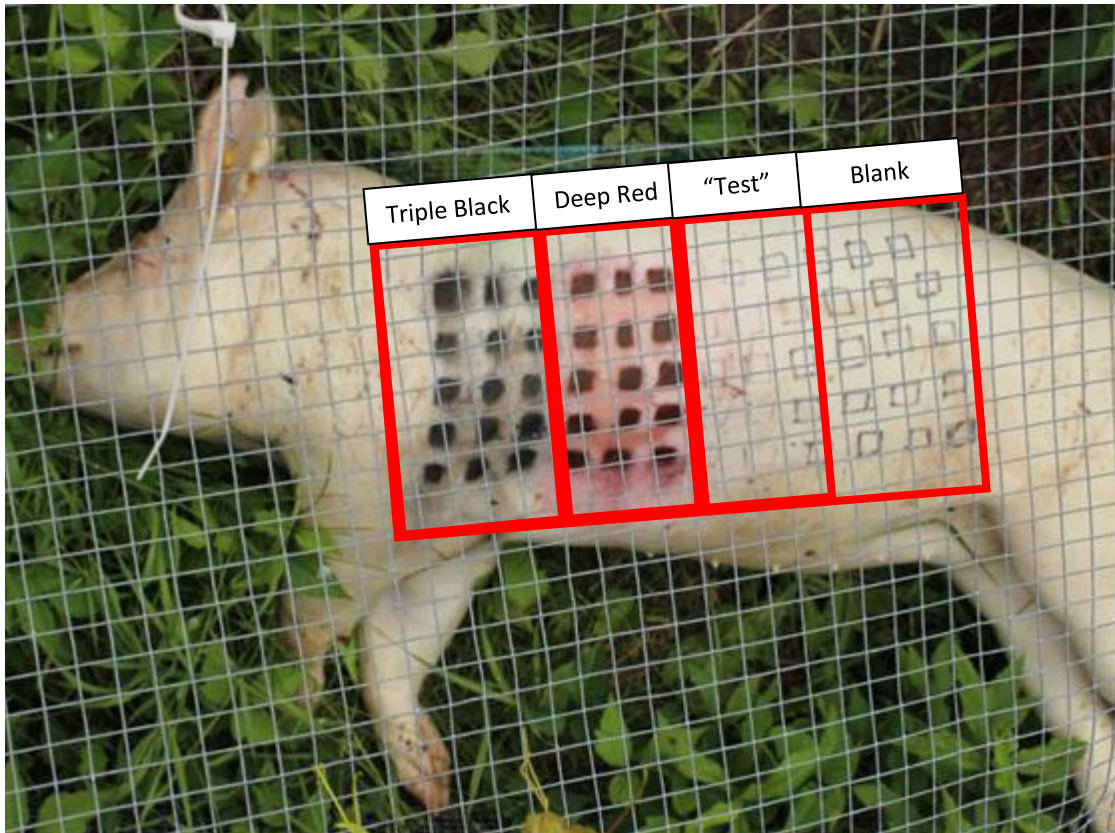


**Figure 3.1:** Positioning of tattoos and blanks on porcine sample

Once the tissue preparation method for SEM-EDS analysis was developed, one sample from each row of the Deep Red tattoo, Triple Black tattoo, and the blank tissue areas were selected. Samples were cut in half length-wise and a section of less than 1 mm in width was extracted. The extracted tissue was dried by immersing the tissue in a series of ethanol (Koptec Opta 200 proof, Lot #109615, VWR, Radnor, PA) diluted with water; 25%, 50%, 75%, and 95% v/v for one hour in each dilution. The tissue was then rinsed three times with 100% ethanol for 30 minutes each. The samples were fixed in 4% glutaraldehyde buffered with 0.1 M sodium phosphate at a pH of 7.4 for 2 hours then rinsed with the 0.1 M phosphate buffer. Following this, the tissue was fixed with 2% osmium tetroxide solution (EM grade, SPI-Chem, SPI Supplies,



West Chester, PA, Spl# 2595) for 2 hours and rinsed with 0.1 M phosphate buffer. The samples were then dried in a Leica Microsystems EM CPD300 critical point dryer (Buffalo Grove, IL) using liquid carbon dioxide as the transitional fluid. The prepared samples were then cross-sectioned height-wise to expose the layer of the skin which contained the tattoo ink and mounted onto a 9 mm stub with a carbon conductive tab.

### 3.4 SEM-EDS Analysis of Tissue Samples

The tissue samples were analyzed using the same parameters as those used in the SEM-EDS analysis of the tattoo ink samples; the only parameter difference is the 1500X magnification used for tissue samples. Each sample was analyzed in the Map mode of the Aztec software with a process time set to 6 (This corresponds to the Jeol 6610LV SEM/ JED-2300 EDS, Jeol, Tokyo, Japan instrument), a pixel dwell time of 100  $\mu$ s, and 2048 channels. The map image was overlaid on a backscatter image collected with the Aztec software. The backscatter image was obtained with an image scan size of 2048 pixels and a dwell time of 8  $\mu$ s. Maps were analyzed at three locations on each tissue sample; locations were chosen on the tattooed samples based on ink visibility, whereas on the blank samples, map locations were selected based on visual similarity to the tissue surrounding the ink observed in the tattoo samples. The maps were then directly assessed for tattoo ink component contents.

## Chapter 4 Statistical Differentiation of Tattoo Inks Based on Organic and Inorganic Content

To determine the chemical composition of a tattoo ink, both the organic and inorganic composition must be known as the pigments can be either organic or inorganic in nature. Both x-ray fluorescence (XRF) spectroscopy, which is used to detect inorganic components of a sample, and infrared (IR) spectroscopy, which is used to detect organic bonds between atoms, were used in this study to characterize a range of popular tattoo inks. The spectra were analyzed through two multivariate statistical analysis procedures, principal components analysis (PCA) and hierarchical cluster analysis (HCA) in order to determine the similarities and differences between the compositions of the tattoo inks. The results of the XRF and IR spectroscopic analyses, along with the multivariate statistical analysis, are discussed below.

### 4.1 X-ray Fluorescence Spectroscopy Analysis of Tattoo Inks

Figure 4.1 shows an overlay of representative XRF spectra of True Blue and Sky Blue inks. All the spectra have a peak near 2.838 keV, corresponding to the  $L\alpha$  spectral line for palladium (Pd), which is present in the detector of the spectrometer. The variability in intensity of the Pd peak among different inks is likely due to several factors such as secondary fluorescence or absorption of x-rays by other elements within the sample. Background subtraction of the Pd peak was not possible as this requires knowledge of the percent composition of the organic elements within the samples.

The XRF spectrum of the True Blue ink (Figure 4.1) displays peaks at 8.049 keV and 8.949 keV corresponding to the  $K\alpha$  and  $K\beta$  spectral lines, respectively, for copper (Cu). Copper phthalocyanine (Table 1.1), is a pigment known to be present in blue inks (1, 2); and hence, Cu contributions were expected. The spectrum of True Blue also has peaks at 4.509 keV and 4.929

keV (Figure 4.1) corresponding to  $K_{\alpha}$  and  $K_{\beta}$  the spectral lines for titanium (Ti), respectively. The intensity of these spectral lines is an order of magnitude larger than the spectral lines corresponding to Cu. These spectral lines are consistent with titanium dioxide, a white pigment (Table 1.1) that is used as a whitening agent (2, 3).

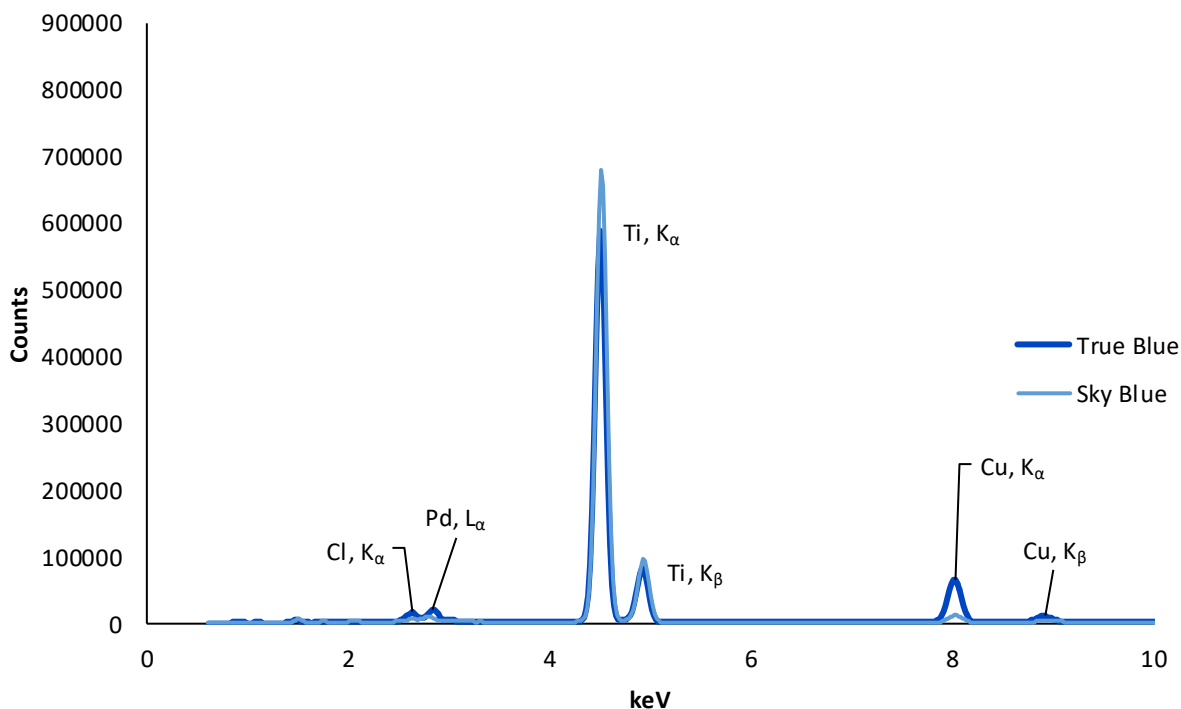


**Figure 4.1:** Representative XRF spectra of True Blue and Sky Blue inks. The specific transition and element are labeled for each major peak in each spectrum.

Previous studies by Miranda and the Dutch Environmental Protection Agency reported that titanium dioxide is not unique to blue inks; rather, this pigment is found in almost every ink color to change the shade of the ink or to increase opacity (1, 3, 4). This can be observed when comparing the XRF spectrum of True Blue ink with the spectrum of Sky Blue ink (Figure 4.1), a lighter shade of blue. Both inks have peaks corresponding to Ti and Cu, but the ratio of the

intensity of the Ti to Cu peaks in the Sky Blue ink is 58:1 compared to 9:1 in the True Blue ink.

The higher Ti content in Sky Blue leads to a lighter shade of blue than True Blue.

The main component of modern day black inks is carbon black, an organic pigment, which is not expected to contain any other elements. Carbon black, however, is often produced by burning materials, which can cause sulfur-containing compounds to be incorporated into the ink (1). This content can be observed in the XRF spectrum of Lining Black (Figure 4.2) which has peaks near 2.309 keV corresponding to  $K_{\alpha}$  for sulfur (S). The spectrum also has a peak at 6.409 keV corresponding to the  $K_{\alpha}$  spectral line for iron (Fe). This spectral line is also observed in the spectrum of Lipstick Red at the same order of magnitude as in Lining Black (Figure 4.2). However, the spectrum for the Dark Red ink (Figure 4.2) contained peaks corresponding to Fe that were four times more intense than the iron peaks observed in the spectra of Lipstick Red and Lining Black, suggesting a purposeful inclusion of Fe in these inks.

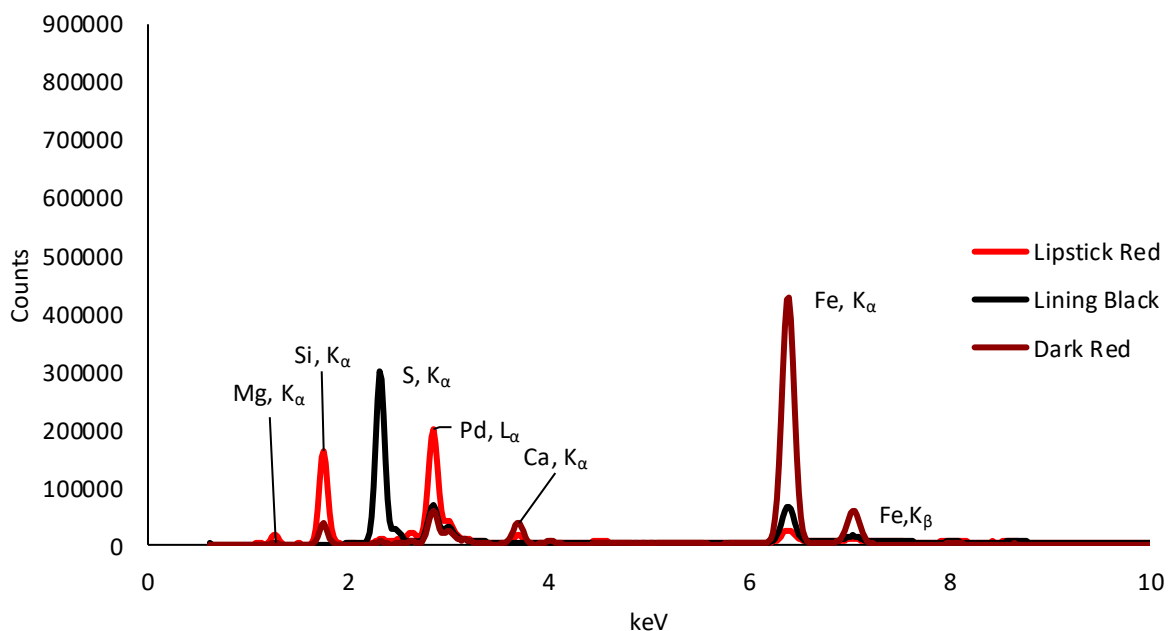


**Figure 4.2:** Representative XRF spectra of Lipstick Red, Lining Black, and Dark Red inks. The specific transition and element are labeled for each major peak in each spectrum.

This difference in magnitude suggests either that the Fe is included in Dark Red to make the ink a darker shade of red compared to Lipstick Red or the Fe in Lipstick Red and Lining Black comes from an unknown source such as possible contamination during the manufacturing process. As black ink pigments consist of carbon black and some red inks are known to be organic-based (1), the low intensity peaks corresponding to Fe in Lining Black and Lipstick Red suggest both inks are organic-based.

Lipstick red also has peaks at 1.749 keV corresponding to the  $K_{\alpha}$  spectral line for silicon (Si). This result was unexpected because previous studies analyzing the inorganic components of tattoo ink did not indicate silicon as a red pigment component (2, 3). However, a study by the Danish Environmental Protection Agency (3) showed that aluminum silicate compounds were incorporated into some inks as a thixotropic agent to control the viscosity of the ink for injection. This use is a possible explanation for the Si in the red inks; however, a pigment origin cannot be ruled out as the red inks found in this study have not been previously analyzed.

$K_{\alpha}$  spectral lines for calcium (Ca) and magnesium (Mg) were also observed in the spectra of red inks (Figure 4.2). The study done by the Danish Environmental Protection Agency had also shown one instance of calcium contributing to red pigment color in the form of pigment Red 63.1 (Table 1.1). However, this pigment is described as being a dark purple-red and is unlikely to be incorporated into lighter shades of red like Lipstick Red (3). Sulfur is also found in pigment 63.1 which is not observed in the spectra of any of the red inks which suggests this is not the pigment used in the red inks. Other sources such as calcium carbonate contamination in water, which can be used as the solvent in tattoo ink, do exist. This suggests that the calcium may not have been purposefully included in the manufacturing process of the ink. However, magnesium

has previously been detected in red inks by Forte *et al.* via inductively coupled plasma mass spectrometry (ICP-MS) (2). The previous literature, along with the Mg and Fe peaks being on the same order of magnitude makes it unclear whether or not Mg is present in the Lipstick Red ink as a pigment component. A possible source of this could be magnesium aluminum silicates, which are also used as thixotropic agents in inks, like the aluminum silicates mentioned earlier (3). This is one explanation for why both Si and Mg are found in the same inks.

Spectra for Lime Green, Caramel, Lightning Yellow and Canary Yellow are shown in Figure 4.3. These spectra contain a peak at 2.629 keV, the  $K_{\alpha}$  spectral line for chlorine (Cl). As halogens like Cl are electron-withdrawing groups, they are often used in pigments to change the color of the pigment. Green inks contain the pigment chlorinated copper phthalocyanine (Table 1.1) which has the same organic structure as copper phthalocyanine (Table 1.1) in blue inks, except with chlorinated functional groups, allowing the differentiation between blue and green inks. Canary Yellow's Cl  $K_{\alpha}$  spectral line is 1/25<sup>th</sup> the intensity of Lightning Yellow (Figure 4.3B). The presence of Cl in Lightning Yellow in a higher concentration would suggest that a different pigment is being used in each ink like such as in the blue and green inks. The presence of Cl in Caramel implies a similar pigment to that of the yellows and greens with the Fe changing the color of the ink to a brown.

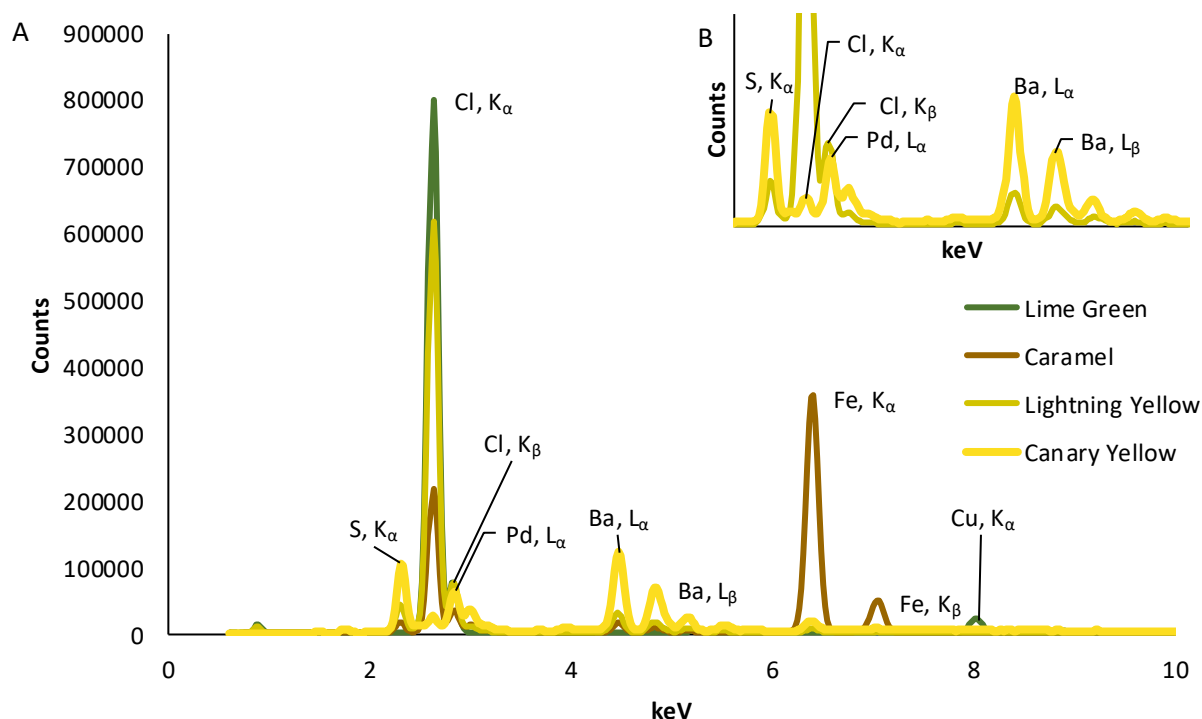


**Figure 4.3:** (A) Representative XRF spectra of Lime Green, Caramel, Lightning Yellow, and Canary Yellow inks. The specific transition and element are labeled for each major peak in each spectrum. The inlaid graph (B) shows a magnified spectrum of Lightning Yellow and Canary Yellow between 2 and 6 keV and 0 and 200,000 counts.

Peak at 4.469 keV and 4.829 keV corresponding to  $L_{\alpha}$  and  $L_{\beta}$  for barium (Ba) as well as the  $K_{\alpha}$  for sulfur (S) are found in the XRF spectra for Lightning Yellow, Canary Yellow, and Caramel but not in Lime Green. This suggests the presence of barium sulfate, a known whitening/ thixotropic agent different from that found in the red inks (1). All of the XRF ink spectra can be seen in supplemental Figure A 4.1 to Figure A 4.22.

Overall, XRF spectral peaks corresponding to Cu, Cl, Fe, Ti, S, Ba, and Si can lead to chemical differentiation of inks. However, Cu and Cl are the only two elements directly attributable to color in every ink which they are observed. Iron and Ti can affect the color of the ink, but are thought to affect the shade more than the color in the inks observed while Ba, S, and Si affect mainly the viscosity of the ink. This implies organic components that cannot be detected

by the XRF spectrometer contribute more to the color of the inks. This issue can be resolved by combining the XRF spectral analysis with IR spectral analysis to obtain information on the organic composition of the ink.

#### 4.2 IR analysis of Tattoo Inks

Representative IR spectra of True Blue and Sky Blue inks are shown in Figure 4.4A. In the IR spectrum of the True Blue, absorptions were observed at 756, 781, 1066, and 1088  $\text{cm}^{-1}$ . Basova *et al.* previously reported that these peaks are associated with isoindole groups and the bridging nitrogens between these groups found in copper phthalocyanine seen in Table 1.1 (5). Basova *et al.* also state that the peaks at 756  $\text{cm}^{-1}$  and 781  $\text{cm}^{-1}$  are due to  $\text{Cu-N}_\alpha$  and  $\text{C}_\alpha\text{-N}_\alpha\text{-C}_\alpha$  vibrations.

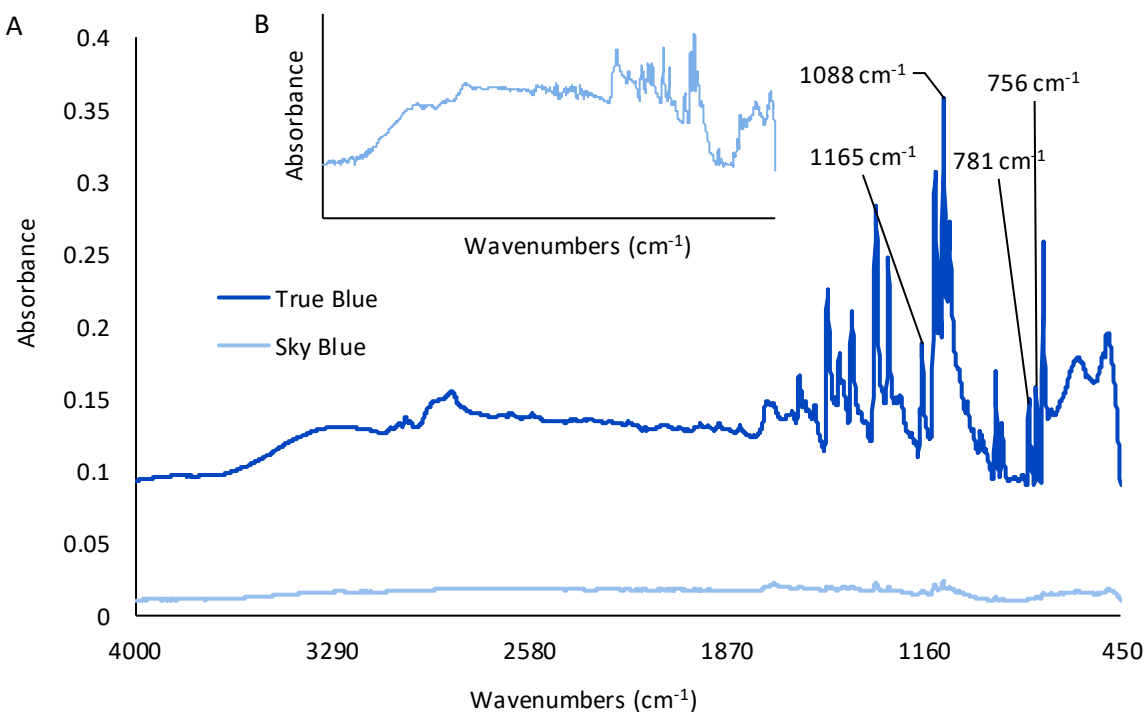


**Figure 4.4:** (A) Overlay of representative absorbance IR spectra of True Blue and Sky Blue inks. The specific wavenumber is labeled for structurally indicative peaks in each spectrum. (B) Sky Blue IR with the absorbance scale set between 0.005 and 0.025.

The peak at 1066  $\text{cm}^{-1}$  can also be attributed to a  $\text{C}_\alpha\text{-N}_\alpha\text{-C}_\alpha$  vibration as well as the  $\text{N}_\alpha\text{-Cu-N}_\alpha$  vibration and the peak at 1088  $\text{cm}^{-1}$  can also be attributed to the  $\text{C}_\alpha\text{-N}_\alpha$  vibration as well as



the  $N_{\alpha}$ -Cu- $N_{\alpha}$  vibration. A peak at  $1165\text{ cm}^{-1}$  is also observed, which is assigned to C-C bond consistent with phthalocyanine (5). When the Sky Blue and True Blue ink are on the same absorbance scale (Figure 4.5A), the Sky Blue ink spectrum appears to have no significant peaks. However, when the Sky Blue IR spectrum is shown with a magnified scale (Figure 4.4B), it can be seen that it has many of the same absorbance peaks as in the True Blue ink. Since they contain the same absorptions in their IR spectra, this further supports that the difference between the Sky Blue and True Blue inks is not due to their organic composition. The difference between the two inks is the shade of the ink which is caused by Ti observed in the XRF spectra. This Ti could also explain why Sky Blue does not have an intense IR absorbance. The most likely source of Ti in tattoo inks is titanium dioxide. Titanium dioxide reflects light in the IR light region (6). Since the Ti reflects light from the IR instrument, less light is available to be absorbed by the organic components, leading to the lower absorption.

There are no peaks observed in the IR spectra of Lining Black (Figure 4.5). This is because the main pigment of black inks, carbon black, has no significant IR absorbing bonds. If the ink were to be detected by IR spectroscopic analysis in tissue, most likely the signal from the tissue would shadow the featureless spectra of the black inks. In this case, XRF spectroscopic analysis would be more useful since S is able to be detected in the black inks.

In the Lipstick Red and Dark Red ink IR spectra (Figure 4.5), absorptions were observed at  $1016$ ,  $1226$ , and  $3166\text{ cm}^{-1}$ , which are attributed to  $\text{CH}_3$ , C-C-C in-plane deformations, and CH aromatic vibrations. Bands near  $3300\text{ cm}^{-1}$  were also observed which are attributed to NH bond vibrations. The presence of these functional groups is consistent with quinacridone pigments (Table 1.1) found in red tattoo inks (1, 7). The IR spectra of Lipstick Red and Crimson Red are the

same. The difference between these inks can be observed in the XRF spectra, in which a difference in Fe content can be observed. This further shows that the Fe in the Dark Red ink is used to change the shade of the ink and is not the sole contributor to the pigment color.

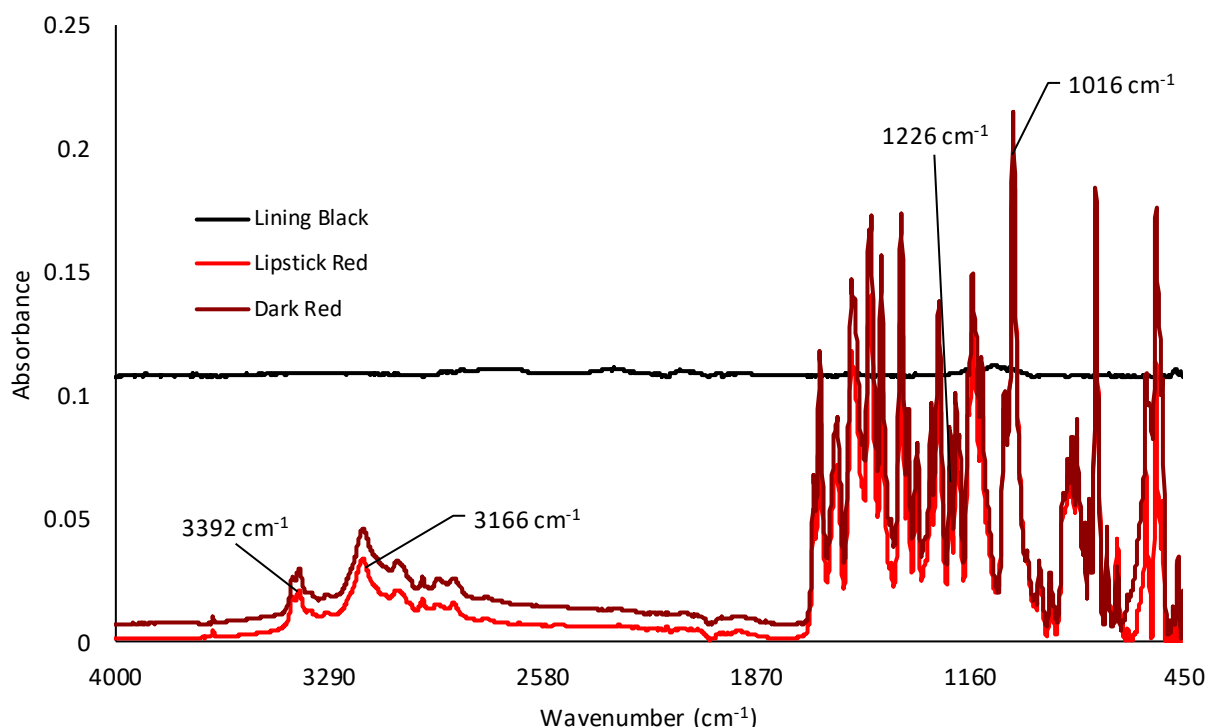


**Figure 4.5:** (A) Overlaid IR spectra of Lining Black, Lipstick Red, and Dark Red inks. The specific wavenumber is labeled for structurally indicative peaks in each spectrum.

Overall, IR absorptions that give information on the organic components of inks can be used to distinguish blue, black, and red inks. Similarly, differences in IR absorptions among the other ink colors were apparent, leading to distinction. However, the presence of metallic components like Fe and Ti which are not detected by IR spectroscopy can help determine the shade of the ink. Thus combining IR spectra with XRF spectra enables greater characterization of the inks for distinction of different colors. Due to the large number of variables in the XRF and IR spectra, these data were further probed using multivariate statistical analysis to investigate the

association and discrimination of the inks. The IR spectra of all analyzed inks are presented in supplemental Figures A 4.23 to A 4.48

### 4.3 Multivariate Statistical Analysis of Tattoo Ink Spectra

#### 4.3.1 XRF and IR Feature Selection for Statistical Analysis

Principal components analysis was used to visualize the differences in inorganic and organic compositions of tattoo inks of different colors as well as similarities between inks of the same color produced by different manufacturers on a subset of the inks. Studies by van Es *et al.* and Hoehse *et al.* previously showed that combining data produced by different instruments led to greater discrimination of samples when analyzed together rather than separately (8, 9).

Initially, both the XRF and IR spectra of each tattoo ink in the initial subset were normalized and analyzed via PCA. In the resulting scores plot (Figure 4.6A), each tattoo ink is represented by the representative color. Replicates are shown for each ink: for some inks, a total of ten samples are shown corresponding to sample replicates while for others, three samples are shown corresponding to instrument replicates. Based on the first two principal components (PCs), distinction of the three most common colors, red, black, and blue, was observed with the exception of Triple Black and Dark Red which overlap. The blank filter paper samples are also clearly separated from the inks and show reproducibility.

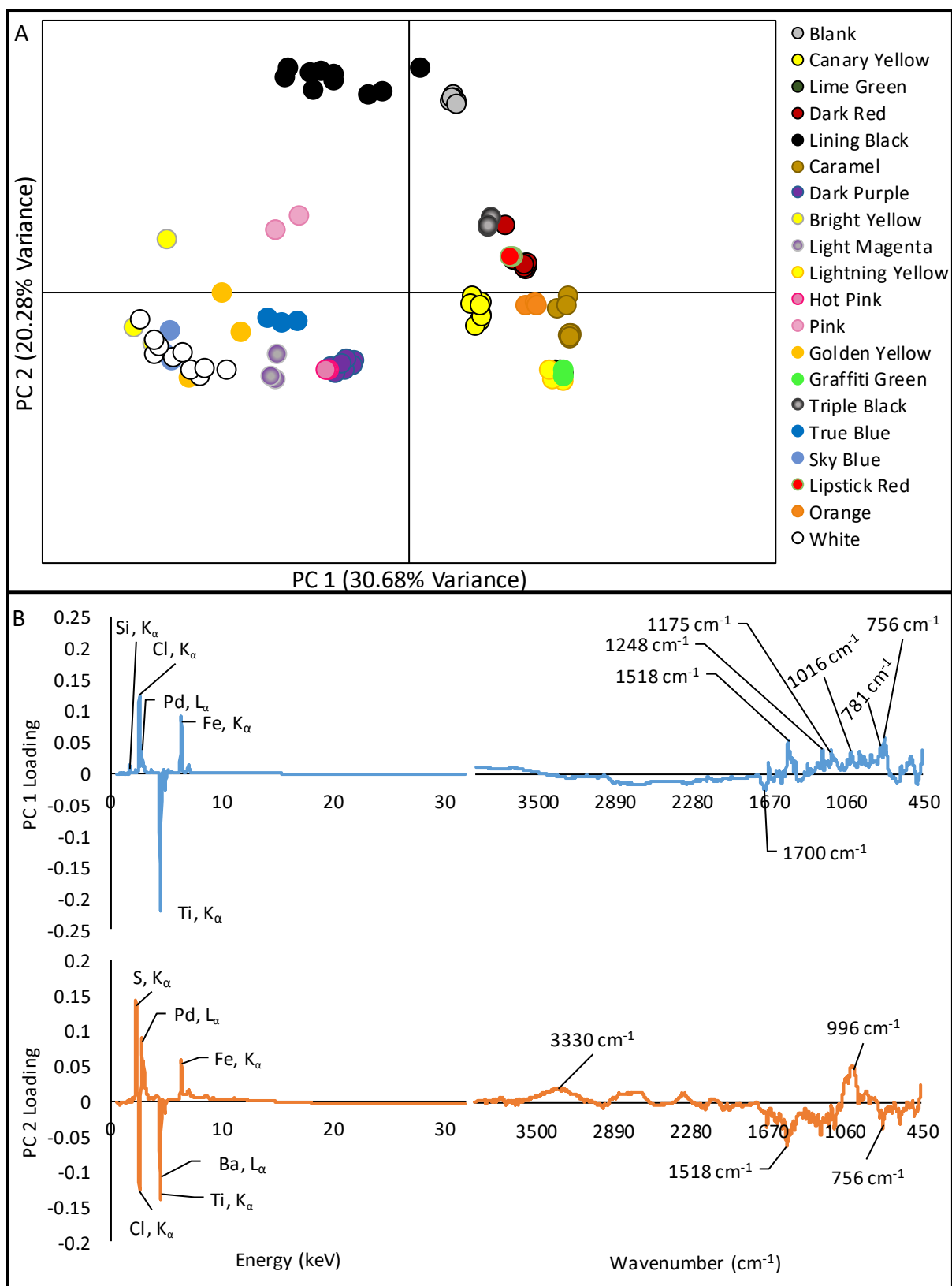


**Figure 4.6:** Principal components analysis of tattoo inks based on IR and XRF spectra. (A) Scores plots for first two principal components (PCs) and (B) corresponding loadings plots for first two PCs

The Triple Black replicates are positioned positively on PCs 1 and 2 while the Lining Black replicates are positioned negatively on PC 1 and positively on PC 2. This is caused by the standard normal variate (SNV) normalization of the dataset. In both black inks, no significant IR bands exist in the raw spectrum. When the featureless spectra are SNV normalized, peaks that are caused by drift in the IR background are accentuated. An example of this can be seen in Figure 4.7 which shows raw IR spectra of black and red inks as well as the corresponding SNV normalized spectra. The SNV normalization causes a peak near  $1000\text{ cm}^{-1}$  to increase in intensity in the spectrum of Lining Black. In the loadings plot for PC 2 (Figure 4.6B), this variable is weighted positively and has the greatest influence of all IR variables. Despite the influence, this variable is can be seen as the main IR peak in the blank spectra, and is therefore attributed to being an artifact. However, this artifact is not observed in all of the black inks, resulting in the distinction observed in the scores plot.

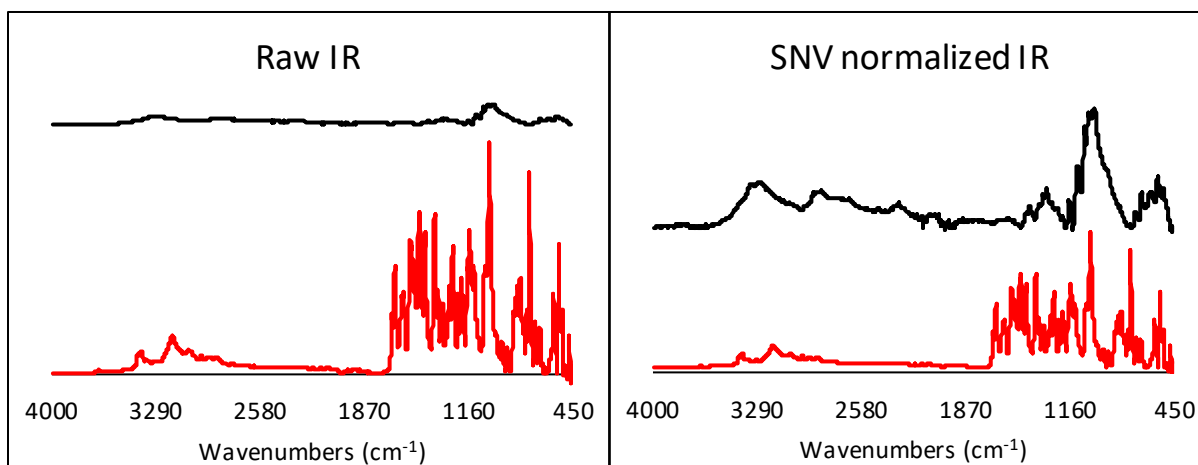


**Figure 4.7:** Raw IR spectra of a Lining Black ink (Top Left) and Lipstick Red ink (Bottom Left) compared to the SNV-normalized spectra (Top and Bottom Right respectively)

In the scores plot, the White ink is one of the most variable inks on PC 1 and overlap is observed between these replicates and the Sky Blue, Bright Yellow and Golden Yellow. This is most likely due to the whitening agent, titanium dioxide being present in all four inks. Titanium

is the largest peak in all four colors and has the largest negative contribution to both PC 1 and PC 2. Variables such as isoindole, copper, and azo peaks that differentiate the light-colored inks from the white ink have significantly less influence than titanium in PC 1 and 2, causing the overlap among these inks in the scores plots.

The loadings plots show the discrepancy in the number of variables between the XRF and IR spectral datasets, with the XRF spectral dataset containing 1570 variables and the IR dataset containing 3551. Normally this would cause the IR data to have more of a contribution to the PCA. However, the IR spectral data also loads at less than half the intensity of the XRF spectral data due to a difference in scales between the two data types. Of the major XRF spectral peaks loading in PC 1 and PC 2, four of the five peaks are the same in both PC 1 and PC 2: Fe, Cl, Pd, and Ti, with the fifth peak, S being the highest loading peak in PC 2. This means that the relative positions of samples on the scores plot are primarily determined by five variables in the XRF spectral data. Several scaling methods were attempted to set the IR and XRF spectral data to the same magnitude; however, this discrepancy in the number of variables between the datasets caused the IR data to contribute more to the PCA when both datasets were set to the same intensity scale. This causes the data to be artificially biased to one dataset.

To account for the discrepancy in the number of variables and intensities between the XRF and IR spectral datasets, feature selection was used to identify the most relevant variables in both the XRF and IR spectra. From the observation of the XRF spectra of the analyzed tattoo inks, silicon (Si, 1.749 keV), sulfur (S, 2.309 keV), chlorine (Cl, 2.629 keV), barium (Ba, 4.469 keV), titanium (Ti, 4.509 keV), iron (Fe, 6.409 keV), and copper (Cu, 8.049 keV) were selected as being

the most important variables to distinguish the inks. These elements also correspond to prevalent elements found in past literature (1-3, 10).

IR variables were selected both from experimental data as well as literature values. This was necessary to account for instrument variation and effects from the tattoo ink matrix. Thus the variables selected based on the eight most intense peaks in the loadings plots for PC 1 and PC 2 (Figure 4.6B) that corresponded to literature values for IR spectrum peaks found in known tattoo ink pigment spectra (1, 5-7) and consisted of  $3330\text{ cm}^{-1}$ ,  $1700\text{ cm}^{-1}$ ,  $1518\text{ cm}^{-1}$ ,  $1248\text{ cm}^{-1}$ ,  $1175\text{ cm}^{-1}$ ,  $1016\text{ cm}^{-1}$ ,  $781\text{ cm}^{-1}$ , and  $756\text{ cm}^{-1}$  (labeled in Figure 4.6B). These bands can be attributed to several different bond frequencies depending on the pigment. In the following discussion and figures, these bands will be referred to as NH-O (ring), C=O, C=N, Amide, Azo, C-polycyclic, C-N-C, and isoindole, respectively.

#### 4.3.2 Principal Components Analysis of the Reduced Variable Dataset

PCA was performed on the reduced variable XRF and IR dataset. From the scree plot (Figure 4.8), 90.97% of the total variance is described by the first six PCs with higher PCs describing 4% or less of the total variance each. As a minimum of two PCs are necessary, this would suggest the optimal number is between two and six.

Six variables are weighted most positively on PC 1: IR absorptions corresponding to C-N-C bonds, isoindole groups, azo groups, C-N bonds, and amide bonds as well as the XRF peak for Cl (Figure 4.9). The variables weighted most negatively on PC 1 are IR absorptions corresponding to C=O bonds as well as XRF peaks corresponding to Ba and Ti.

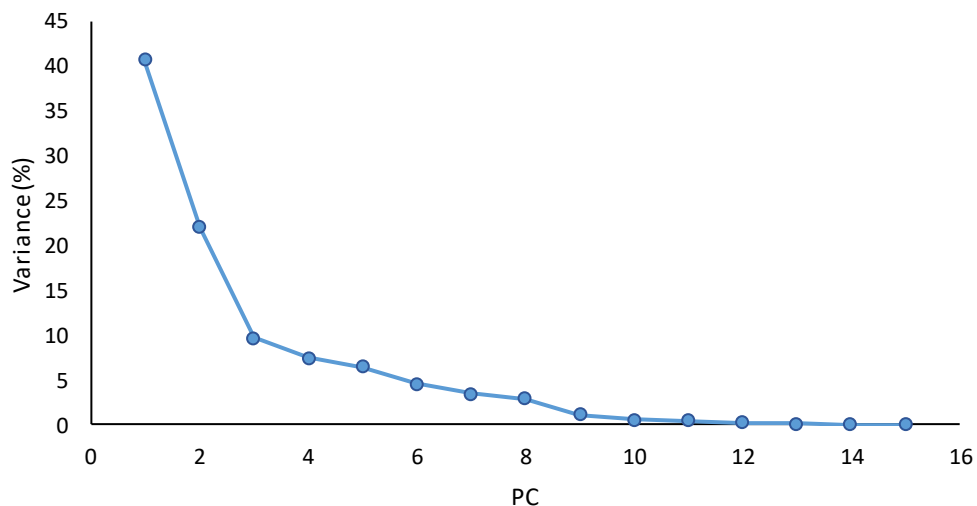


**Figure 4.8:** Scree plot describing the variance of each PC in the PCA analyzed feature selected IR and XRF spectral data

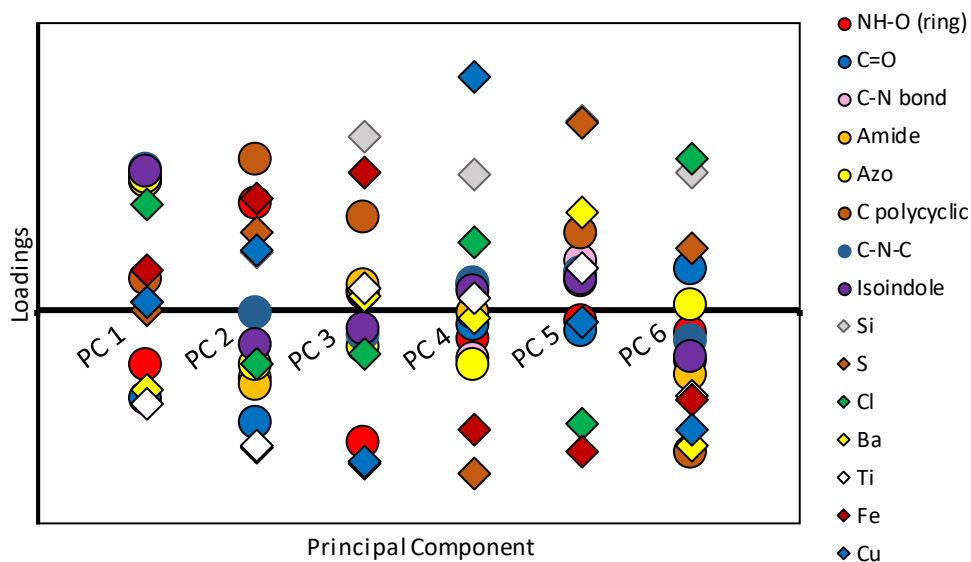


**Figure 4.9:** Loadings plot for PCs 1-6 of the PCA of the reduced variable IR and XRF spectra

These same variables load negatively on PC 2. XRF variables corresponding to Cu, Fe, and S are weighted positively on PC 2 along with the IR absorption corresponding to C-polycyclic bonds. It should be noted that all of the IR variables and XRF peaks corresponding to Ti, Ba, and



Cl have been the most influential variables in the first two PCs. Also, XRF peaks related to Cu, S, and Fe load positively on PC 2. This shows improvement over the non-reduced variable dataset in which only five XRF peaks influenced the first two PCs. In addition, the XRF peaks related to Fe, Si, S, and Cu, are among the most influential variables in PCs 3 and 4 for the reduced variable PCA. This means that any variance described by PCs 5 and 6 (11.01% variance total) will already be portrayed in PCs 1-4, suggesting that PCs 5 and 6 are likely not necessary for further analysis.

Based on the analysis of the loadings plot, PCs 1-4, which account for 79.97% of the total variance, were considered sufficient to investigate the association and discrimination of the tattoo inks. Scores plots showing the positioning of the inks on the first four PCs are shown in Figure 4.10. In the scores plot for PC 1 vs PC 2 (Figure 4.10A), green and yellow inks are positioned positively on PC 1 and negatively on PC 2; blue, purple, pink, white and light colored inks are positioned negatively on both PCs; the red inks are positioned close to zero on PC 1 and positively on PC 2; while the black inks are negative on PC 1 and positive on PC 2. This positioning is similar to the positioning observed in the scores plot for PCs 1 and 2 for the full dataset prior to feature selection (Figure 4.6A), and describes 11.79% more variance.

The exception is the positioning of the red inks and Triple Black. This is due to the higher contribution of the IR data to the reduced dataset PCA. Both the reds and Triple Black have IR absorbances near the C-polycyclic band. Since this absorbance is the most influential peak in PC 2 this causes the inks to be repositioned positively on this PC. Along with this, both inks contain Fe which is weighted positively on PC 1 in the full IR and XRF dataset. However, Fe has almost no influence on PC 1 in the reduced dataset PCA, causing both inks to position closer to zero on PC 1. PC 1 and PC 2 show differentiation of the red inks from the orange and yellow inks as well as a

closer positioning of Triple Black with Lining Black in the reduced variable dataset than in the full dataset. However, replicates of Lining Black overlap with filter paper (blank) replicates in the first 2 PCs for the reduced variable dataset. This did not occur in the full dataset and has been caused by the presence of an IR absorbance near the C-polycyclic band in the filter paper samples. However, in PC 4 of the reduced dataset, the blank and black inks are distinguished based on S, the most negatively loading variable on this PC, causing the black inks to be positioned more negatively than the blank

When a reduced set of variables is used for PCA, most replicates of similar colors position closely. There is less variation among replicates of White ink in the reduced variable dataset than in the full dataset in PCs 1 and 2 (Figure 4.6 and Figure 4.10A). Further, there is less overlap of White with light colored inks which is primarily observed in PC 2 of the reduced variable dataset. Both yellow inks that overlapped the white in the full dataset had absorbances corresponding to C-polycyclic bonds, while Sky Blue, which also overlapped the White in the full dataset, contains copper. White does not have either peak. Both the Cu and C-polycyclic peaks have little to no effect on the first 2 PCs in the full dataset, but have a positive influence on PC 2 in the reduced dataset, causing the separation among Sky Blue, Bright Yellow, Golden Yellow, and White in PC 2 of the reduced dataset.

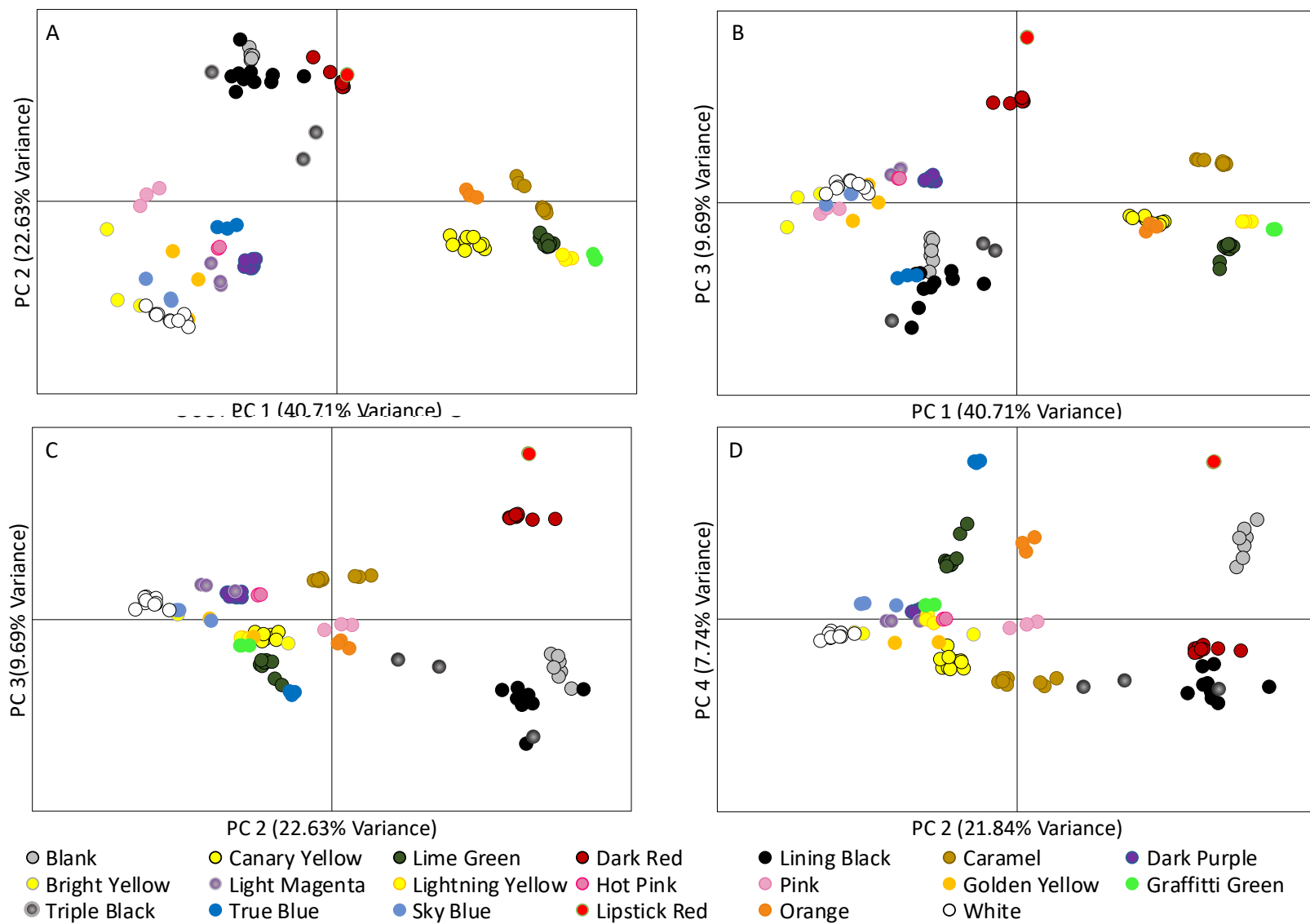


**Figure 4.10:** PCA scores plots for (A) PC 1 vs PC 2, (B) PC 1 vs PC 3, (C) PC 2 vs PC 3 and (D) PC 3 vs PC 4 of the feature selected IR and XRF spectra

More improvement in ink differentiation between the full and reduced variable datasets can be observed among the yellow and green inks. For example, the Lightning Yellow, Graffiti Green, and Lime Green inks no longer overlap with differentiation among these inks now observed on PC 1. This is due to differences in intensities of C-N, C-N-C, and isoindole related peaks in the IR spectra of these inks, which previously had been masked by the influence of more intense XRF spectra peaks in the full dataset PCA. Yellow pigments are known to consist of azo pigments, which typically do not contain C-N-C bonds or isoindole functional groups. However, both functional groups are found within copper phthalocyanines which are associated with blue and green pigments. Since Lightning Yellow contains both of these functional groups as well as Cl; this suggests that the yellow pigment used in Lightning Yellow is possibly a type of chlorinated isoindole containing pigment. Such pigments are known to produce yellow colors (11); however, no literature is available in which the presence of these pigments in tattoo ink is reported.

Within the reduced variable dataset, improvements were seen from the total dataset within the first 2 PCs. However, further chemical differences between inks were observed in higher PCs. In PCs 3 and 4, the red inks are distinguished from each other. This indicates the differences in the Fe and Si composition of Lipstick Red and Dark Red, both of which are highly influential on PCs 3 and 4.

More differentiation between Sky Blue and the other light colored inks can also be seen in PC 4. This differentiation is due to the presence of copper in Sky Blue (containing the pigment copper phthalocyanine), which is the highest positively loading peak in PC 4, causing Sky Blue to be positioned more positively than the other light colored inks on this PC. The high influence of

Cu on PC 4 also causes separation among the Lime Green, Nuclear Green, and Lightning Yellow inks with the Lightning Yellow ink positioned slightly more negative due to lack of Cu.

One advantage of the use of PCA is that sample data can be projected onto the PCA at a later time without affecting the resulting statistics. This would allow analysts to analyze an initial set of known tattoo inks and then compare possible inks from evidence to the already analyzed set on the same PCA. In order to see if the inks initially analyzed in the PCA would be a representative sample set of all tattoo inks, a test set of inks (Table 3.1) was projected onto the PCA

In Figure 4.11, many of the projected inks are positioned closely to inks of similar color in each of the scores plots. However, three inks, Bright Orange, Scarlet Red, and Light Red, are not positioned near similar colors. Bright Orange is positioned close to Hot Pink or Pink in all 4 PCs. The pink inks are primarily organic based with the C-N and polycyclic bands in the IR spectra being the most intense peaks. Bright Orange also has these as its main bands in its IR spectrum suggesting they may both be azo pigments. The metallic composition of Bright Orange distinguishes it from Orange because it has a Ti peak that is an order of magnitude larger than the Orange ink. Along with this Orange also contains Fe while Bright Orange does not.

Light Red and Scarlet Red consistently are positioned near Orange. These reds have many of the same variables as Lipstick Red; however, in contrast to Lipstick Red, these reds do not contain Si but have more intense IR peaks associated with C-N-C bonds. This suggests that these inks contain similar azo pigments to the Orange ink.

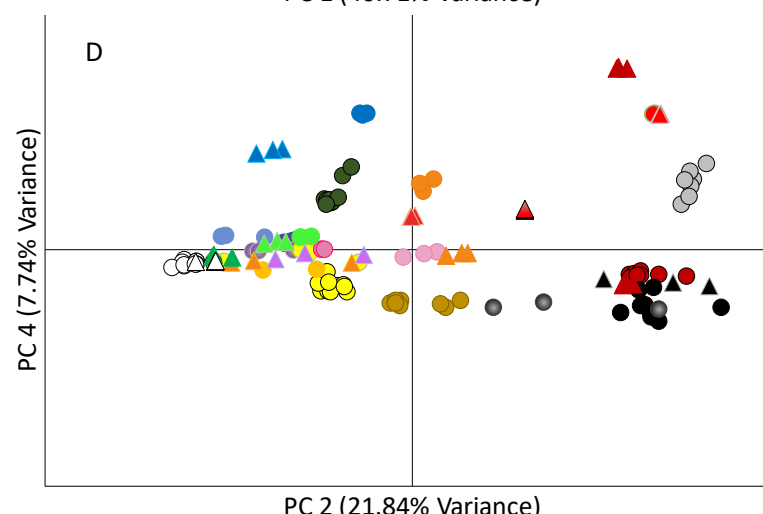
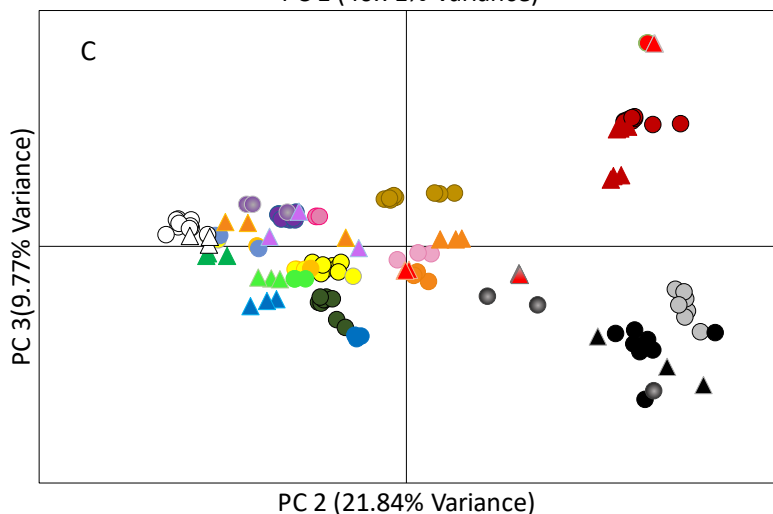
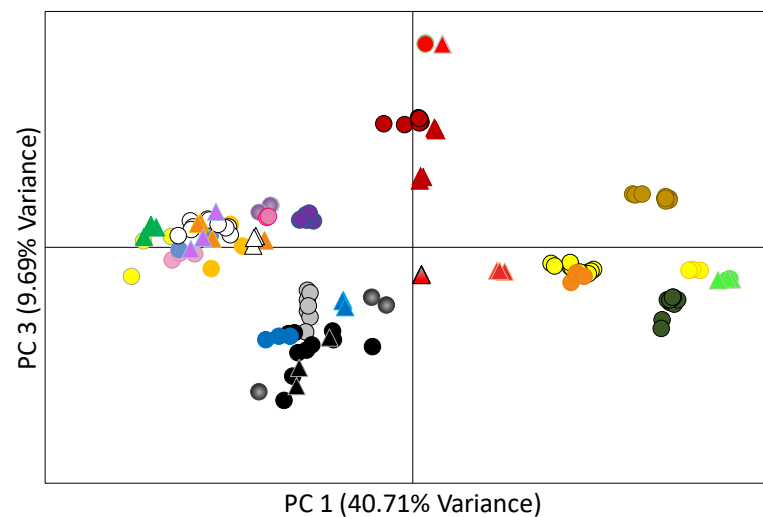
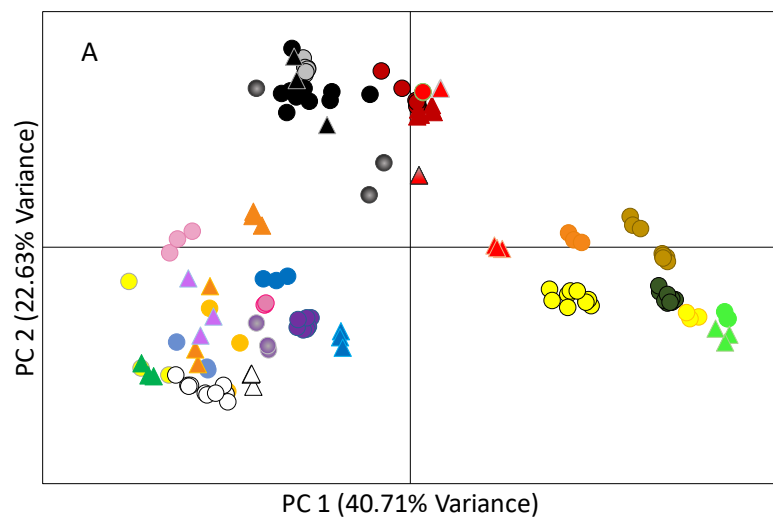


**Figure 4.11:** Projected PCA scores plots for (A) PC 1 vs PC 2, (B) PC 1 vs PC 3, (C) PC 2 vs PC 3 and (D) PC 3 vs PC 4 of feature selected IR and XRF spectra

Through PCA, most of the inks were able to be correctly differentiated from inks of different colors. However, some of the inks, especially lighter colored inks that contain titanium, show only minute differences in the PCA that visually cannot be differentiated in the scores plot. To investigate further differentiation of the inks, additional statistical analysis was investigated.

#### 4.3.3 Hierarchical Cluster Analysis

PCA only allows for a visual interpretation of the scores plots on which the samples are projected. Although a majority of the inks group with similar colored inks in PCA, the lack of a quantitative measure of the degree of correlation and discrimination in PCA lends itself to subjectivity in analysis which could cause analysts to arrive at differing conclusions. To overcome these issues, hierarchical cluster analysis (HCA), which provides quantitative information of the similarity between groups of samples, may be performed. In this case, HCA was performed on the scores of each sample on the first 4 PCs of the PCA. The resulting HCA dendrogram is shown in Figure 4.12 with clusters of inks forming at a similarity level of 86.0% or greater indicated. Most of the replicates were formed groups at similarity levels of higher than 95%, the exceptions to this being the light colored inks and the black inks. The first cluster of non-replicate samples occurs at over 93%. Since the goal of the HCA is to group inks of the similar colors together, a lower similarity level was chosen to display.

The clusters of inks observed in the HCA dendrogram corroborates many of the conclusions that were made based on groups of inks observed in the first 4 PCs. For instance, the 6 different red inks form five different clusters at a similarity level of 86%. However, it was observed that the clusters formed by Dark Red and Deep Red cluster at 86.3% suggesting they

have very similar composition. Lipstick Red and Crimson Red cluster at 55.7% similarity before forming a group with the reds associated with high metallic contents (Dark Red and Deep Red) at 29% similarity. Scarlet Red and Light Red (the red inks with low silicon content) group with each other at a similarity level of 64.0% and never group with the other red inks. This suggests that there are 5 distinct compositions among the red inks.

Similar to the PCA scores, variability is observed among the black inks most likely due to the sporadic spectra caused by SNV normalization of featureless spectra. In the HCA, there are six clusters of black ink at the selected similarity consisting of 3 inks. All of the black inks cluster together at a little over 60%. However, the next sample the black inks cluster with is the filter paper (blank) samples which they do not cluster to until less than 50% similarity.

In HCA there is the clear difference that can be observed among the light-colored inks (Bright Yellow, Bright Orange, Mint Green, Golden Yellow, Pink, and Sky Blue) and the white inks. These inks either partially or completely overlap in PCs 1, 3, and 4 of the PCA due to their high Ti content. In the HCA, the White and Brite White inks form a cluster at a similarity of 86.5% with only one Golden Yellow included in the cluster. The other light colored inks group together but with less specificity. For instance, there is a group that consists of Mint Green, Bright Yellow, and one White replicate which cluster at 93% similarity and another which consists of Sky Blue, Light Purple, and Golden Yellow that cluster at 87% similarity. Both of these light-colored clusters group with each other at 85% similarity before clustering with the white inks at 84% similarity. This suggests that inks in these groups most likely have to be considered as a light color that is not white instead of directly associating them with a color.



#### 4.4 Conclusion

Principal components analysis and hierarchical cluster analysis are two complementary multivariate statistical techniques, each of which provides information the other lacks. PCA can provide information on the variables which affect the clustering of samples while HCA provides numerical measurements of similarity to create a less subjective analysis. Through the use of both PCA and HCA, many of the inks were differentiated according to general color. Inks that lie outside of their color set show that there are likely inks that contain pigments not analyzed in this study that cause them to position differently within both multivariate techniques. Improvement in the differentiation of ink in the PCA is possible by analyzing a wider variety of tattoo inks and incorporating their data into the original PCA.

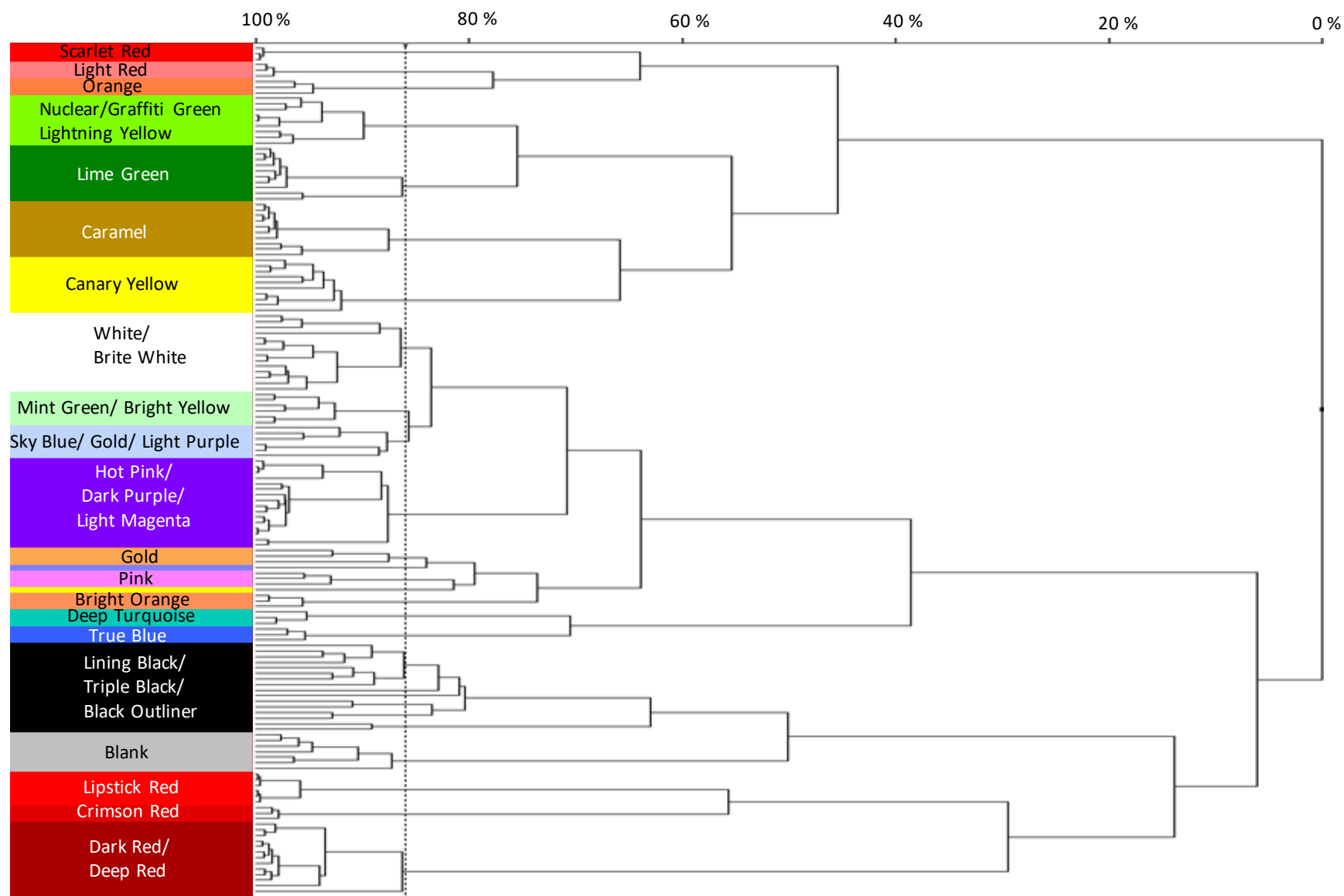


**Figure 4.12:** Projected HCA dendrogram for truncated IR and XRF spectral datasets for PCs 1-4. The dashed line marks 86.0% similarity

## APPENDICES

## Appendix 4.1

### Representative X-ray Fluorescence Spectra of Tattoo Ink samples

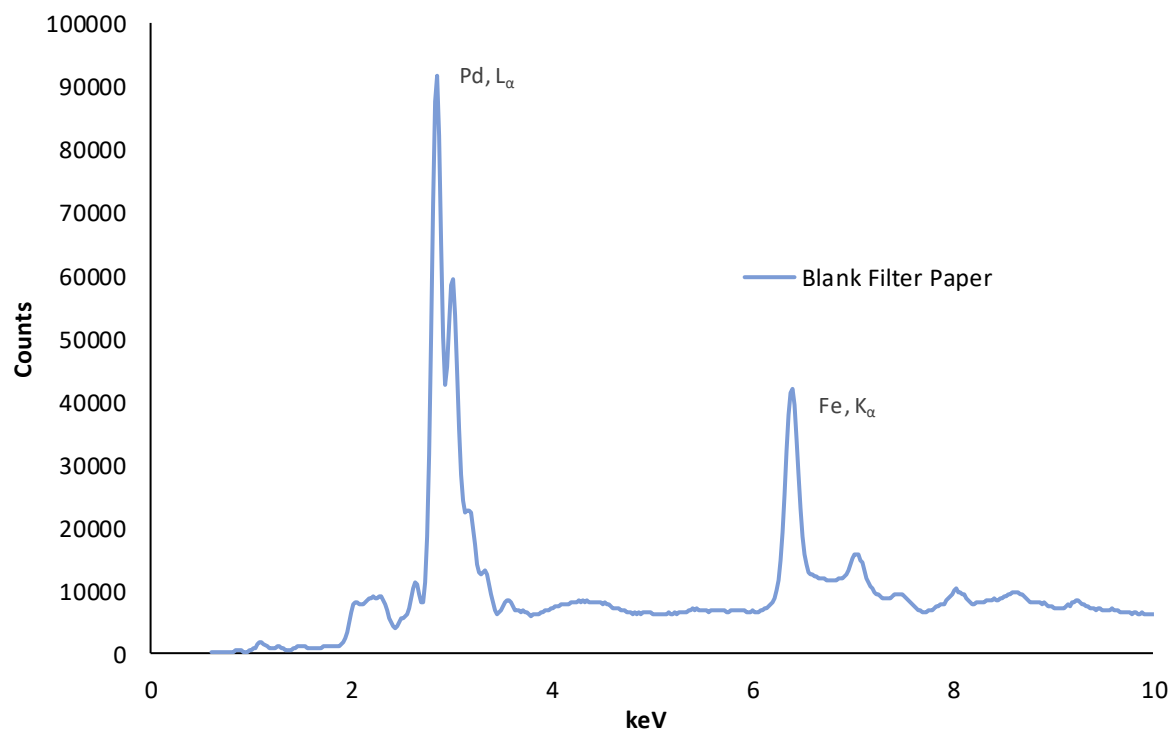


**Figure A 4.1:** Representative XRF spectra of blank filter paper. The specific transition and element are labeled for each major peak in the spectrum.

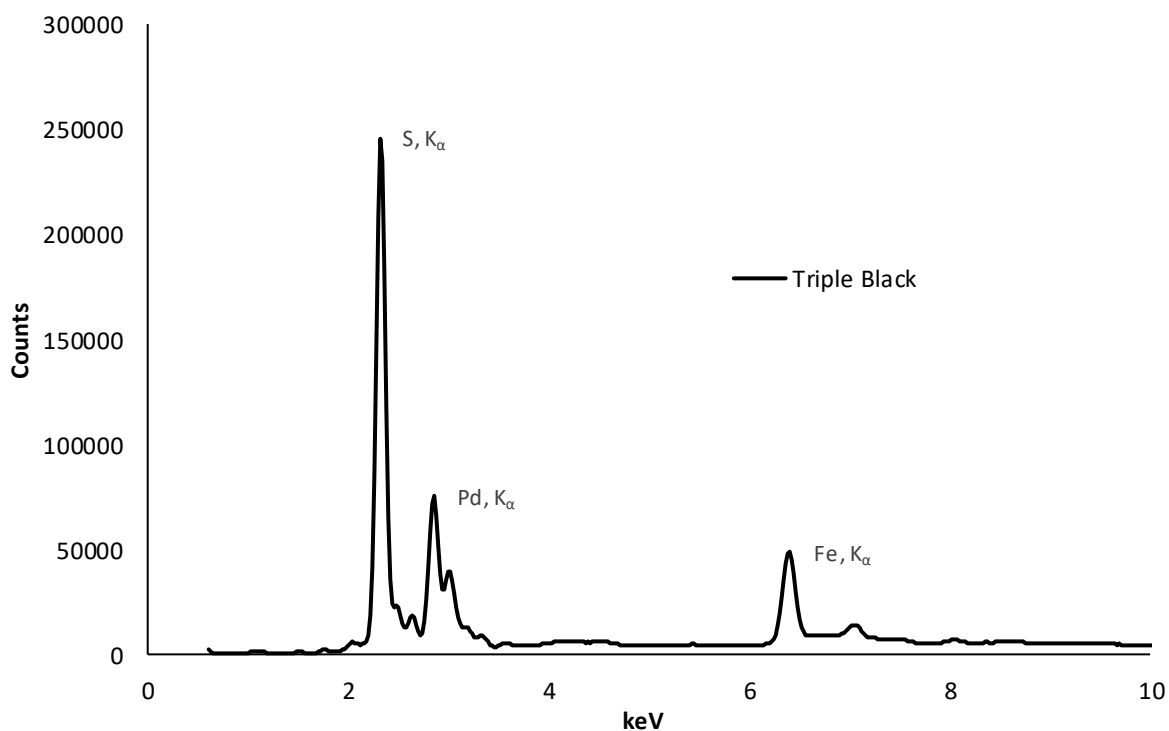


**Figure A 4.2:** Representative XRF spectra of Triple Black. The specific transition and element are labeled for each major peak in the spectrum.

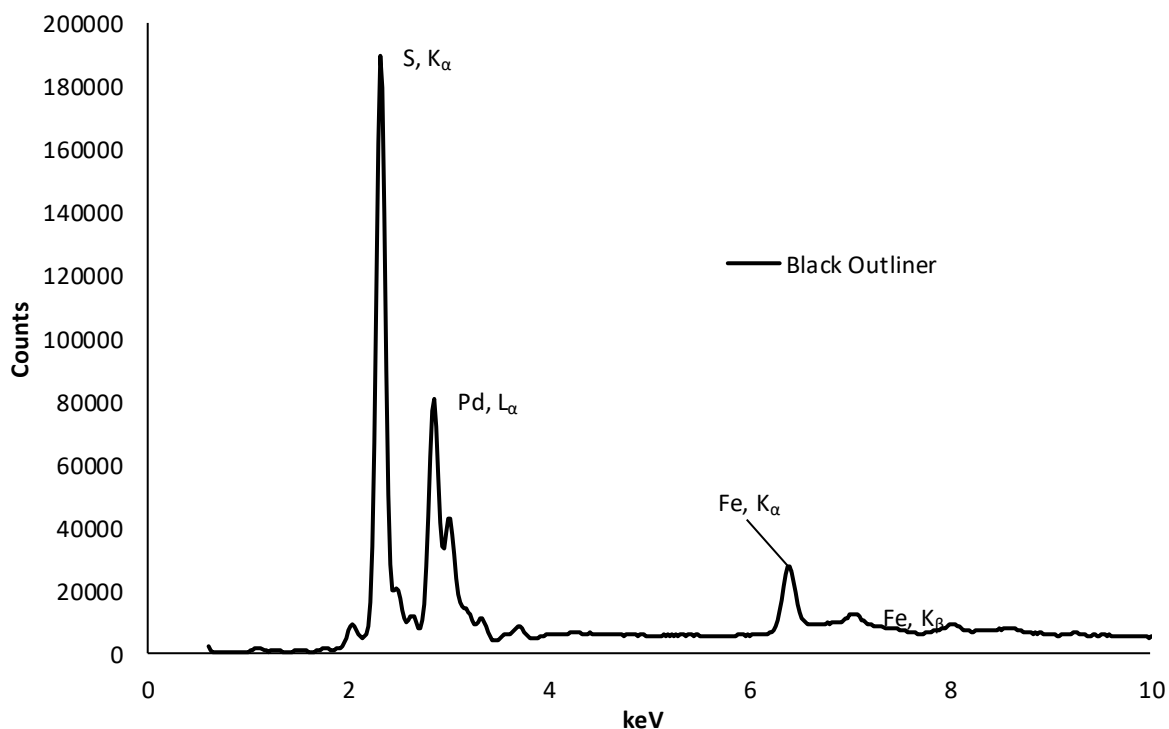


**Figure A 4.3:** Representative XRF spectra of Black Outliner. The specific transition and element are labeled for each major peak in the spectrum.

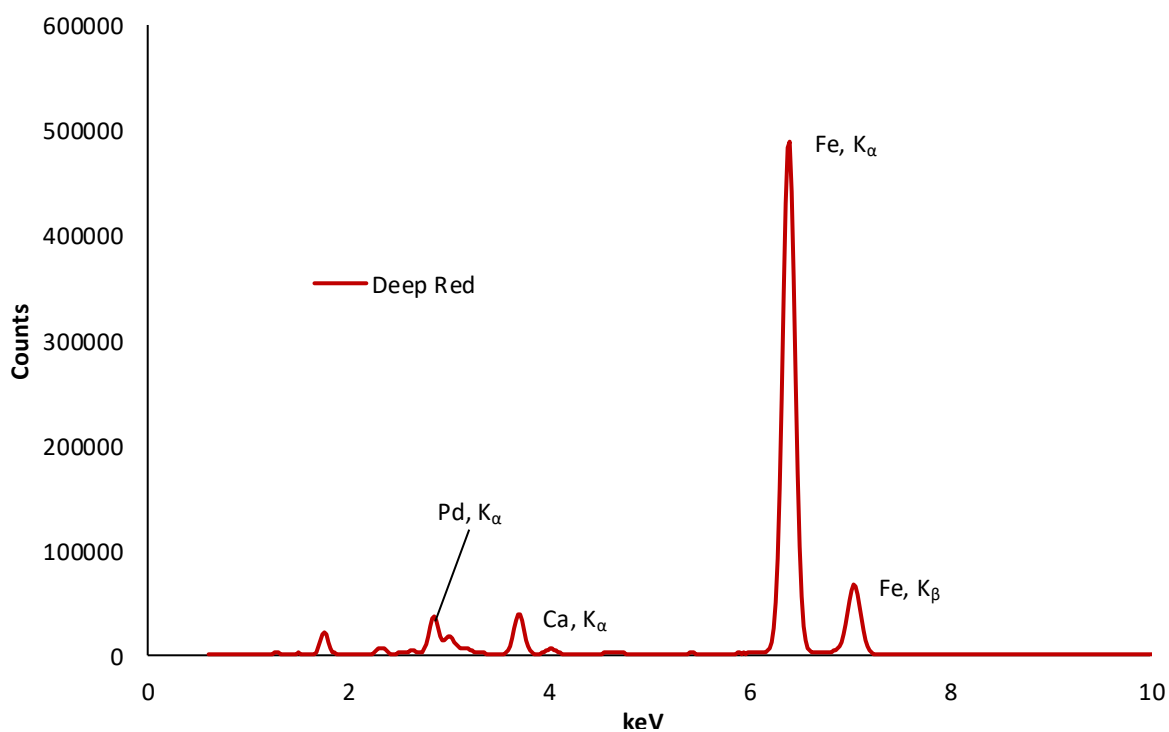


**Figure A 4.4:** Representative XRF spectra of Deep Red. The specific transition and element are labeled for each major peak in the spectrum.

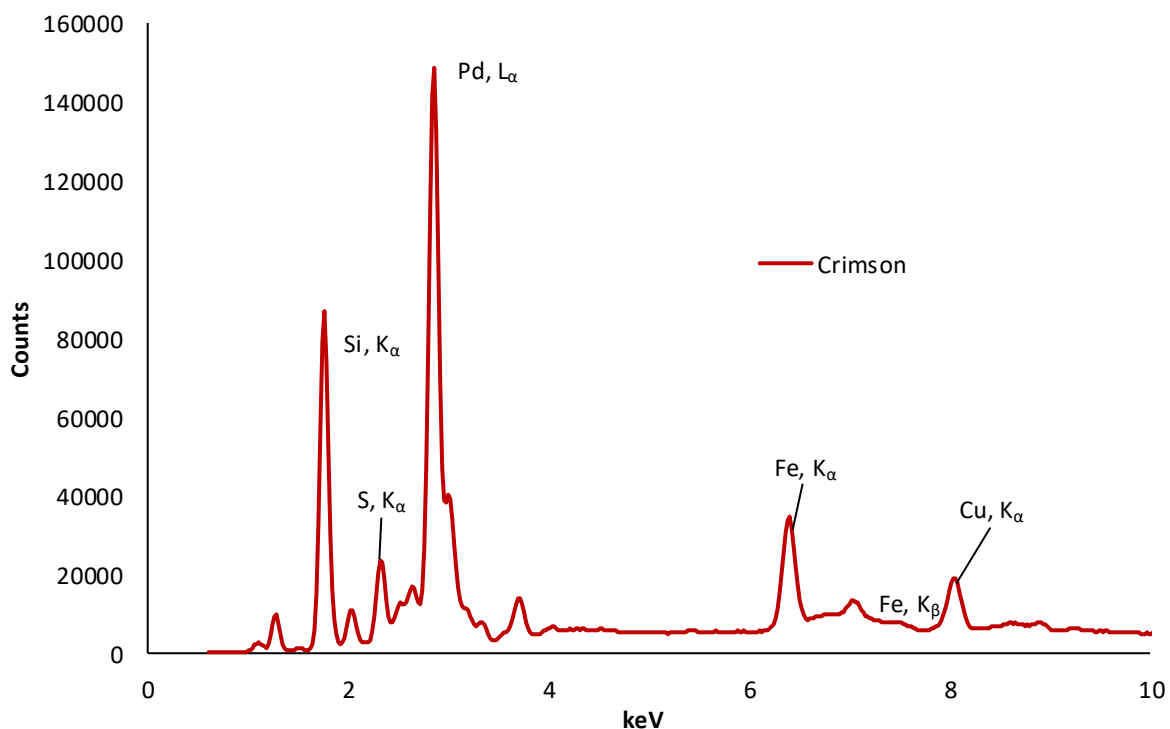


**Figure A 4.5:** Representative XRF spectra of Crimson Red. The specific transition and element are labeled for each major peak in the spectrum.

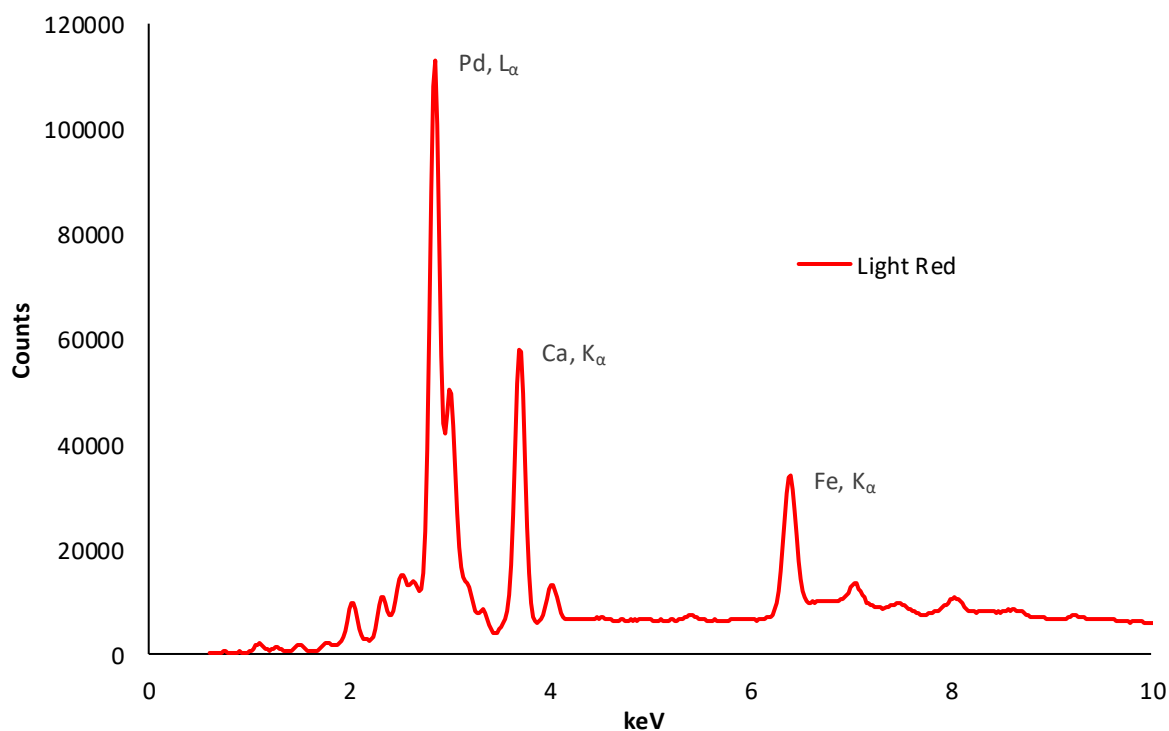


**Figure A 4.6:** Representative XRF spectra of Light Red. The specific transition and element are labeled for each major peak in the spectrum.

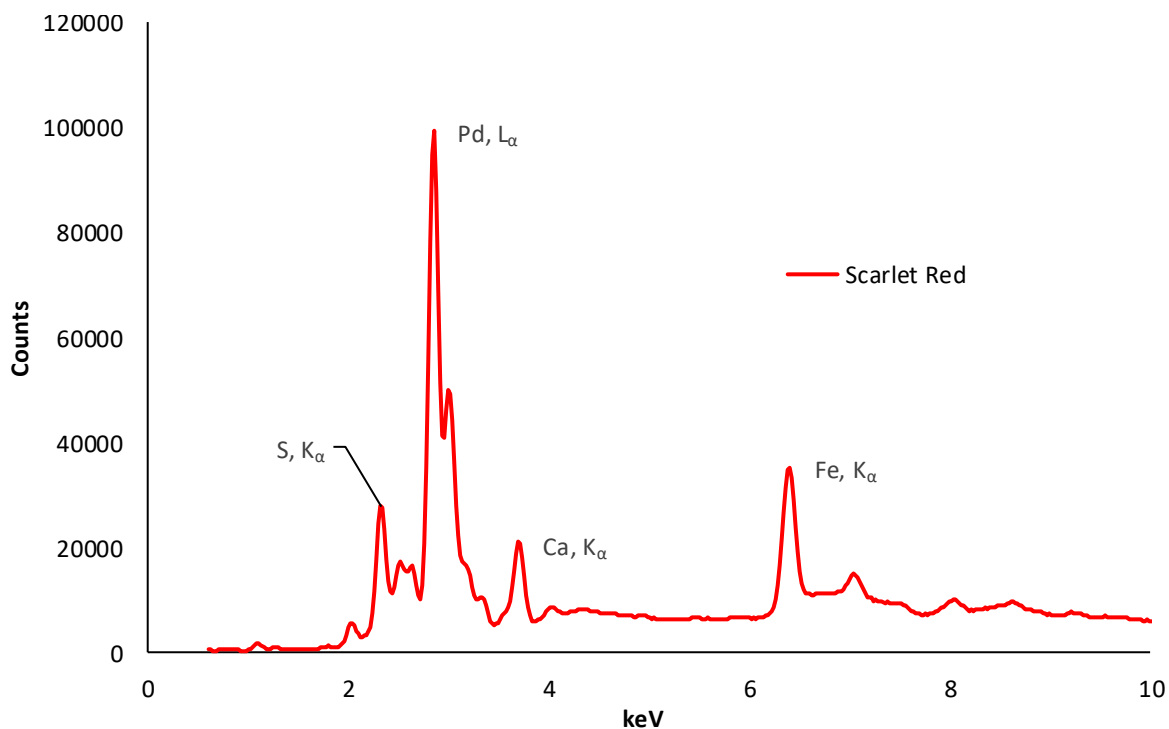


**Figure A 4.7:** Representative XRF spectra of Scarlet Red. The specific transition and element are labeled for each major peak in the spectrum.

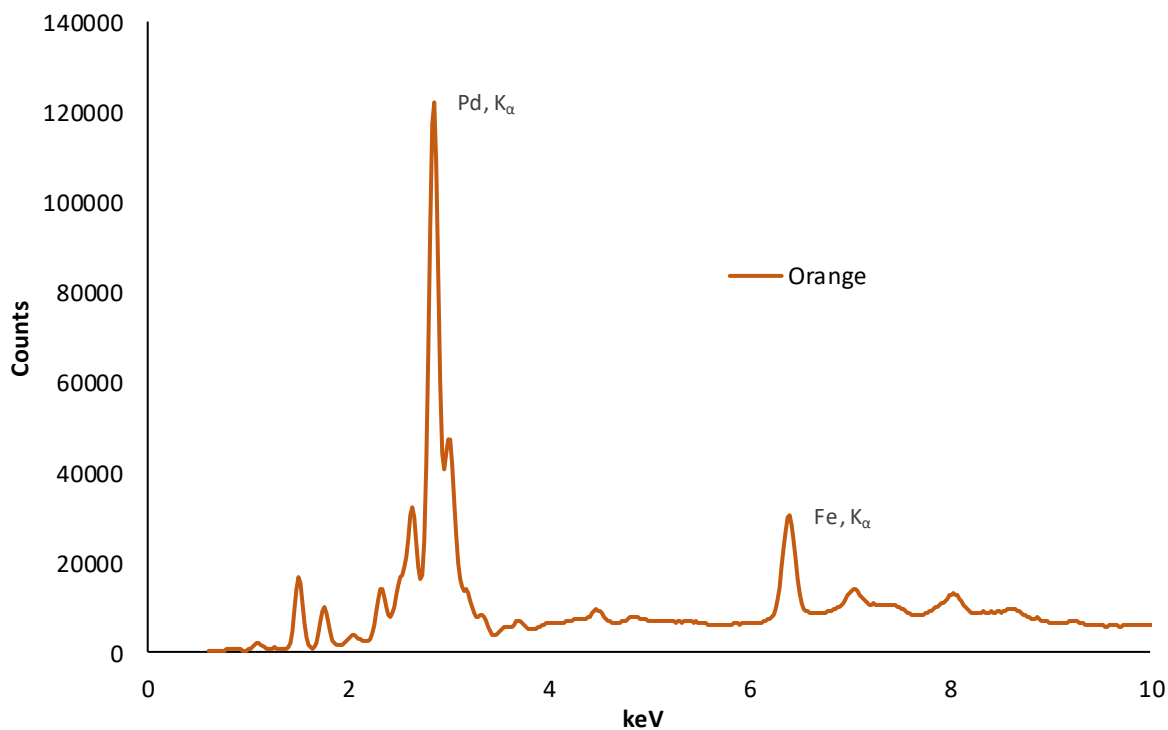


**Figure A 4.8:** Representative XRF spectra of Orange. The specific transition and element are labeled for each major peak in the spectrum.



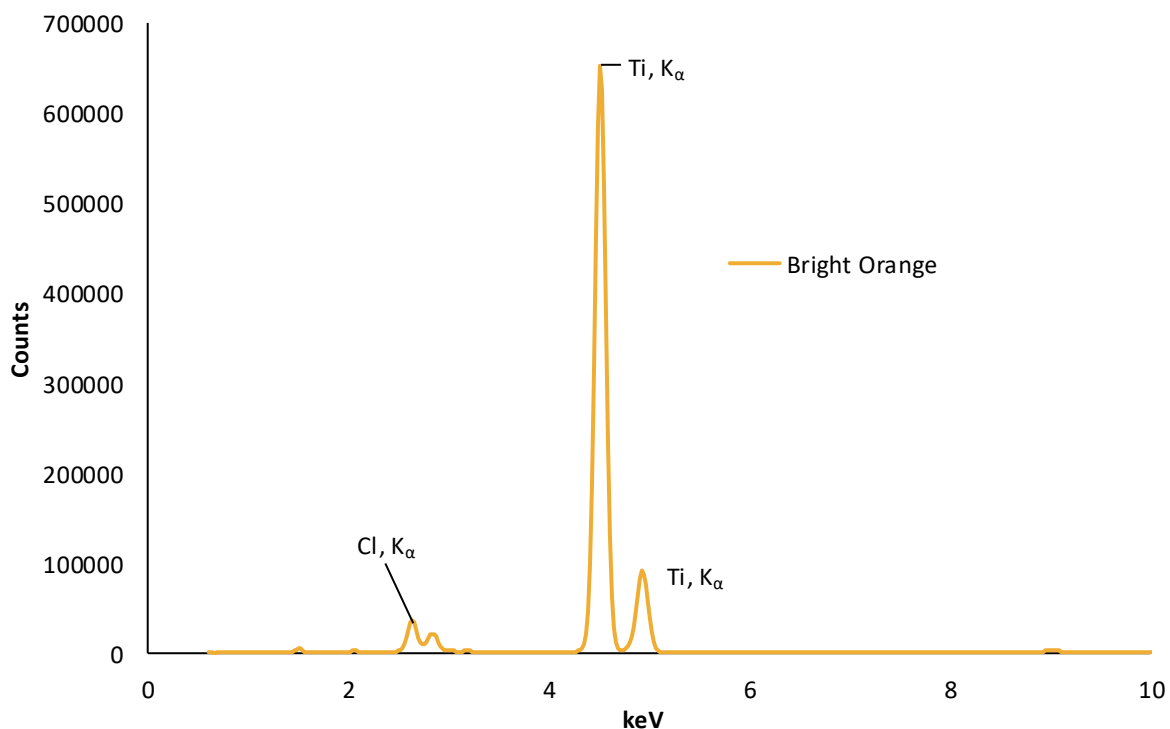


**Figure A 4.9:** Representative XRF spectra of Bright Orange. The specific transition and element are labeled for each major peak in the spectrum.

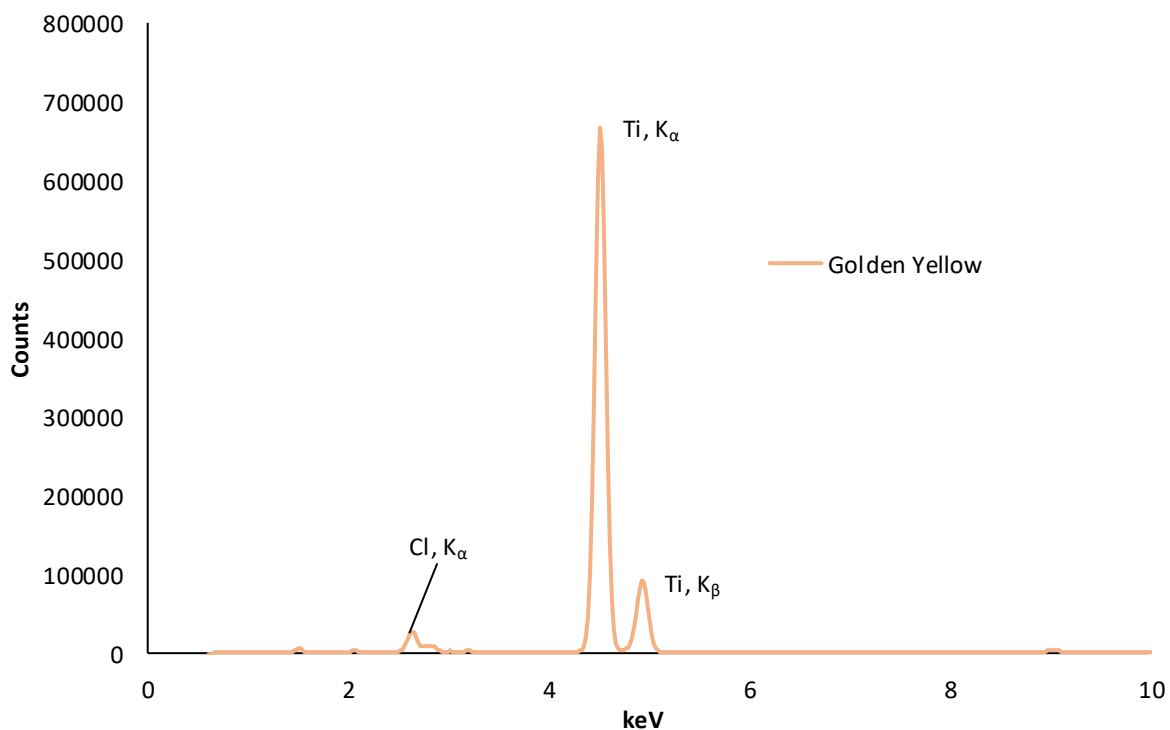


**Figure A 4.10:** Representative XRF spectra of Golden Yellow. The specific transition and element are labeled for each major peak in the spectrum.

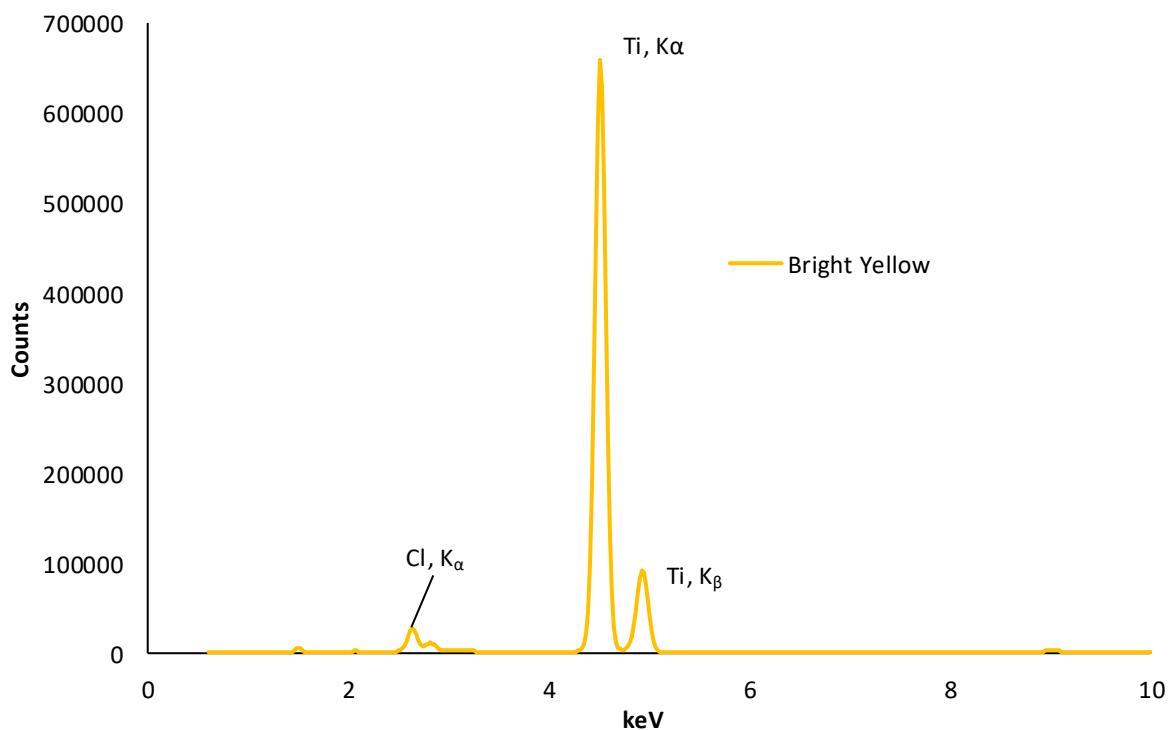


**Figure A 4.11:** Representative XRF spectra of Bright Yellow. The specific transition and element are labeled for each major peak in the spectrum.

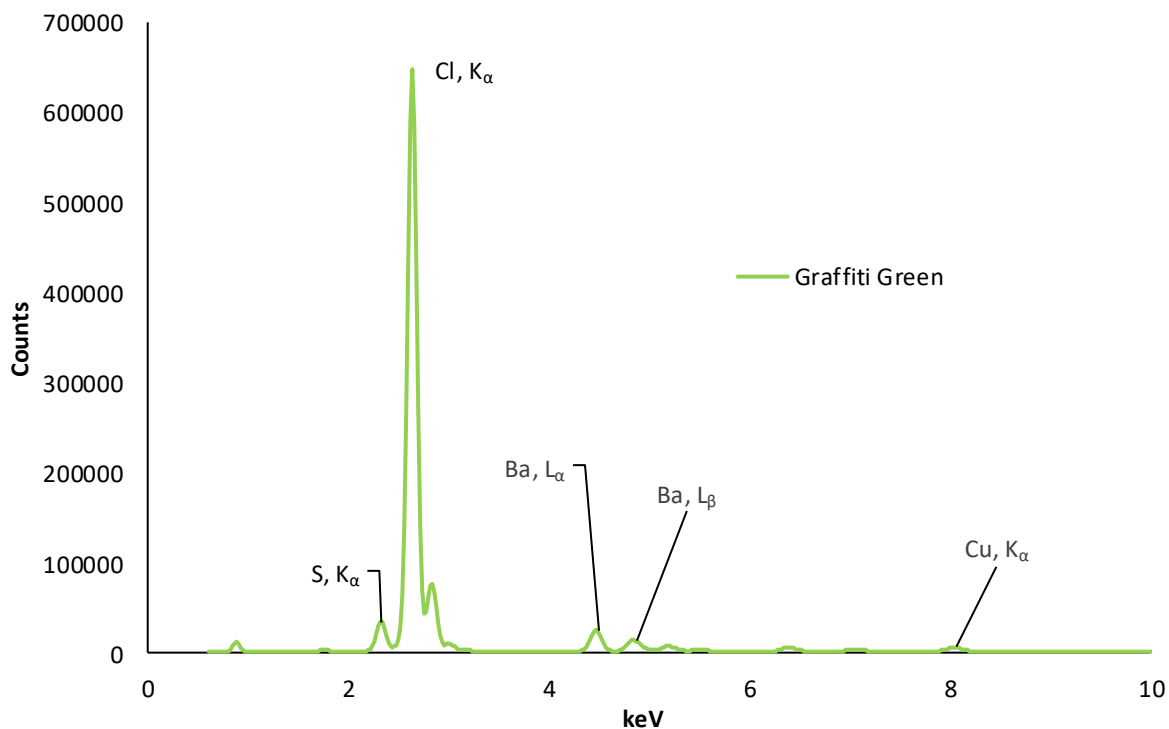


**Figure A 4.12:** Representative XRF spectra of Graffiti Green. The specific transition and element are labeled for each major peak in the spectrum.

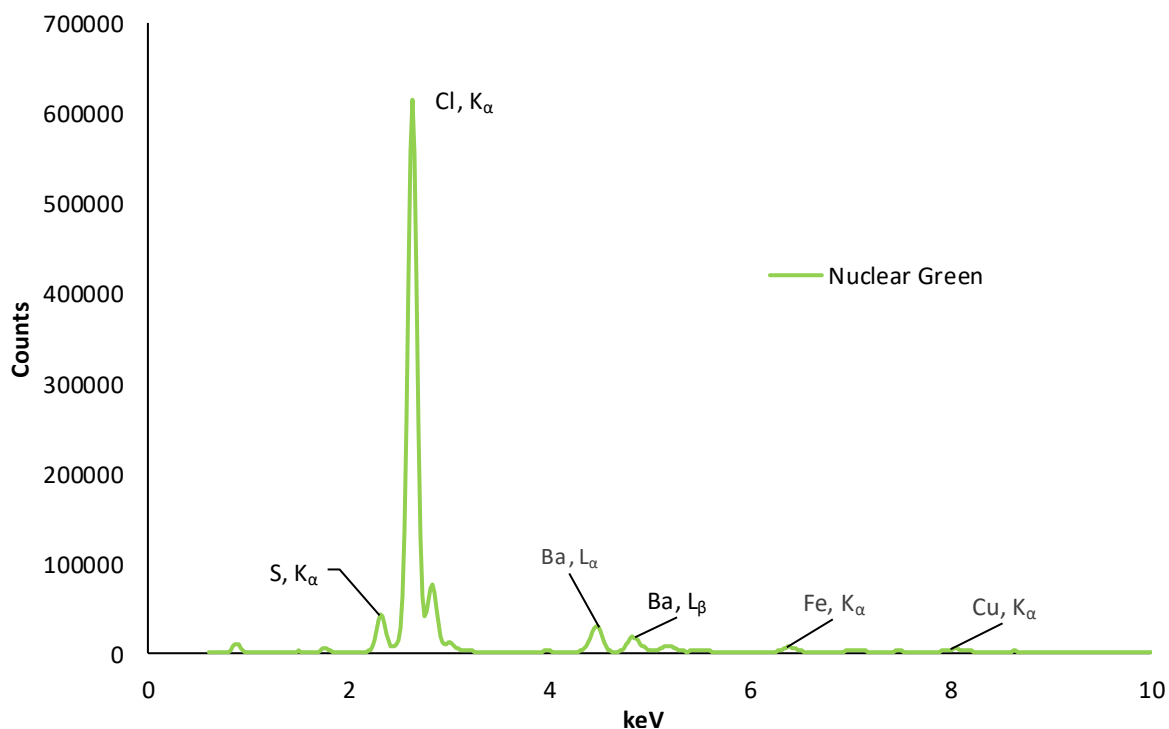


**Figure A 4.13:** Representative XRF spectra of Nuclear Green. The specific transition and element are labeled for each major peak in the spectrum.

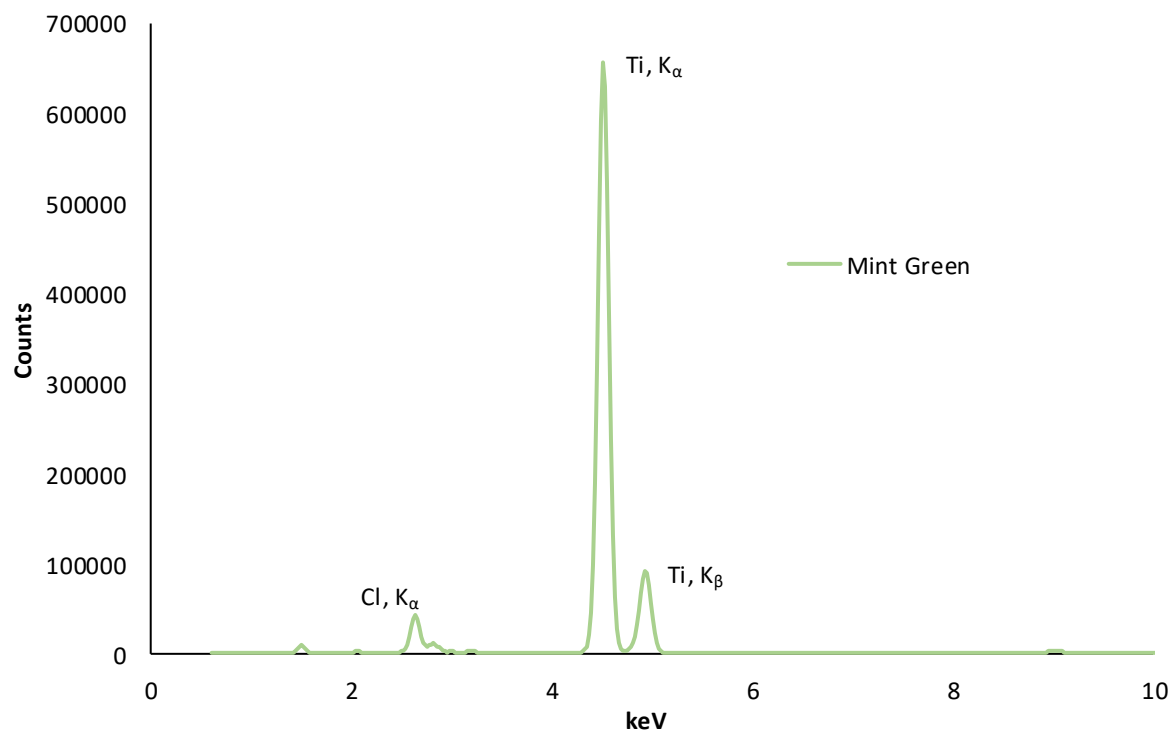


**Figure A 4.14:** Representative XRF spectra of Mint Green. The specific transition and element are labeled for each major peak in the spectrum.

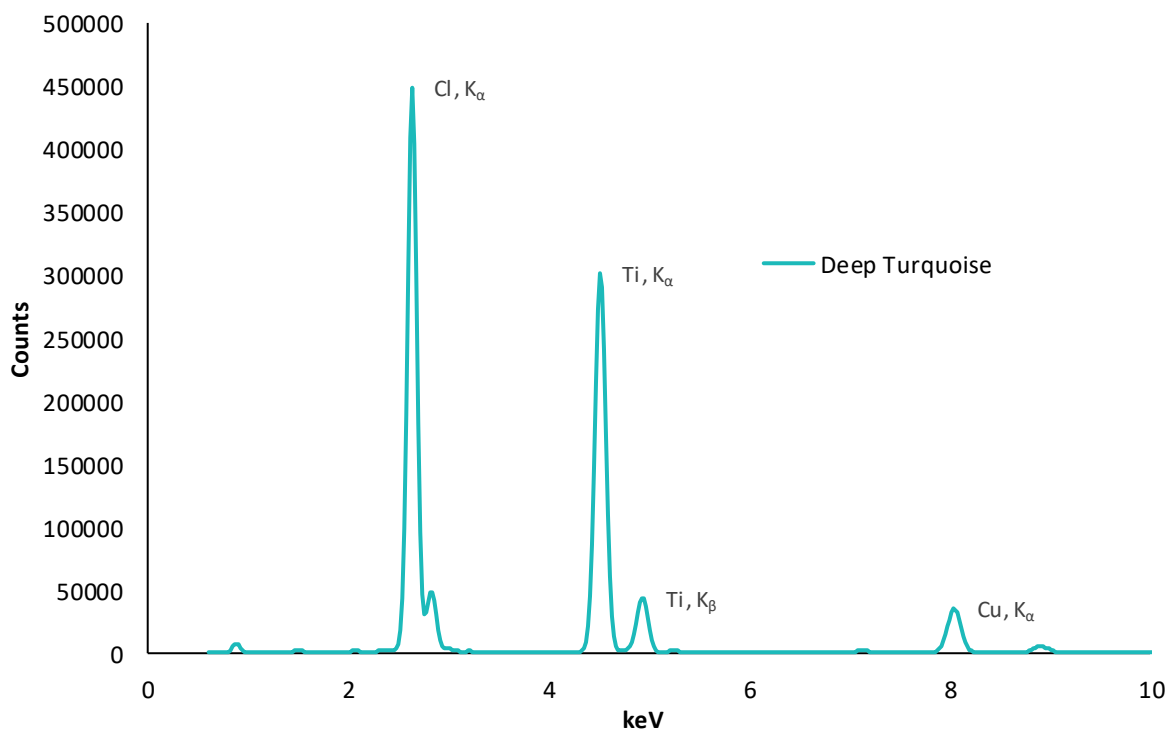


**Figure A 4.15:** Representative XRF spectra of Deep Turquoise. The specific transition and element are labeled for each major peak in the spectrum.

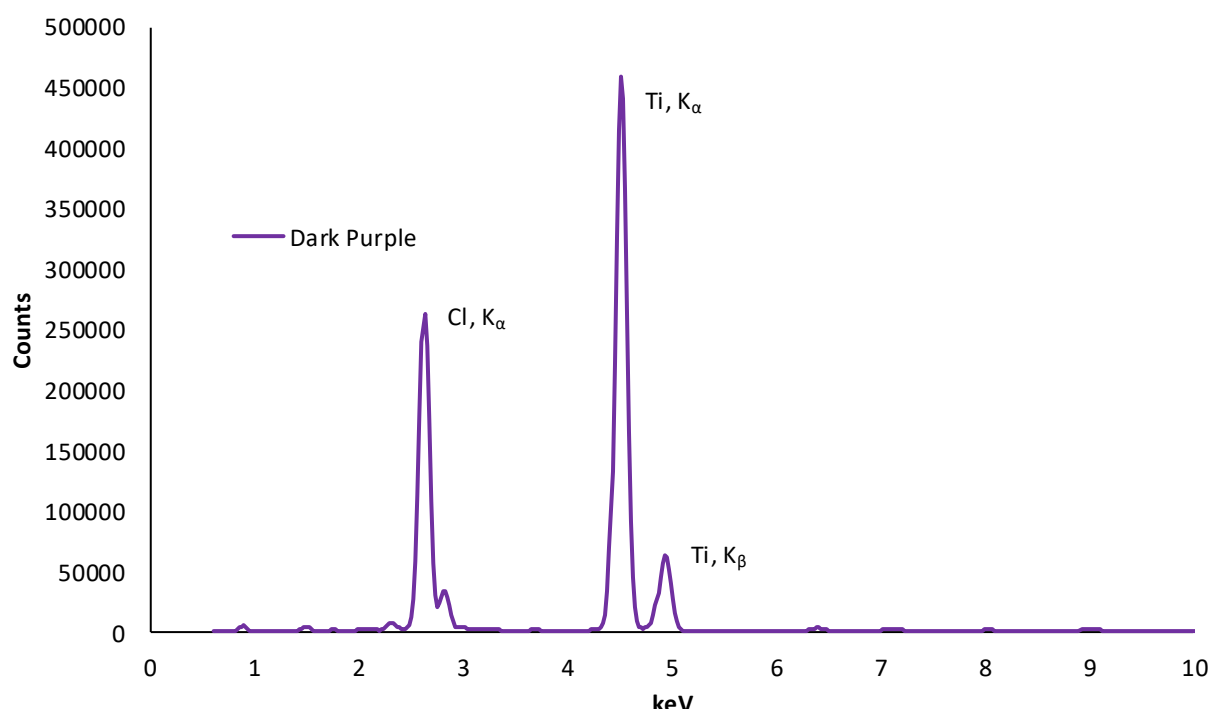


**Figure A 4.16:** Representative XRF spectra of Dark Purple. The specific transition and element are labeled for each major peak in the spectrum.

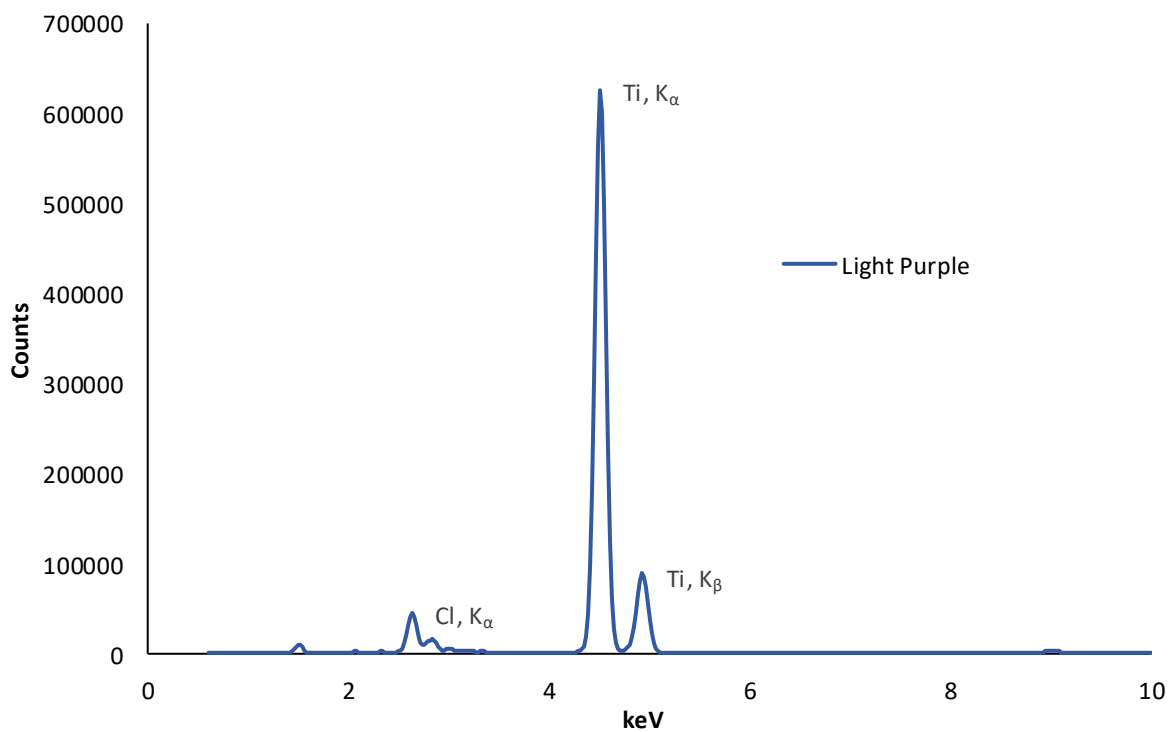


**Figure A 4.17:** Representative XRF spectra of Light Purple. The specific transition and element are labeled for each major peak in the spectrum.

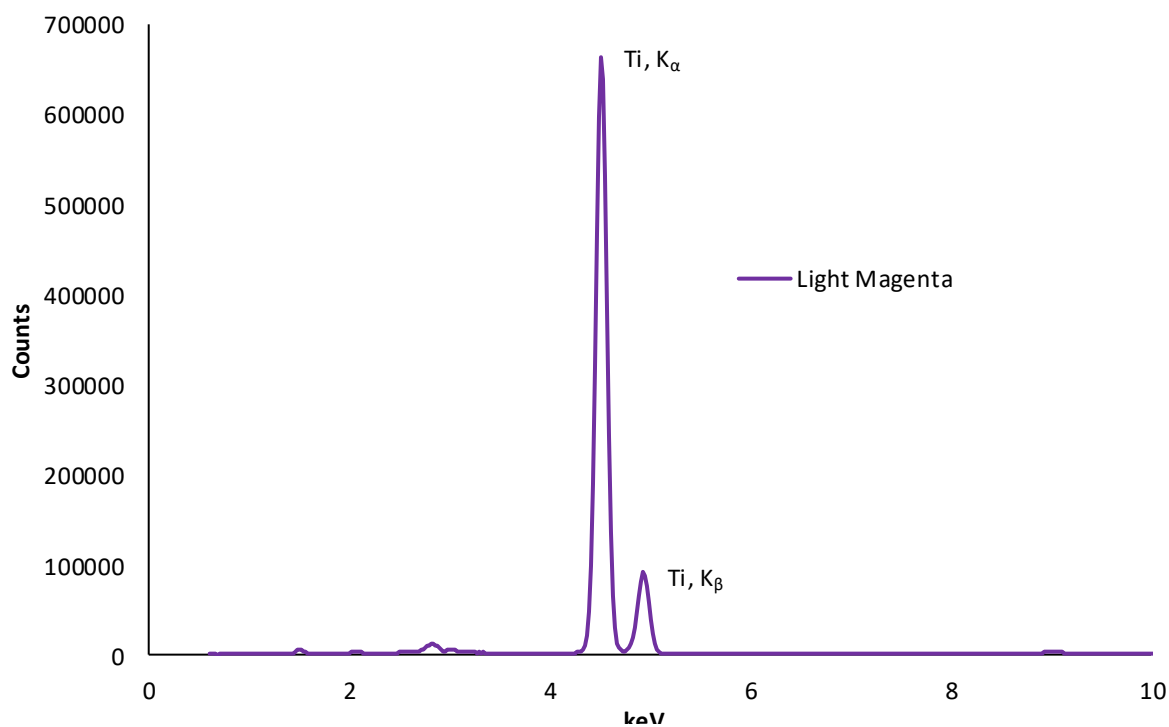


**Figure A 4.18:** Representative XRF spectra of Light Magenta. The specific transition and element are labeled for each major peak in the spectrum.

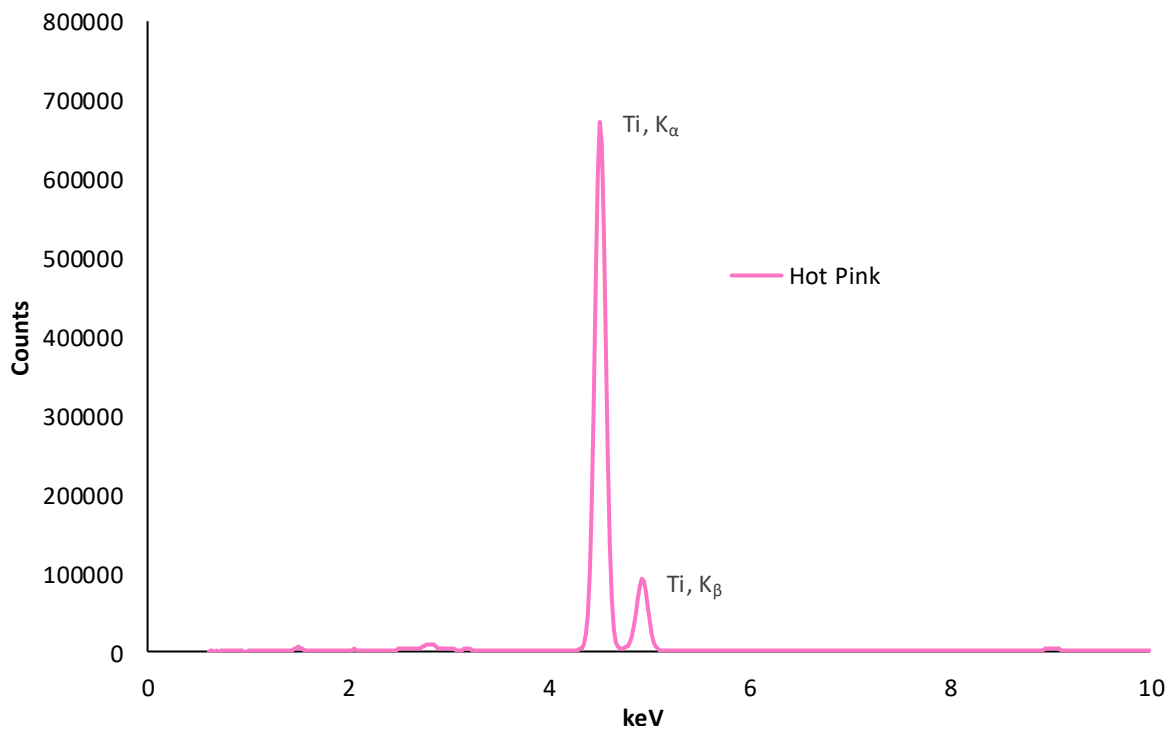


**Figure A 4.19:** Representative XRF spectra of Hot Pink. The specific transition and element are labeled for each major peak in the spectrum.

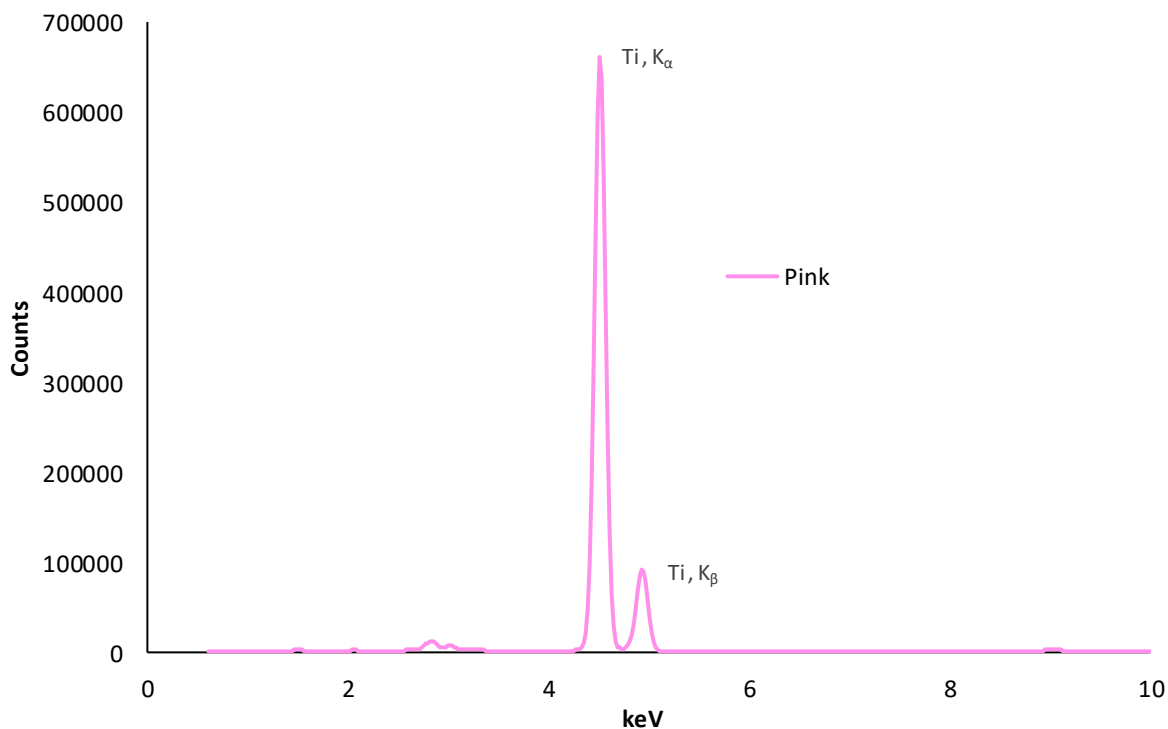


**Figure A 4.20:** Representative XRF spectra of Pink. The specific transition and element are labeled for each major peak in the spectrum.

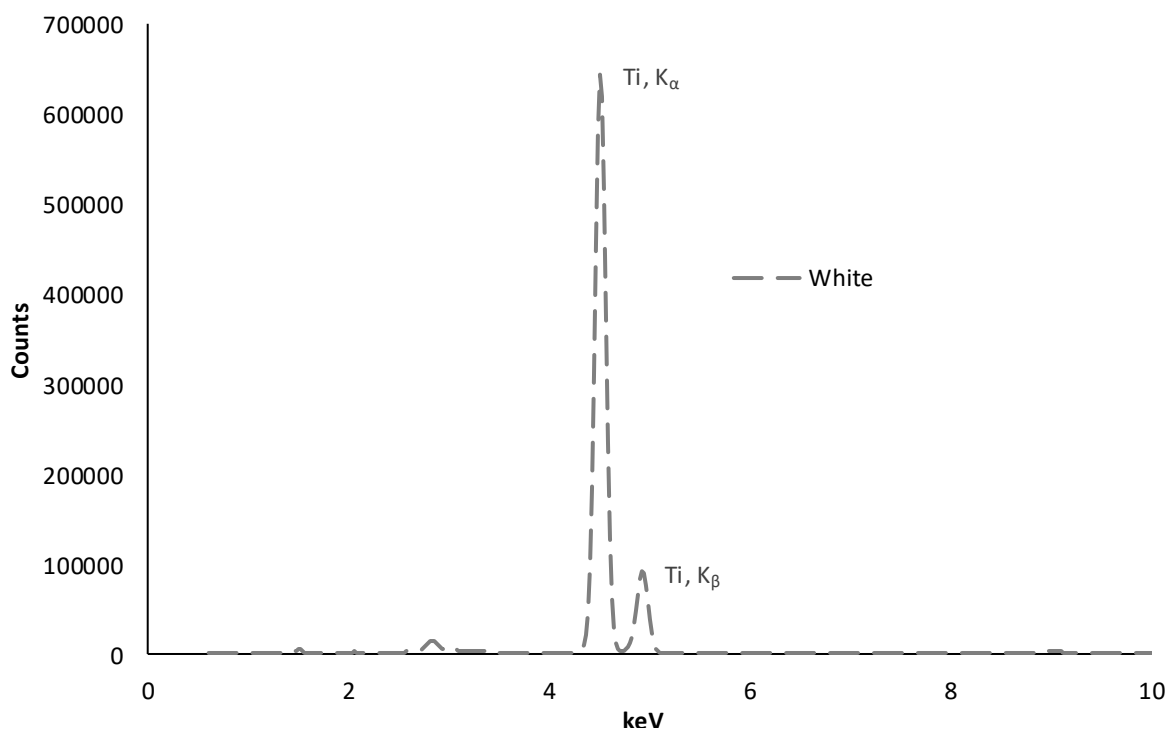


**Figure A 4.21:** Representative XRF spectra of White. The specific transition and element are labeled for each major peak in the spectrum.

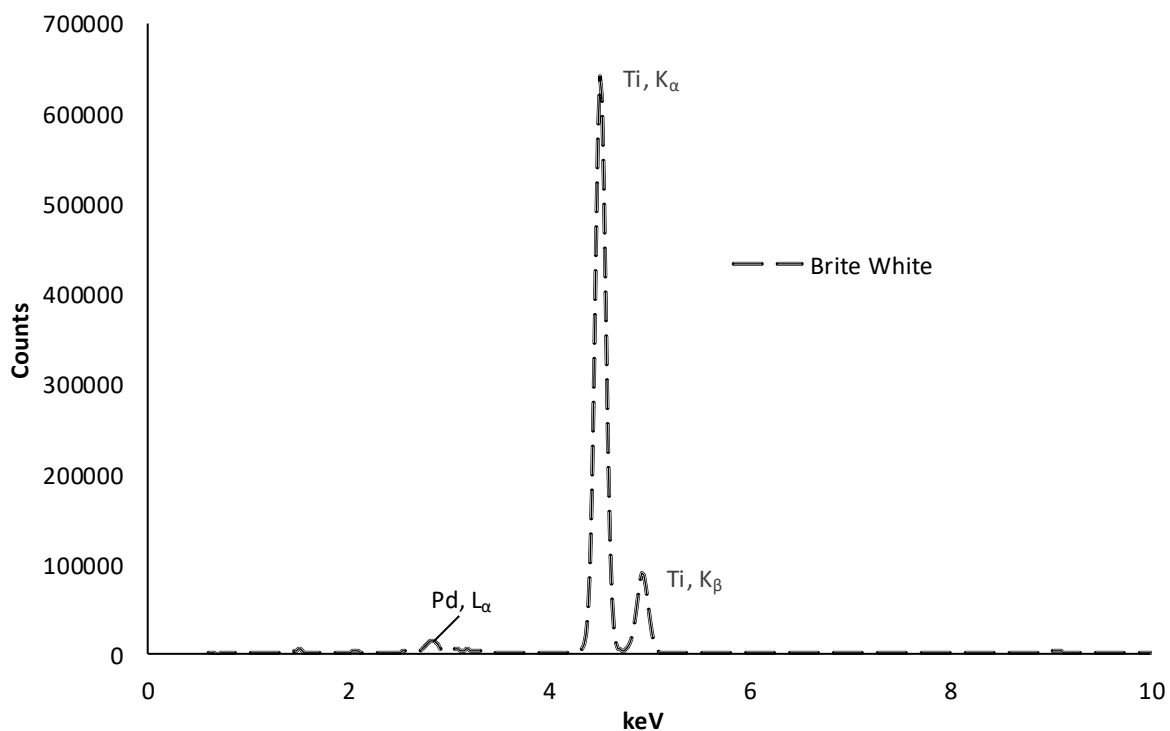


**Figure A 4.22:** Representative XRF spectra of Brite White. The specific transition and element are labeled for each major peak in the spectrum.

## Appendix 4.2

### Representative Infrared Spectra of Tattoo Ink samples



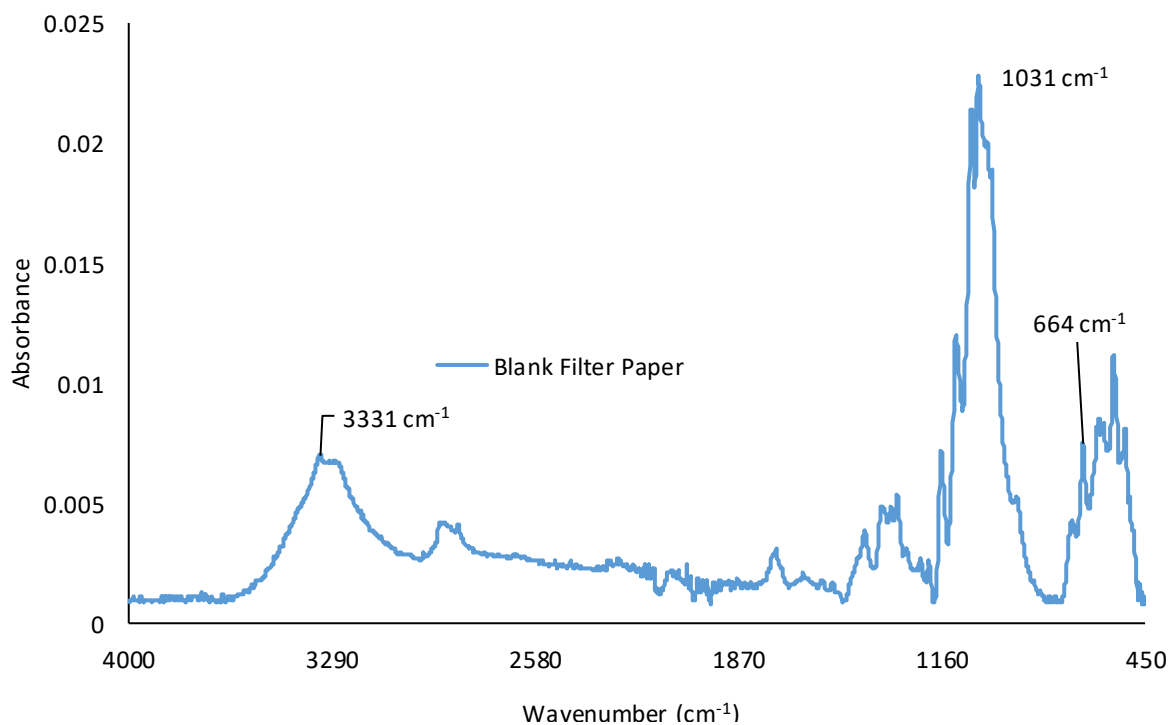


**Figure A 4.23:** Representative IR spectrum of Blank Filter Paper. The specific wavenumber is labeled for structurally indicative peaks in the spectrum.

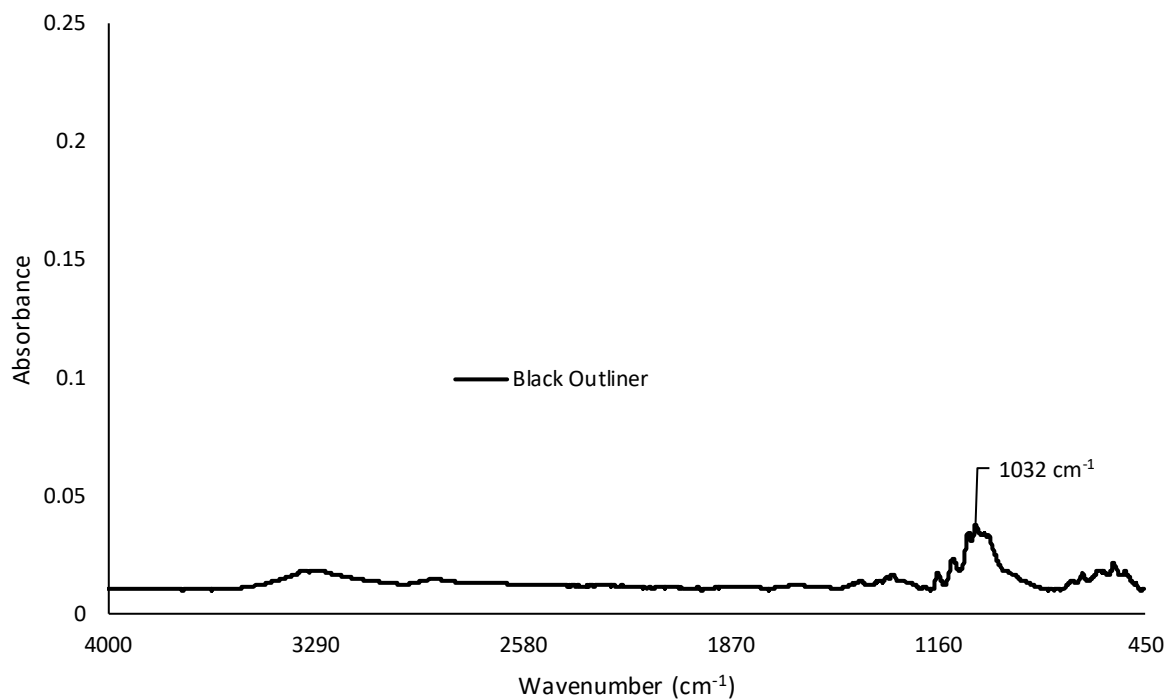


**Figure A 4.24:** Representative IR spectrum of Black Outliner ink. The specific wavenumber is labeled for structurally indicative peaks in the spectrum.

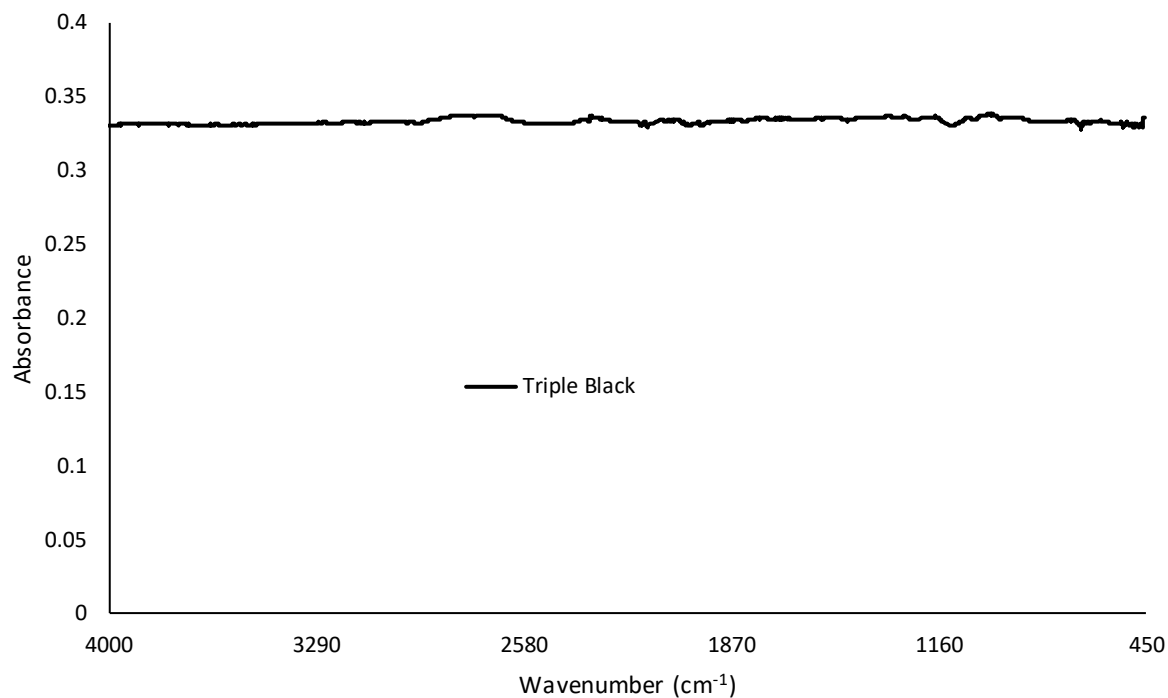


**Figure A 4.25:** Representative IR spectrum of Triple Black ink. The specific wavenumber is labeled for structurally indicative peaks in the spectrum.

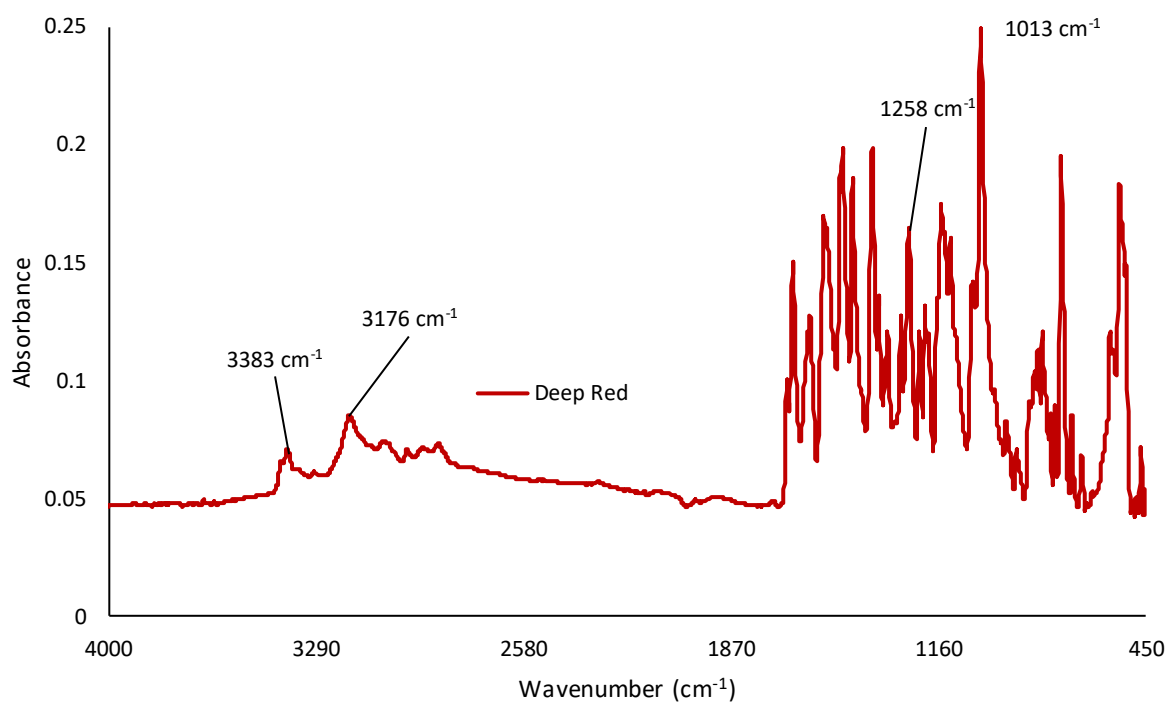


**Figure A 4.26:** Representative IR spectrum of Deep Red ink. The specific wavenumber is labeled for structurally indicative peaks in the spectrum.

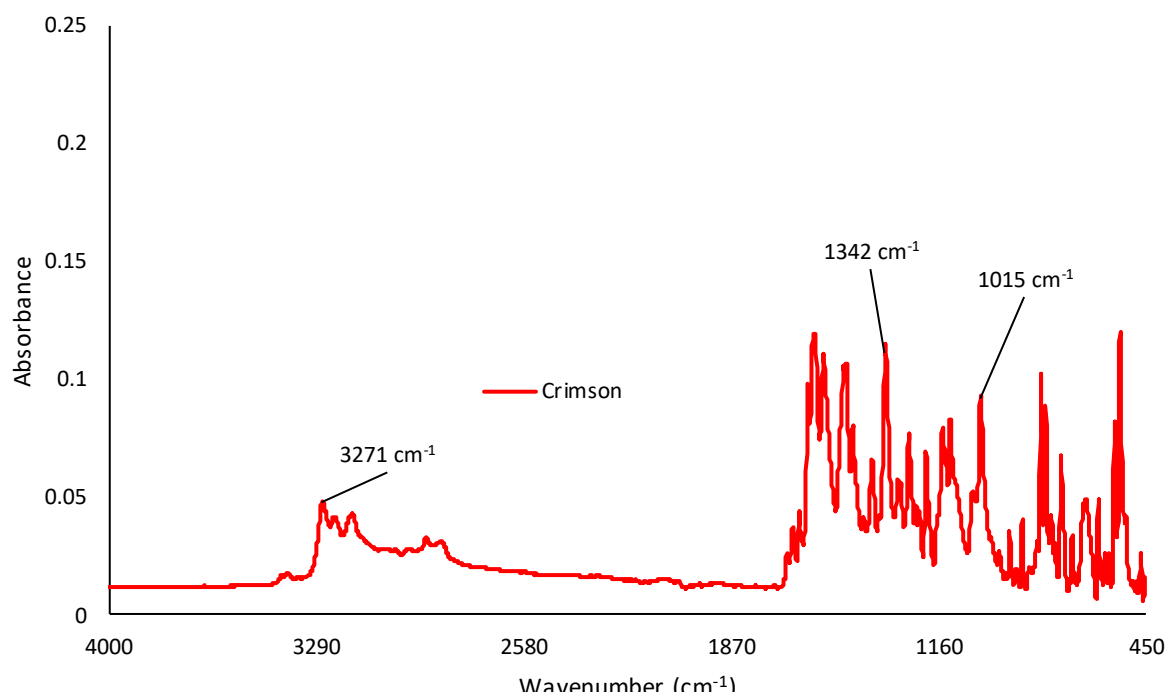


**Figure A 4.27:** Representative IR spectrum of Crimson Red ink. The specific wavenumber is labeled for structurally indicative peaks in the spectrum

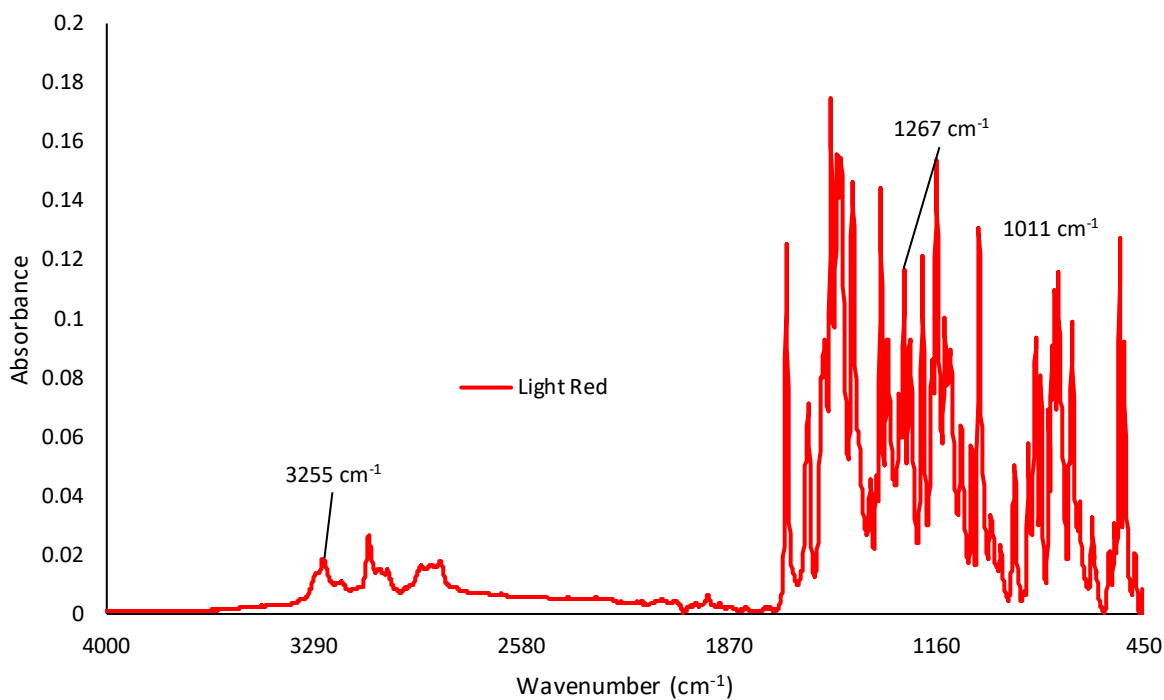


**Figure A 4.28:** Representative IR spectrum of Light Red ink. The specific wavenumber is labeled for structurally indicative peaks in the spectrum

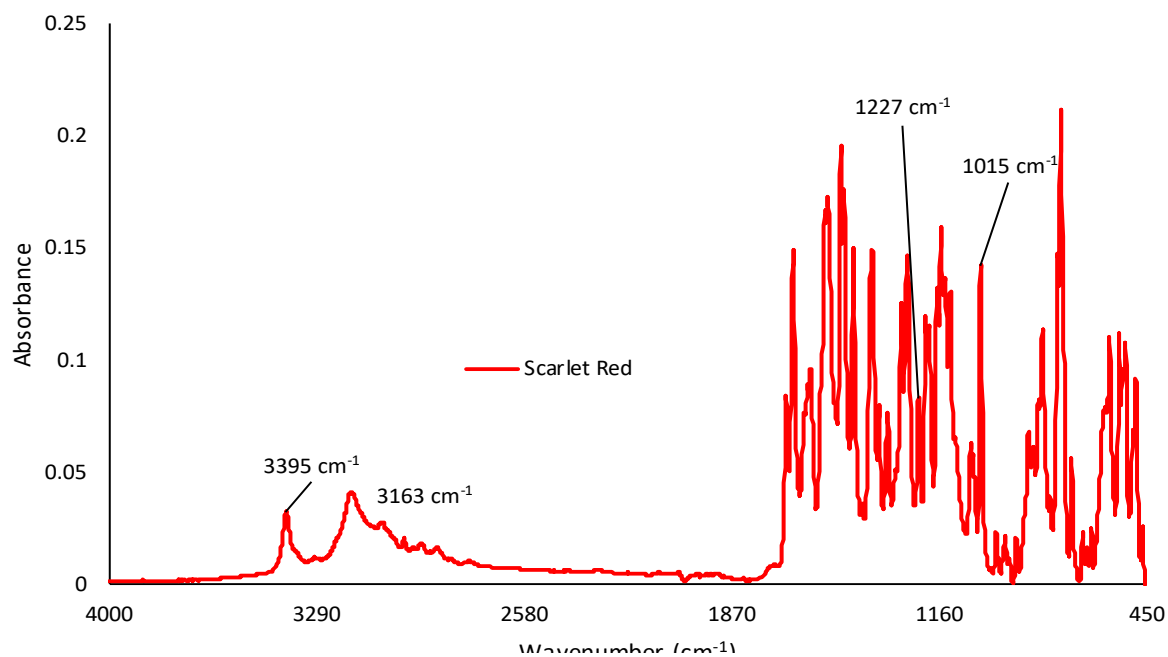


**Figure A 4.29:** Representative IR spectrum of Scarlet Red ink. The specific wavenumber is labeled for structurally indicative peaks in the spectrum

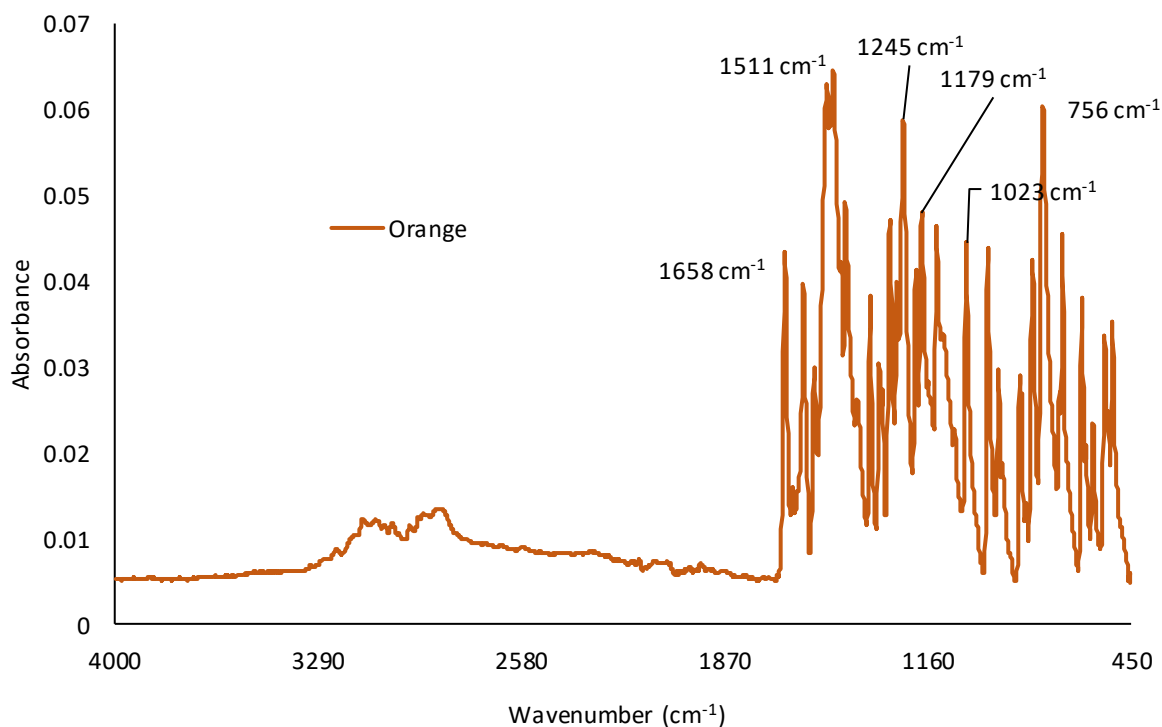


**Figure A 4.30:** Representative IR spectrum of Orange ink. The specific wavenumber is labeled for structurally indicative peaks in the spectrum.

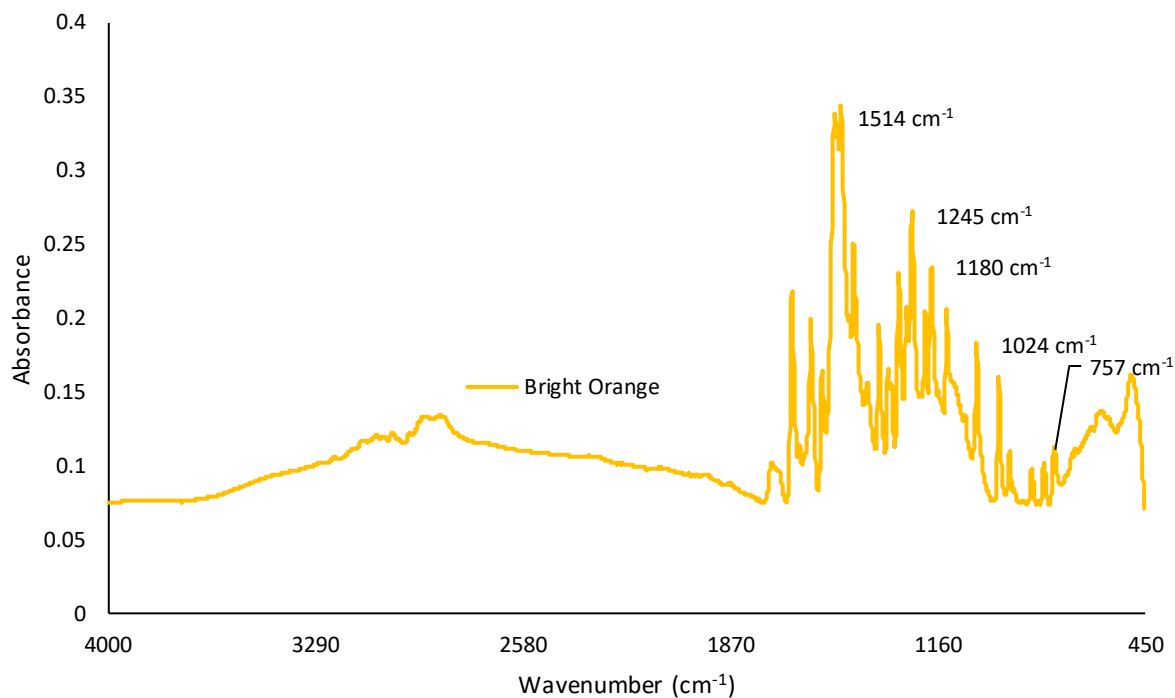


**Figure A 4.31:** Representative IR spectrum of Bright Orange ink. The specific wavenumber is labeled for structurally indicative peaks in the spectrum.

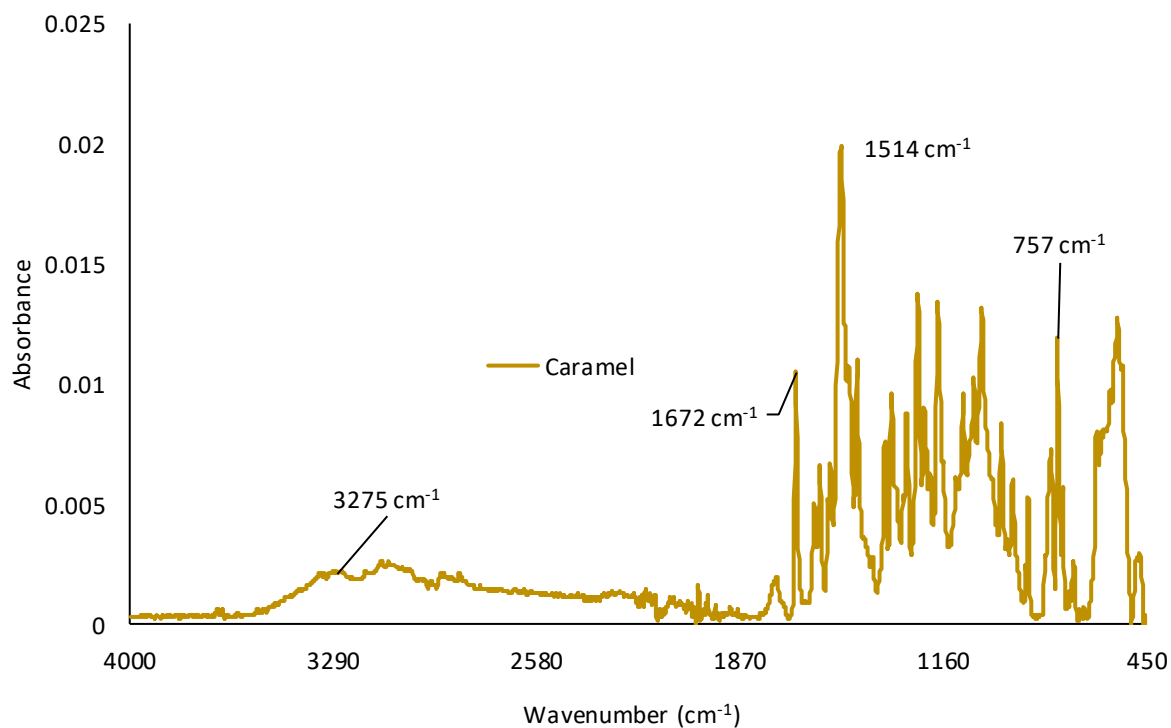


**Figure A 4.32:** Representative IR spectrum of Caramel ink. The specific wavenumber is labeled for structurally indicative peaks in the spectrum.

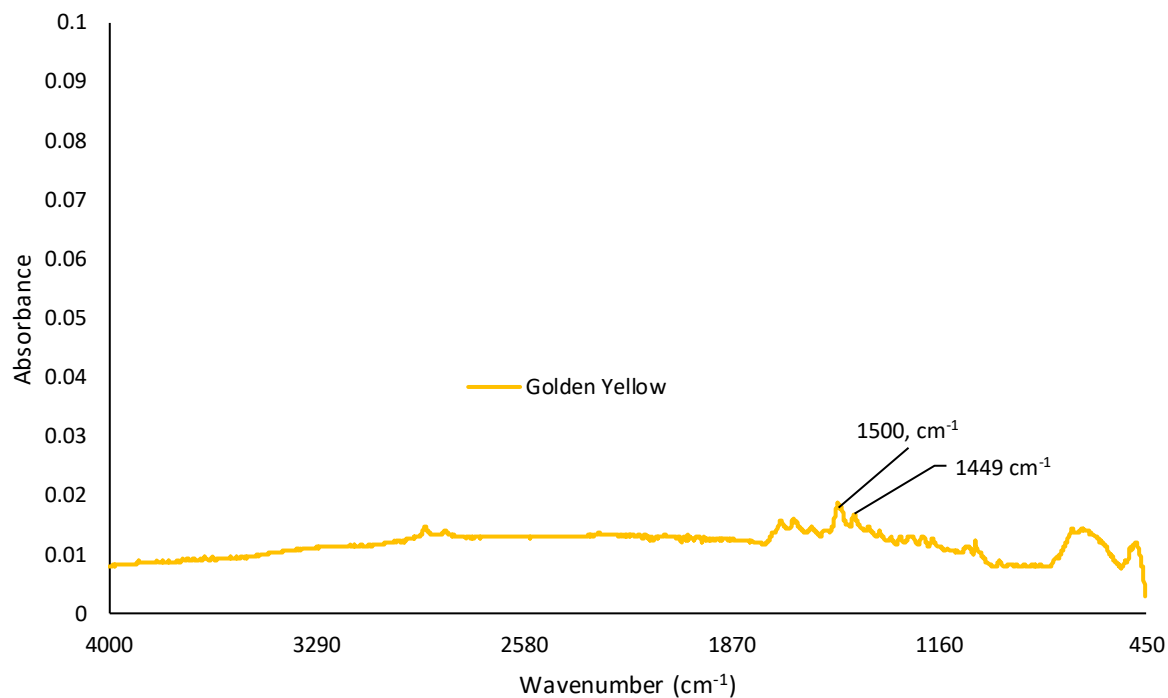


**Figure A 4.33:** Representative IR spectrum of Golden Yellow ink. The specific wavenumber is labeled for structurally indicative peaks in the spectrum

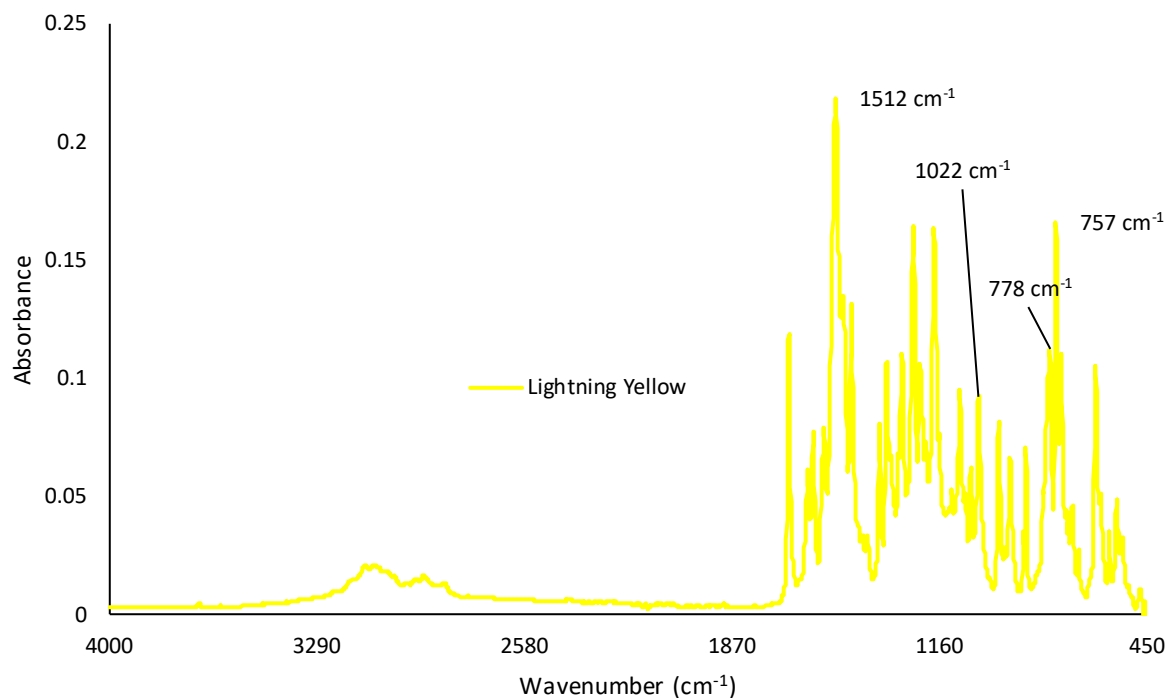


**Figure A 4.34:** Representative IR spectrum of Lightning Yellow ink. The specific wavenumber is labeled for structurally indicative peaks in the spectrum

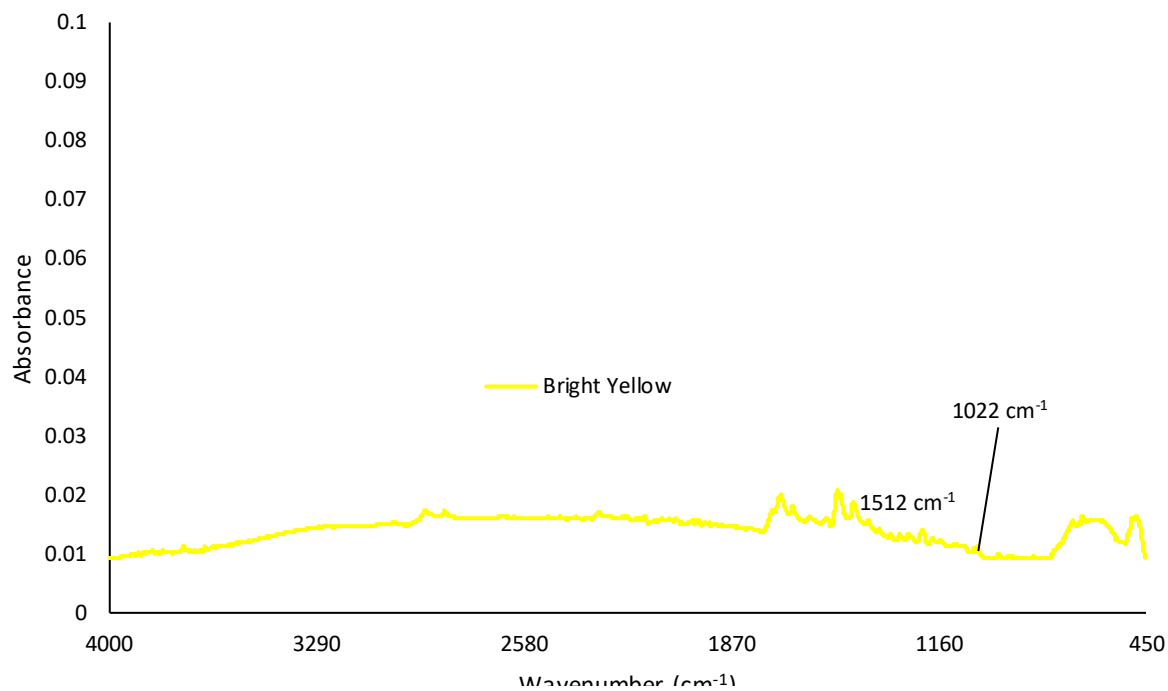


**Figure A 4.35:** Representative IR spectrum of Bright Yellow ink. The specific wavenumber is labeled for structurally indicative peaks in the spectrum

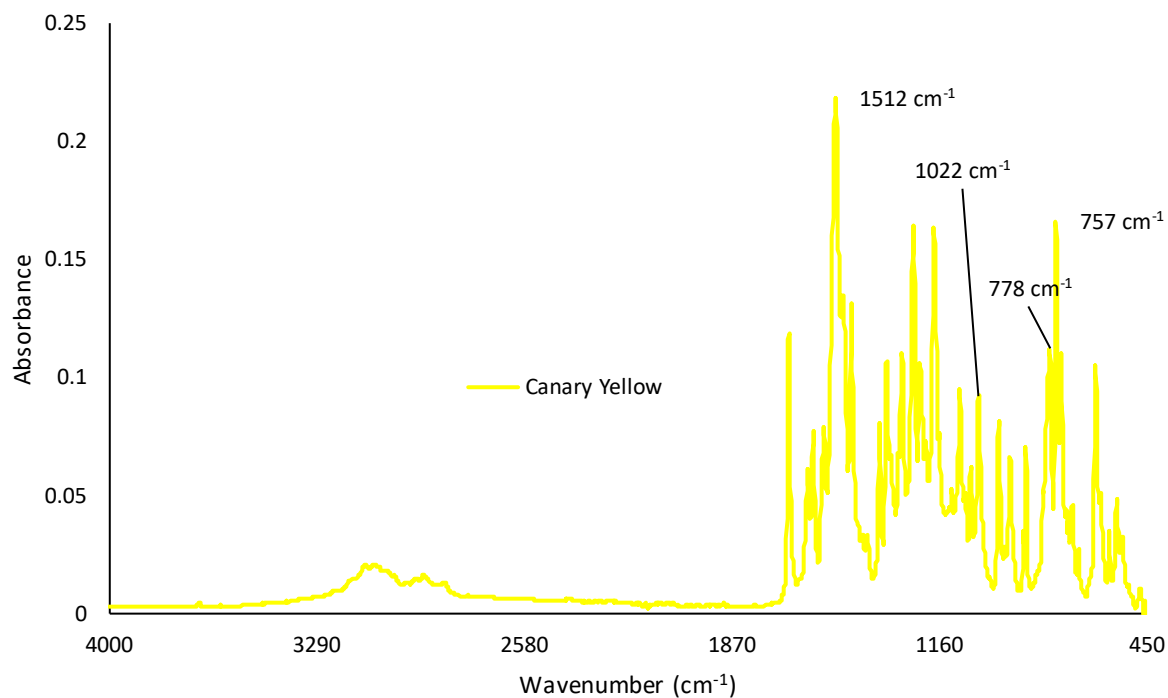


**Figure A 4.36:** Representative IR spectrum of Canary Yellow ink. The specific wavenumber is labeled for structurally indicative peaks in the spectrum

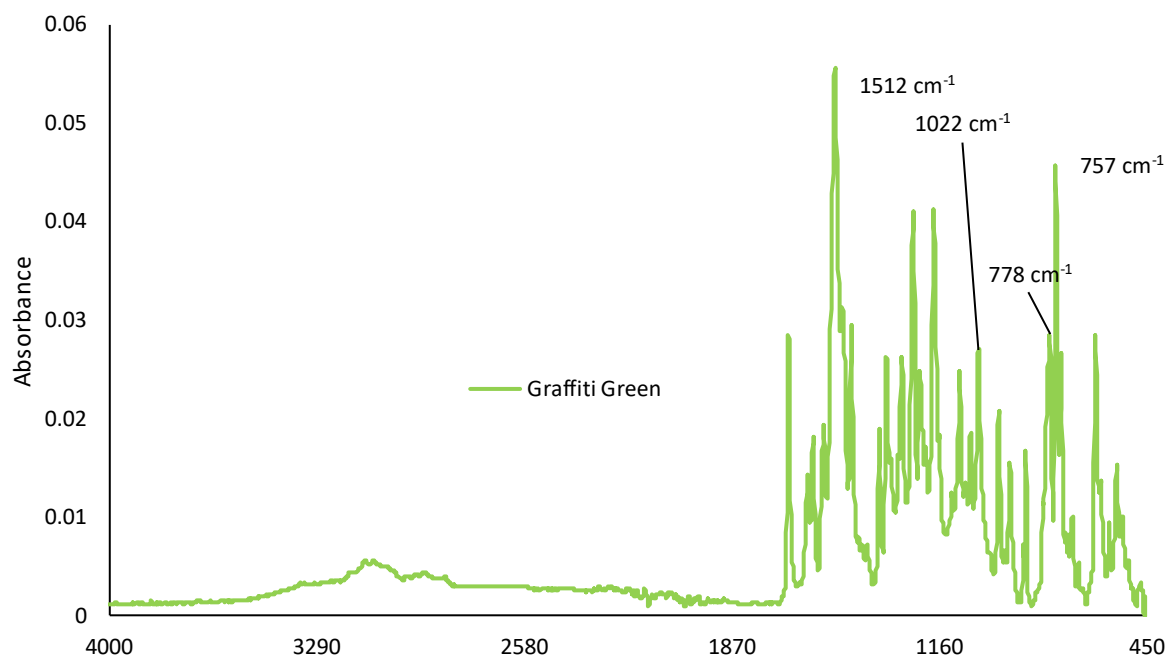


**Figure A 4.37:** Representative IR spectrum of Graffiti Green ink. The specific wavenumber is labeled for structurally indicative peaks in the spectrum

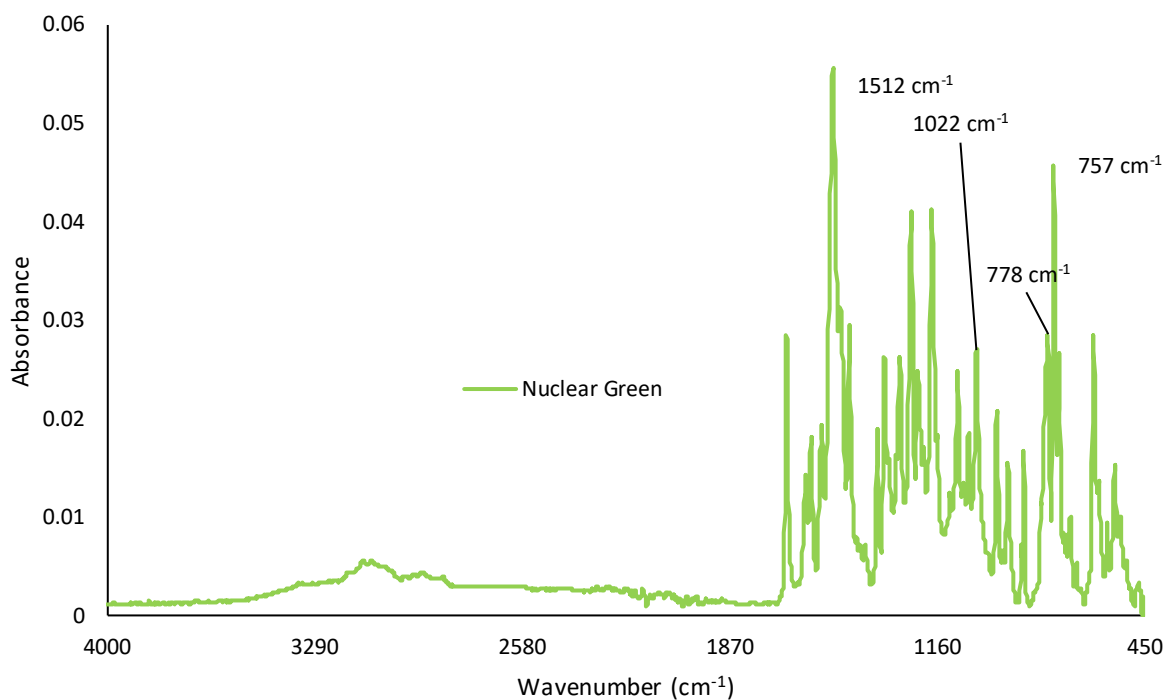


**Figure A 4.38:** Representative IR spectrum of Nuclear Green ink. The specific wavenumber is labeled for structurally indicative peaks in the spectrum



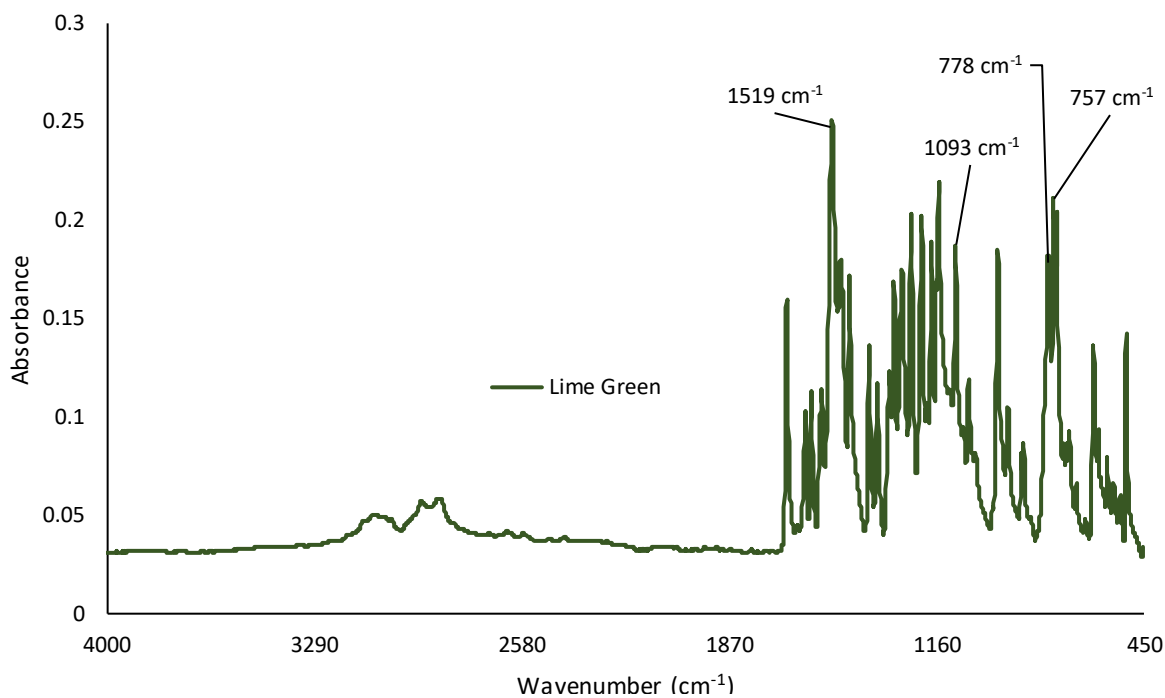


**Figure A 4.39:** Representative IR spectrum of Lime Green ink. The specific wavenumber is labeled for structurally indicative peaks in the spectrum

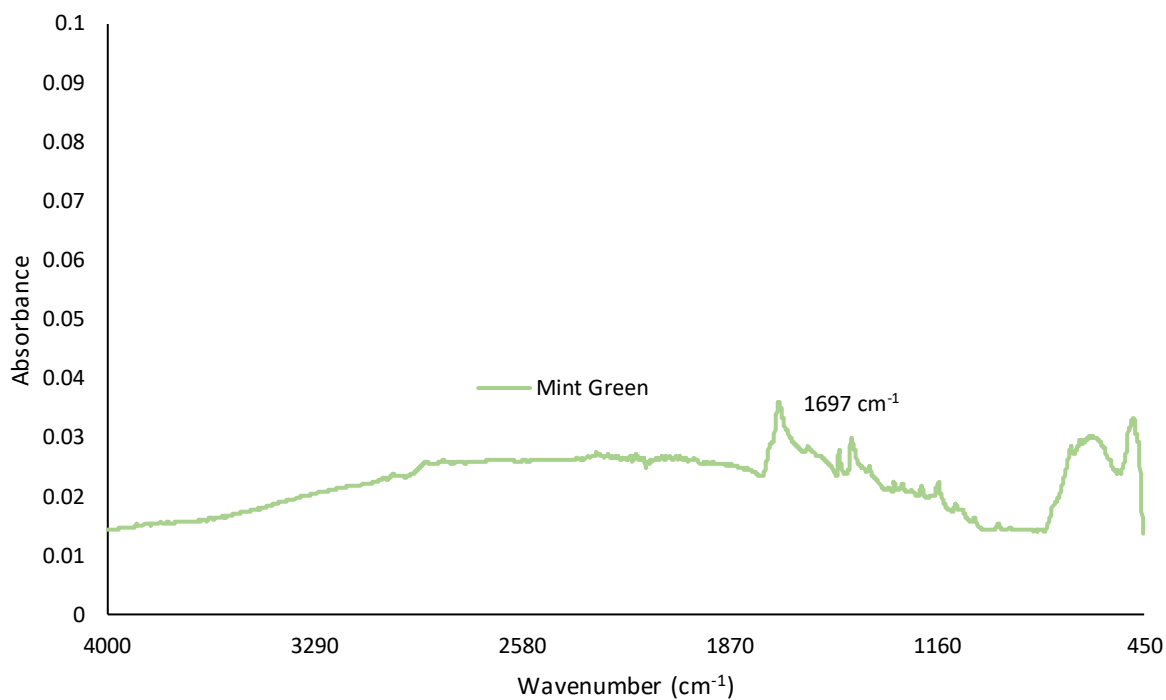


**Figure A 4.40:** Representative IR spectrum of Mint Green ink. The specific wavenumber is labeled for structurally indicative peaks in the spectrum

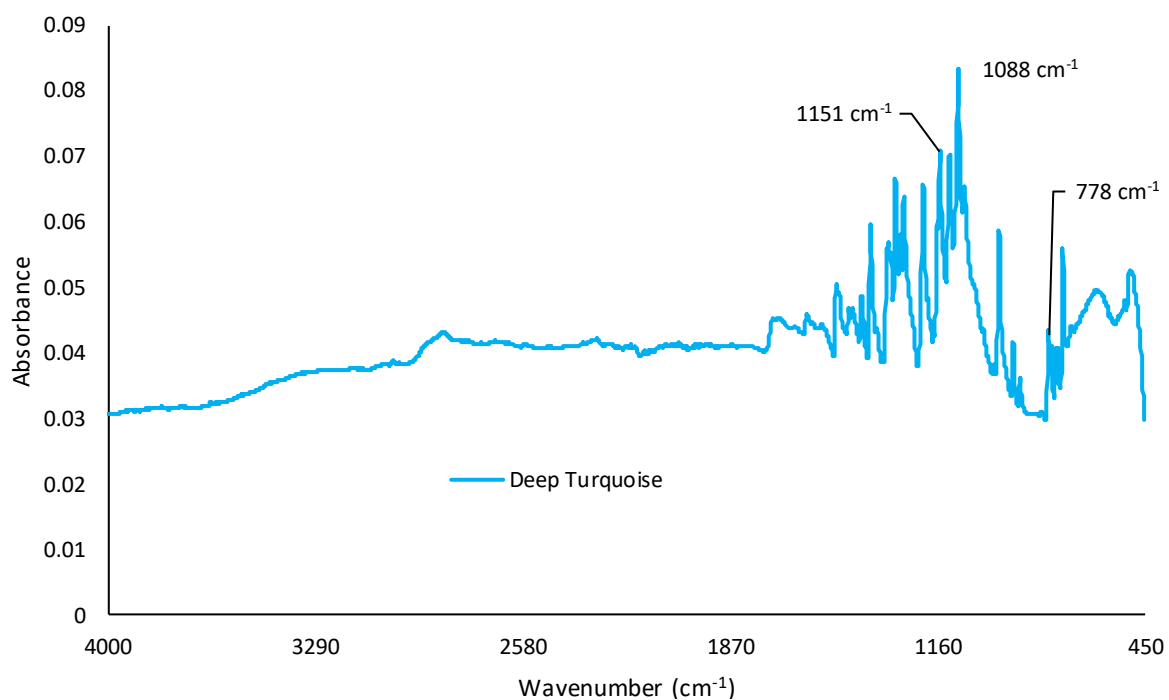


**Figure A 4.41:** Representative IR spectrum of Deep Turquoise ink. The specific wavenumber is labeled for structurally indicative peaks in the spectrum

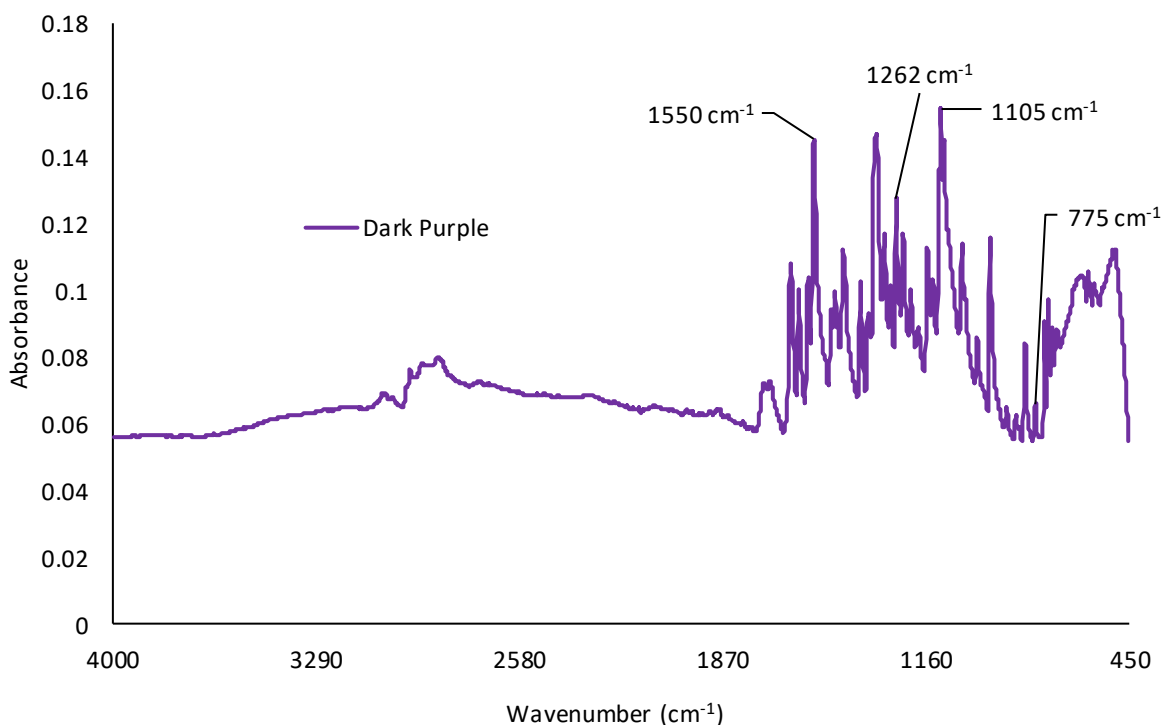


**Figure A 4.42:** Representative IR spectrum of Dark Purple. The specific wavenumber is labeled for structurally indicative peaks in the spectrum.

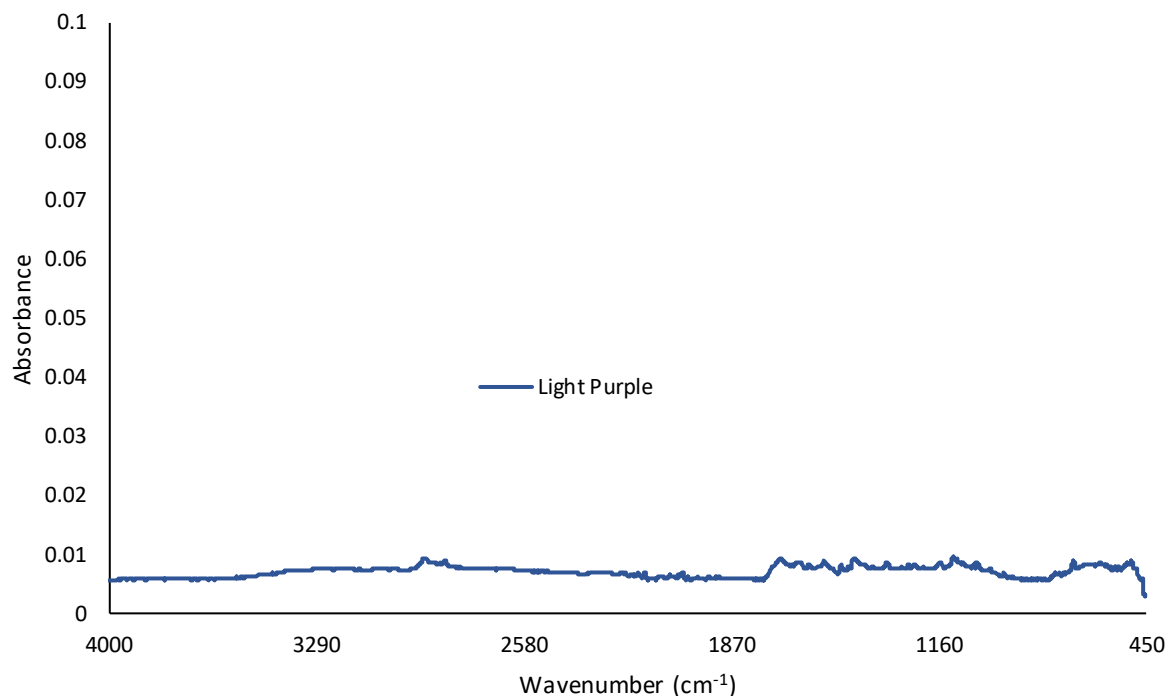


**Figure A 4.43:** Representative IR spectrum of Light Purple. The specific wavenumber is labeled for structurally indicative peaks in the spectrum.

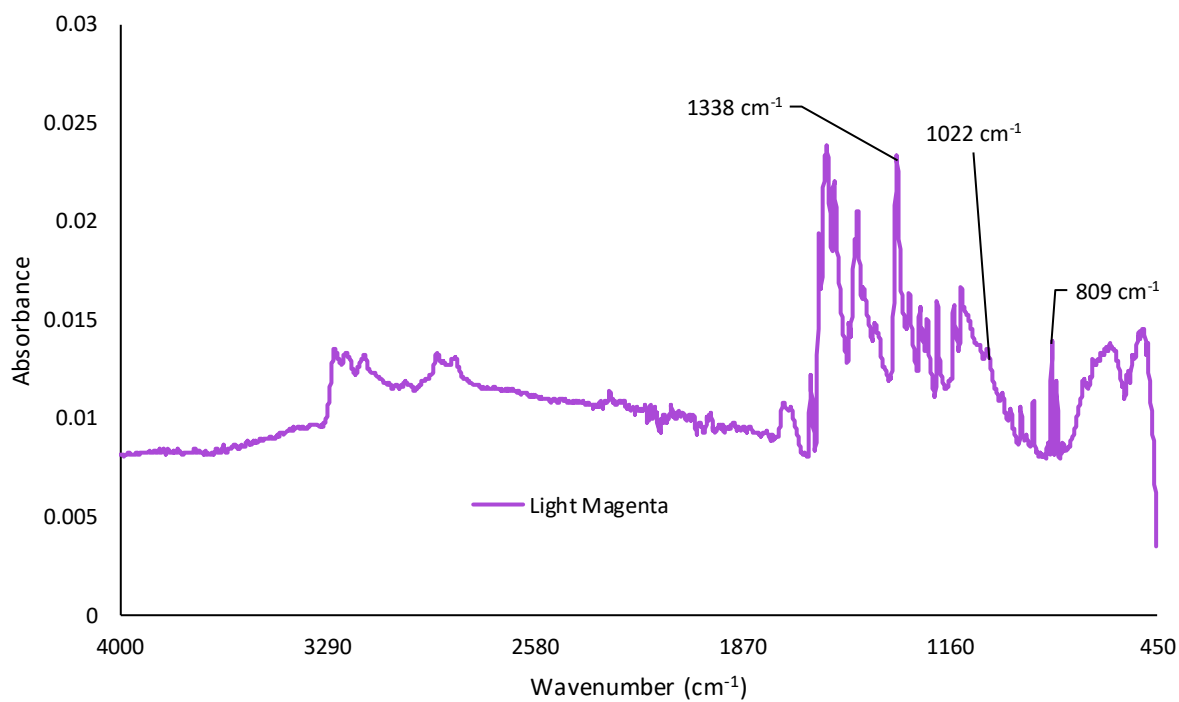


**Figure A 4.44:** Representative IR spectrum of Light Magenta. The specific wavenumber is labeled for structurally indicative peaks in the spectrum.

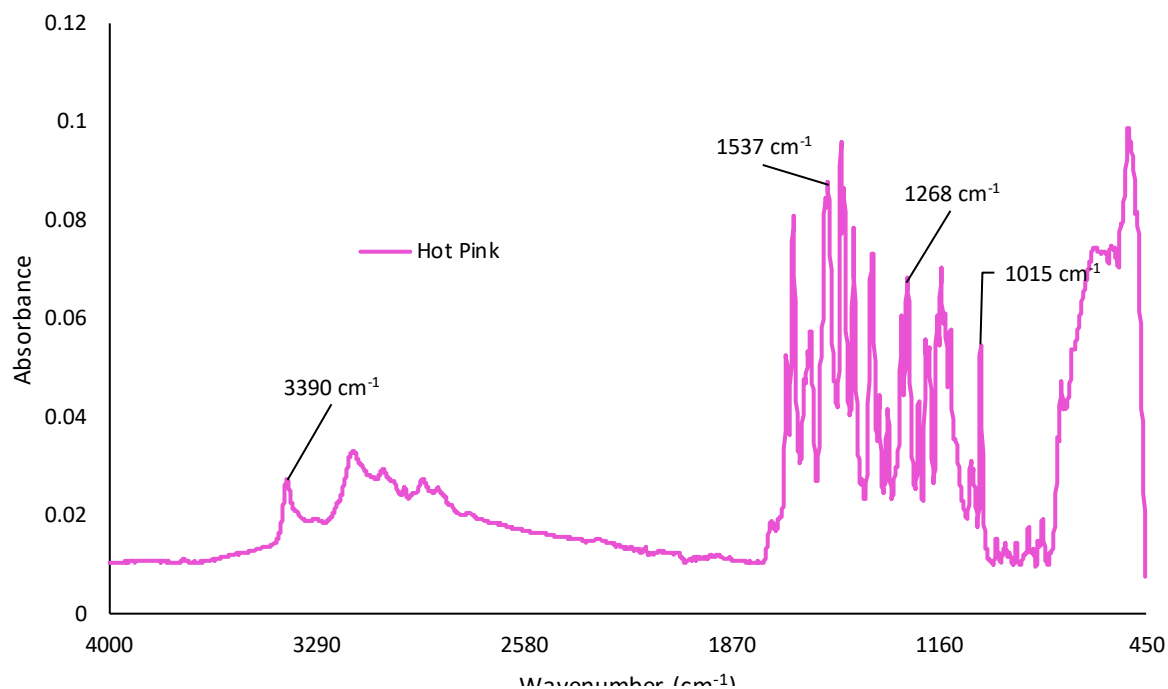


**Figure A 4.45:** Representative IR spectrum of Hot Pink. The specific wavenumber is labeled for structurally indicative peaks in the spectrum.

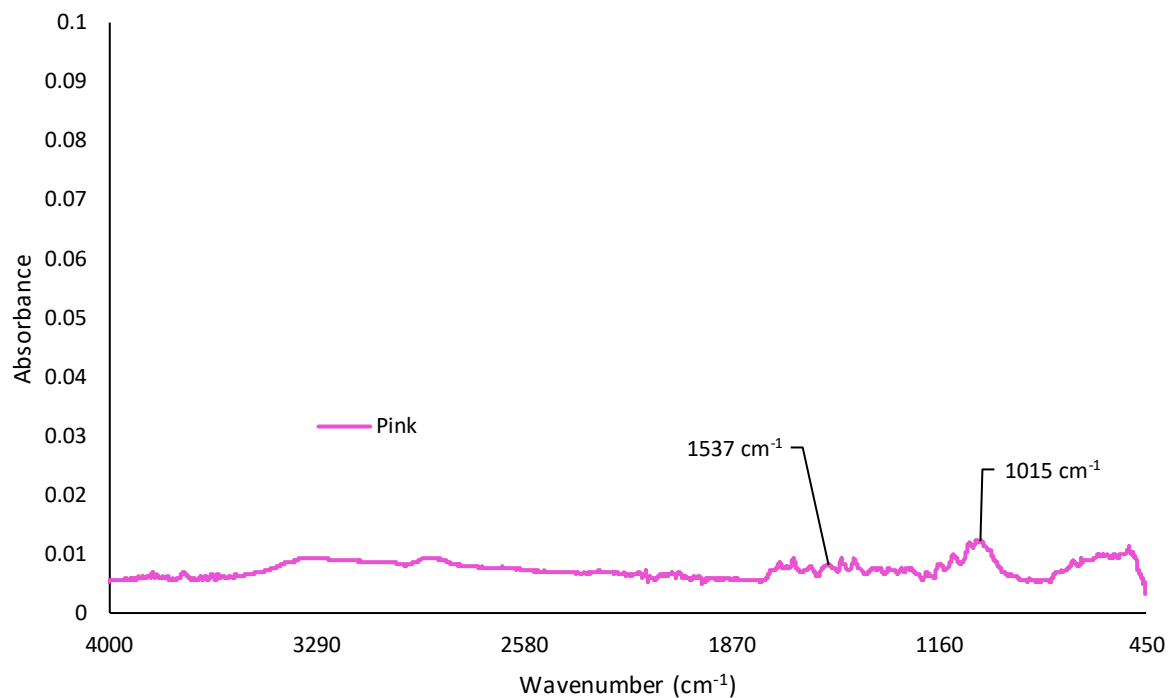


**Figure A 4.46:** Representative IR spectrum of Pink. The specific wavenumber is labeled for structurally indicative peaks in the spectrum.

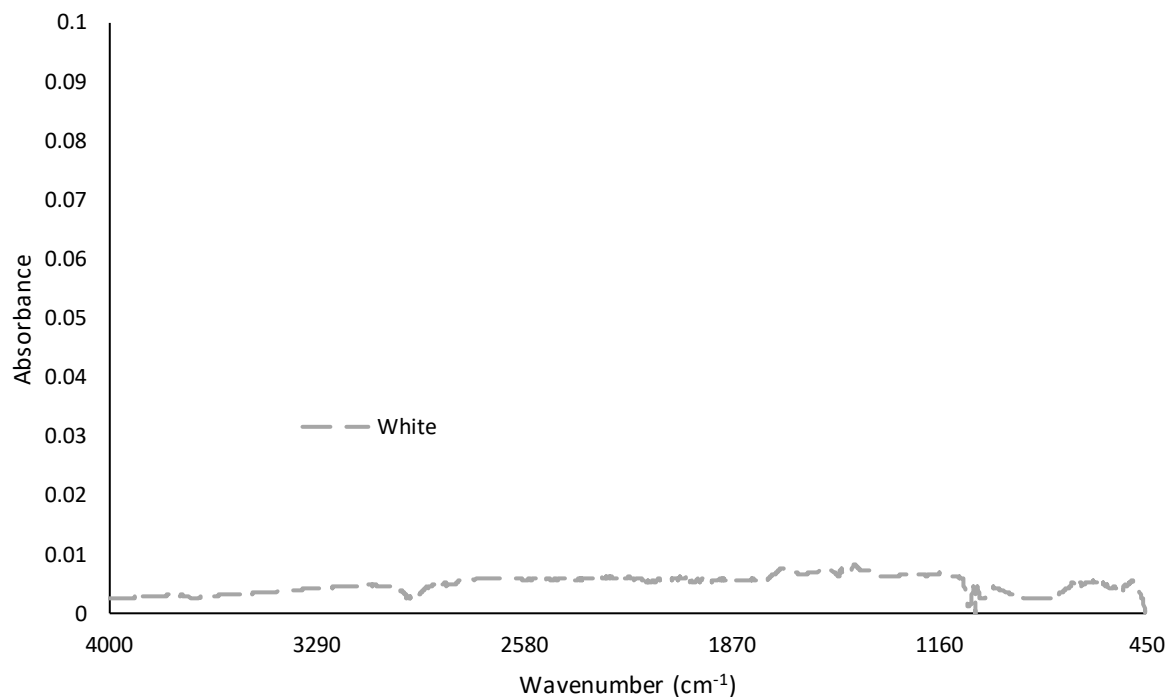


**Figure A 4.47:** Representative IR spectrum of White ink. The specific wavenumber is labeled for structurally indicative peaks in the spectrum.

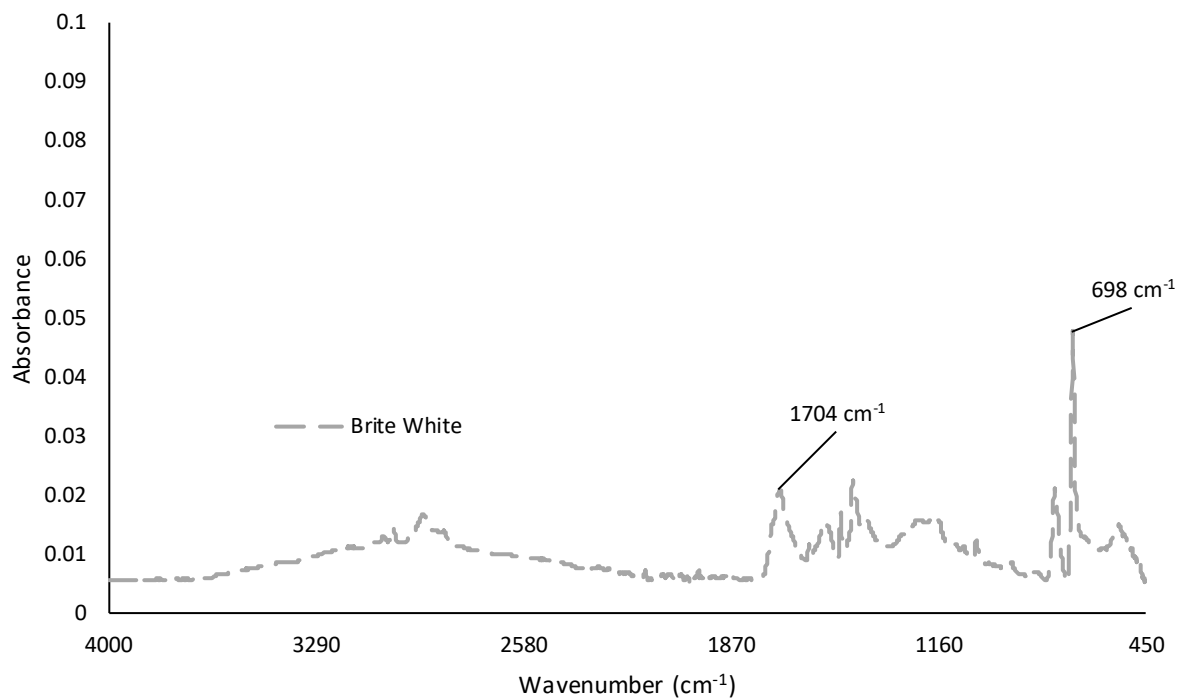


**Figure A 4.48:** Representative IR spectrum of Brite White ink. The specific wavenumber is labeled for structurally indicative peaks in the spectrum.

## REFERENCES

## REFERENCES

1. Miranda MD. Forensic Analysis of Tattoos and Tattoo Inks. 1 ed. Boca Rotan, Fl: CRC Press, 2016.
2. Forte G, Petrucci F, Cristuado A, Bocca B. Market survey on toxic metals contained in tattoo inks. *Science of the Total Environment*. 2009;407:5997-6002.
3. Chemical Substances in Tattoo Ink Survey of chemical substances in consumer products Copenhagen, DK: Miljøstyrelsen; 2012;155.
4. Wamer W, Yin J-j. Photocytotoxicity in human dermal fibroblasts elicited by permanent makeup inks containing titanium dioxide. *J Cosmet Sci*. 2011;62:535-47.
5. Basova T, Kiselev V, Schuster B-E, Peisert H, Chasse T. Experimental and theoretical investigation of vibrational spectra of copper phthalocyanine: polarized single-crystal Raman spectra, isotope effect and DFT calculations. *J Raman Spectrosc*. 2009;40:2080-7.
6. Brady R, Wake L. Principles and formulations for organic coatings with tailored infrared properties. *Progress in Organic Coatings*. 1992;20:1-25.
7. del Puerto E, Domingo C, Garcia J, Ramos G, Sanchez-Cortes S. Adsorption Study and Detection of the High Performance Organic Pigments Quinacridone and 2,9-Dimethylquinacridone on Ag Nanoparticles By Surface-Enhanced Optical Spectroscopy *Langmuir*. 2014;50:753-61.
8. van Es A, de Koeijer J, van der Peijl G. Discrimination of document paper by XRF, LA-ICP-MS and IRMS using multivariate statistical techniques *Science and Justice*. 2009;49:120-6.
9. Hoehse M, Paul A, Gornushkin I, Panne U. Multivariate classification of pigments and inks using combined Raman spectroscopy and LIBS *Anal Bioanal Chem*. 2012;402:1443-50.
10. Timko A, Miller C, Johnson F, Ross V. In Vitro Quantitative Chemical Analysis of Tattoo Pigments. *Arch Dermatol*. 2001;137:143-7.
11. Ropret P, Centeno S, Bukovec P. Raman identification of yellow synthetic organic pigments in modern and contemporary paintings: Reference spectra and case studies *Spectrochimica Acta*. 2008;69 486-97.

## Chapter 5 Mixed Inks and Tissue Sample Results and Discussion

Tattoos often consist of more than one color which may be combined in the body or analysis process. In order for an analysis of the tattoo ink components to successfully aid in the identification of highly decomposed remains, the analysis must be able to differentiate between inks which have been mixed and single inks. In order to determine if this was possible, several mixtures consisting of two inks were made. These ink mixtures were then analyzed with x-ray fluorescence (XRF) and infrared (IR) spectroscopy and processed using the multivariate statistical analyses performed in Chapter 4.

### 5.1 XRF analysis of Ink Mixtures

When the inks were mixed, the XRF spectrum of the mixed ink had peaks present that were present in both inks used to create it; the more ink present of one color in a mixture the more intense the peaks were that were associated with that color. For instance, mixtures of Lipstick Red and True Blue contained peaks associated with silicon (Si), copper (Cu), and titanium (Ti) with Si coming from Lipstick Red and Cu and Ti coming from True Blue (Figure 5.1A). In the Lipstick Red/True Blue 25/75 v/v mixture, the  $K_{\alpha}$  peak at 4.509 keV associated with Ti had an intensity of 582,114 counts. The intensity decreases to 553,340 and 492,549 counts in the mixtures which contain 50% and 25% True Blue, respectively. This would be expected as the amount of Ti should be less since less of the ink which contained Ti was used in these inks.

However, the ratio of intensities between peaks that originate from the same ink remains relatively the same. For instance, the ratio between the Ti  $K_{\alpha}$  peak and the Cu  $K_{\alpha}$  peak in True Blue is 9.2:1, in the Lipstick Red/True Blue 25/75 v/v mixture it is 8.7:1, in the 50/50 v/v mixture it is 8.7:1, and in the 75/25 v/v mixture it is 8.71:1. In comparison, the Ti  $K_{\alpha}$  peak and the Cu  $K_{\alpha}$



peak in Sky Blue ink is 58:1 (Figure 4.1). This would suggest that similar ratios between components from the same ink could lead to the association of the mixed ink with the ink that it originates from.

The Si  $K_{\alpha}$  peak follows the same decreasing intensity pattern with the intensity in the pure Lipstick Red ink being 164,014 counts, the intensity in the 75% Lipstick Red 25% True Blue mixture being 30,890 counts, the intensity in the 50% Lipstick Red 50% True Blue mixture being 10,788 counts, and the intensity in the 25% Lipstick Red 75% True Blue mixture being 3,083 counts. However, unlike with the Ti  $K_{\alpha}$  peaks in the Lipstick Red and True Blue mixtures, there is a large decrease in intensity of the Si  $K_{\alpha}$  peak between the pure ink sample of Lipstick Red and the 75% Lipstick Red 25% True Blue mixture. Also, peaks associated with Iron (Fe) and magnesium (Mg), which are elements found in Lipstick Red, do not appear in the mixed inks. The lack of peaks corresponding to Fe and Mg as well as the large decrease in intensity of the Si  $K_{\alpha}$  peak between the pure ink sample of Lipstick Red and the 75% Lipstick Red 25% True Blue mixture is likely due to the lower concentration of Si, Fe, and Mg in sample or the presence of Ti, the most intense peak in the spectrum, which absorbs x-rays.

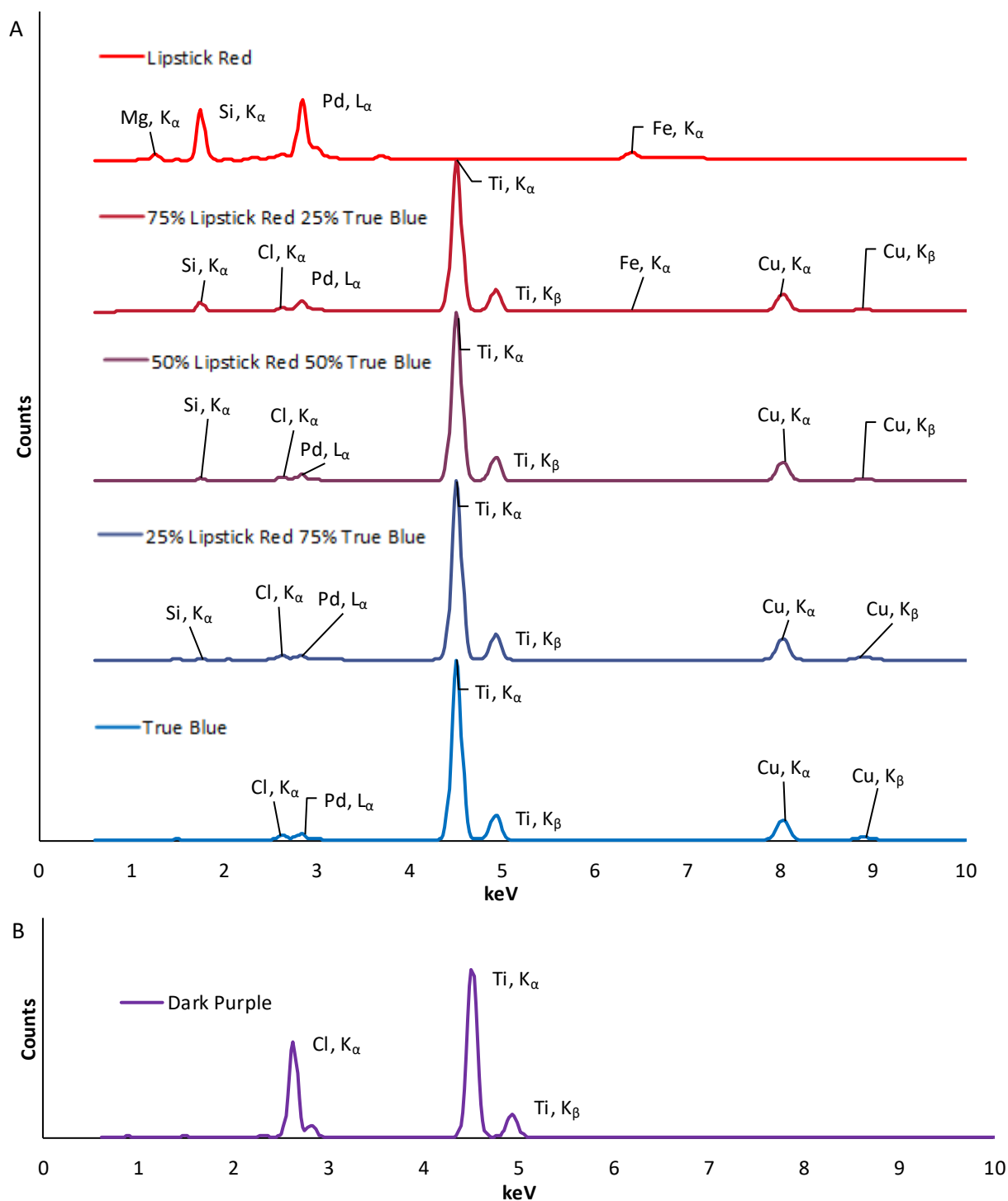


**Figure 5.1:** A) Representative XRF spectra of Lipstick Red and True Blue as well as 25/75, 50/50 and 75/25 v/v mixtures of these inks and B) Representative XRF spectrum of Dark Purple ink

When the 50% Lipstick Red 50% True Blue mixture is compared to the Dark Purple ink (Figure 5.1B), which is visually the closest in manufactured ink color to this ink, two differences are observed. The first is that the Dark Purple ink lacks Cu, which is present in the mixed ink due to copper phthalocyanine in True Blue which it is derived from. Also, the Dark Purple ink has a peak associated with chlorine (Cl) that is orders of magnitude greater than that observed in the mixed ink. These factors allow the Lipstick Red/True Blue 50/50 v/v mixture to be differentiated from the Dark Purple ink based on the inorganic data alone.

Figure 5.2A shows XRF spectra of the series of mixtures of Lightning Yellow and True Blue. In these mixtures, peaks associated with sulfur (S), Cl, Ti, and Cu are observed. Sulfur originates from the Lightning Yellow ink, Cu and Ti originate from the True Blue ink, and Cl originates from both inks. However, a majority comes from Lightning Yellow since the Cl peak in the XRF spectrum of Lightning Yellow is orders of magnitude greater than that observed in the True Blue ink XRF spectrum. Barium (Ba) is observed in the XRF spectrum of the Lightning Yellow ink but not in any of the mixtures due to the overlap of the Ba  $L_{\alpha}$  and  $L_{\beta}$  peaks with the Ti  $K_{\alpha}$  and  $K_{\beta}$  peaks.

Like in the Lipstick Red and True Blue mixtures, the intensity of the peaks correlating to Cu and Ti, present in True Blue, decrease in intensity as the amount of True Blue decreases in the Lightning Yellow and True Blue mixtures. However, the ratio of Ti to Cu remains relatively consistent with the ratio in the mixture which contains 75% True Blue being 9.3:1 and the ratio in the mixture which contains 50% True Blue mixture being 9.0:1. However, the ratio is 7.72:1 in the Lightning Yellow/True Blue 75/25 v/v mixture. The reason for this change for one sample is not clear.

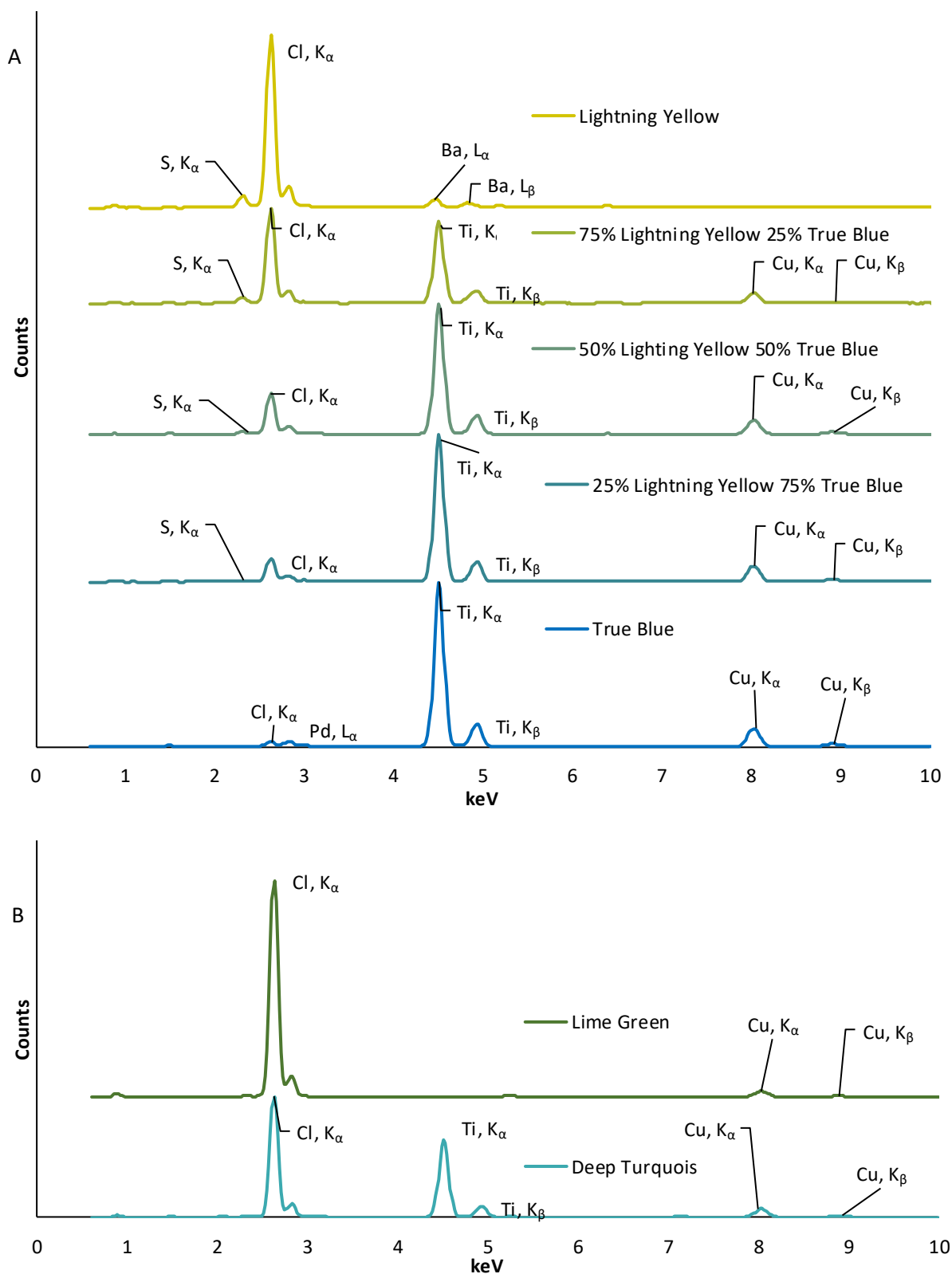


**Figure 5.2:** A) Representative XRF spectra of Lightning Yellow and True Blue as well as 25/75, 50/50 and 75/25 mixtures of these inks and B) Representative XRF spectra of Deep Turquoise and Lime Green

The elements associated with the Lightning Yellow ink, S and Cl, decreased in intensity as the amount of Lightning Yellow ink was decreased among the mixed Lightning Yellow and True Blue samples. For instance, in the Lightning Yellow ink, the Cl  $K_{\alpha}$  peak had an intensity of 617359 counts while the mixed inks that contained 75%, 50%, and 25% Lightning Yellow by volume have Cl  $K_{\alpha}$  peak intensities of 340,511 counts, 146,948 counts, and 84,949 counts respectively. The ratio between the Cl and S  $K_{\alpha}$  peaks also maintained a relatively constant ratio with the Lightning Yellow having a ratio of 14.21:1 Cl:S and the mixtures containing 75%, 50%, and 25% Lightning Yellow by volume having ratios of 14.7:1, 14.8:1, and 14.3:1 respectively. Although there is some contribution to the Cl  $K_{\alpha}$  peak from True Blue, it is not intense enough to skew the ratio. In comparison, the Canary Yellow ink (Figure 4.3) has a Cl:S ratio of 0.24:1, showing again that a ratio of two components found within the same ink could be used to associate mixtures of inks made from that ink with the original ink.

Two manufactured inks that resemble mixtures of Lightning Yellow and True Blue in color are Lime Green, which resembles the color of the Lightning Yellow/True Blue 75/25 v/v mixture, and Deep Turquoise, which resembles the color of the Lightning Yellow/True Blue 50/50 v/v mixture (Figure 5.2B). One component that differentiates the Lime Green ink from the Lightning Yellow/True Blue 75/25 v/v mixture is Ti which is not observed in Lime Green. Sulfur is also not observed in either the Deep Turquoise ink or the Lime Green ink, suggesting that differentiation among these inks and the mixed Lightning Yellow and True Blue ink would be possible based on the inorganic composition.

Due to the few peaks found in both the XRF and IR spectra of black inks, it was thought that the multivariate statistical techniques may not differentiate inks comprised of black ink

and another color from the color the black ink is mixed with. Along with the mixtures already mentioned, two other types of mixtures were also prepared. These consisted of mixtures of Lining Black with either True Blue or Lipstick Red. These mixtures containing Lining Black were made in order to determine if the presence of a black ink could be detected among inks of other colors.

Only two elements are observed in the spectrum of Lining Black, S and Fe (Figure 5.3A and Figure 5.4A). Neither True Blue nor Lipstick Red contains S; therefore, for a mixture of these inks with Lining Black to be distinguished from the original inks, the S  $K_{\alpha}$  peak must be observable. As can be seen in Figure 5.3 and Figure 5.4A, mixtures which contain at least 50% Lining Black by volume have an observable S peak and thus would be differentiated from the ink the Lining Black is mixed with based on the XRF spectra. However, the mixture of Lining Black and True Blue ink which contains 25% Lining Black by volume has a S  $K_{\alpha}$  peak that cannot be reliably differentiated from the baseline of the spectrum. No other peaks are present which would differentiate the mixture containing 25% Lining Black by volume from True Blue. This would suggest that IR would be necessary in order to differentiate this mixture from True Blue.

Inks which are similar in color to Lining Black and Lipstick Red mixtures, such as Deep Red and Dark Red, do not contain S either and would be able to be differentiated from these inks. The Deep Red and Dark Red inks also contain Fe  $K_{\alpha}$  peaks which are at least twice as intense

and Si  $K_{\alpha}$  peaks which are orders of magnitude less intense than peaks observed in the mixtures of Lining Black and Lipstick Red which would also lead to differentiation

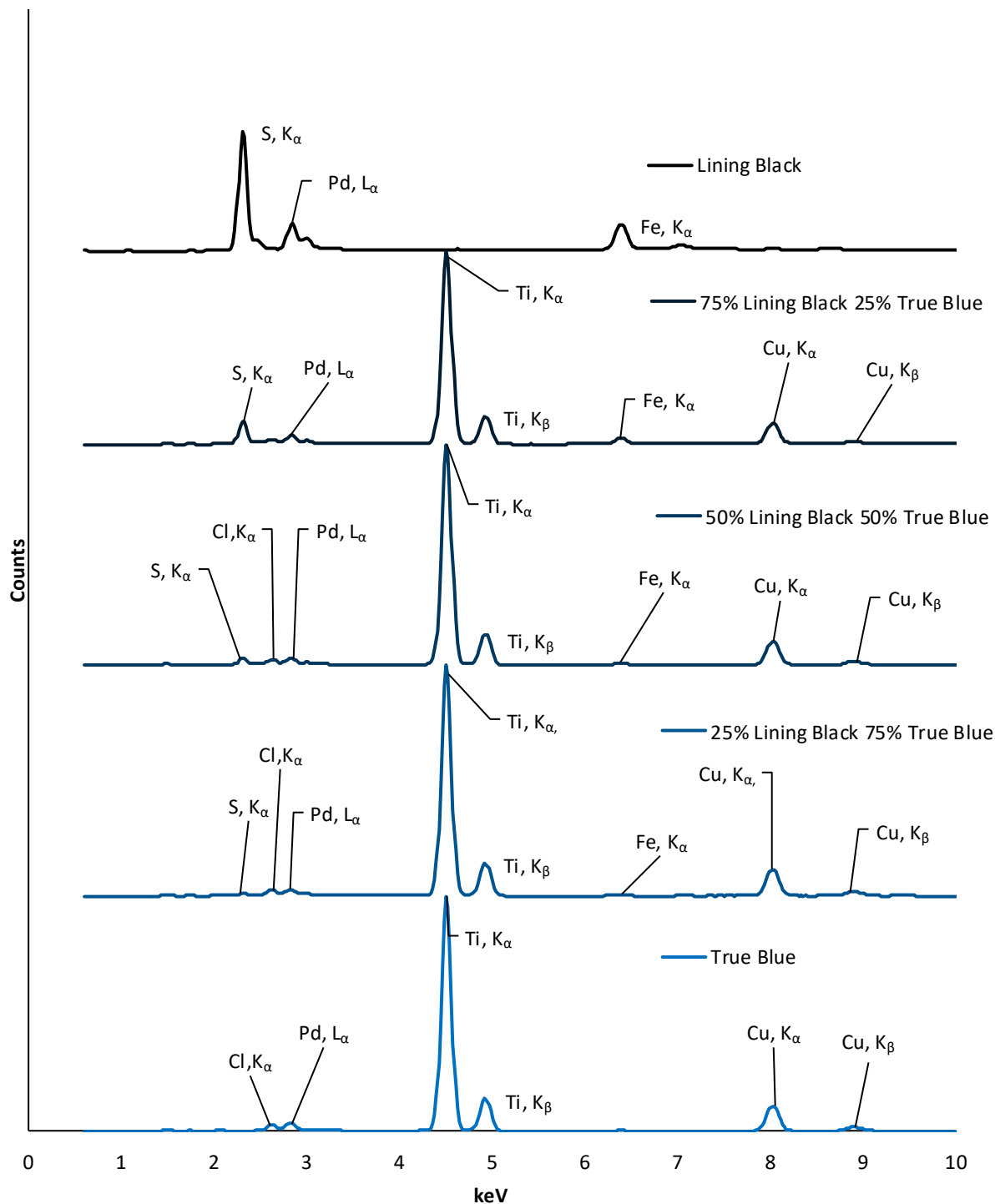


**Figure 5.3:** Representative XRF spectra of Lining Black and True Blue as well as 25/75, 50/50 and 75/25 mixtures of these inks

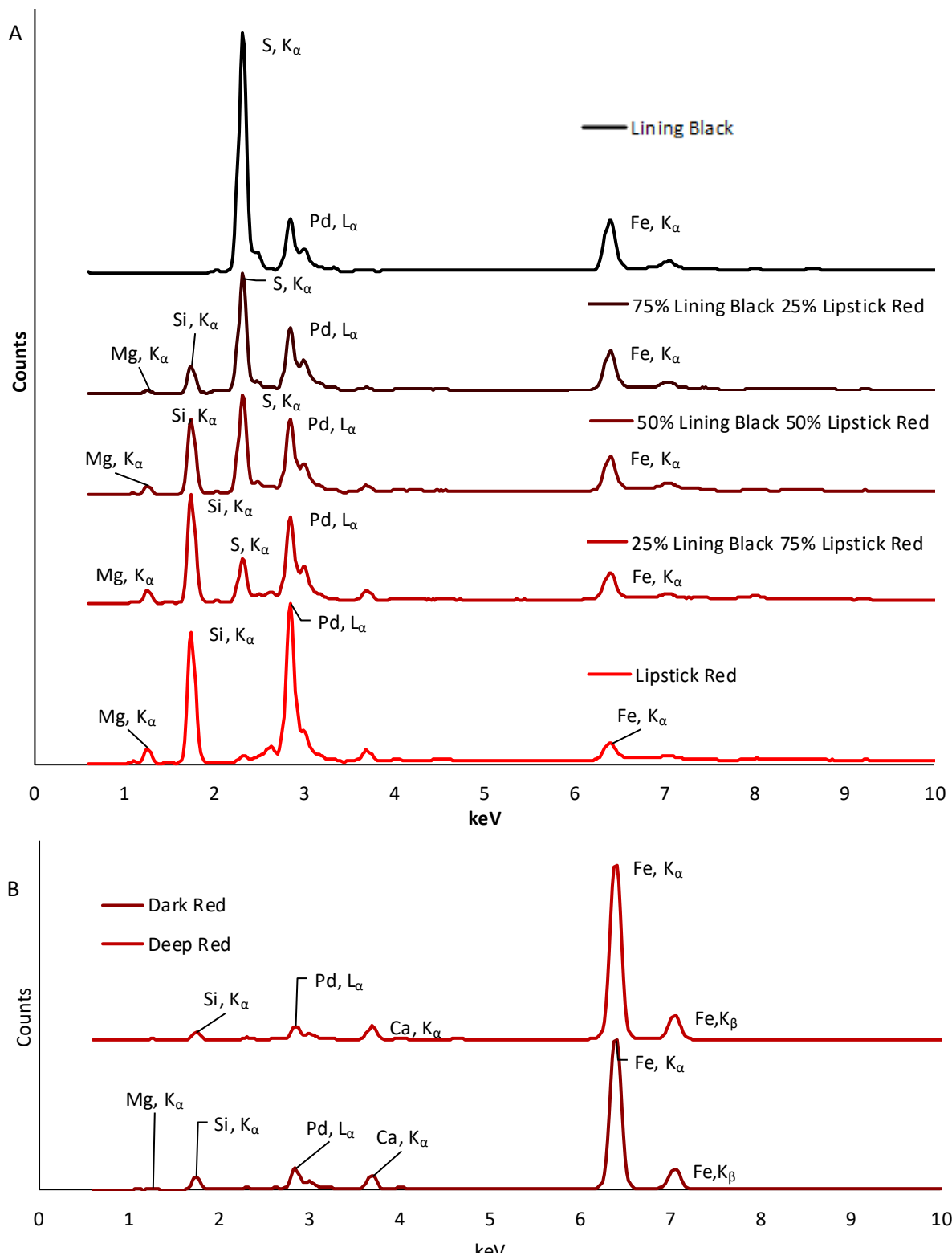


**Figure 5.4:** A) Representative XRF spectra of Lining Black and Lipstick Red as well as 25/75, 50/50 and 75/25 mixtures of these inks and B) Representative XRF spectra of Dark Red and Deep Red



## 5.2 IR analysis of Mixed Ink Samples

The infrared (IR) spectra of mixed inks contain peaks associated with both of the inks that the ink is derived from. In the IR spectra of the Lipstick Red/True Blue 50/50 and Lipstick Red/True Blue 25/75 v/v mixtures, absorptions were observed at 756, 781, 1066, and 1088  $\text{cm}^{-1}$  (Figure 5.5), which are consistent with copper phthalocyanine (1), a blue pigment found in the True Blue ink. However, in the Lipstick Red/True Blue 75/25 v/v mixture IR spectrum, the IR band at 1088  $\text{cm}^{-1}$  is one of the few indicative IR bands associated with copper phthalocyanine present. This is likely due to less copper phthalocyanine being present in the Lipstick Red/True Blue 75/25 v/v mixture, since the absorption is based on the concentration of the component.

Absorptions were also observed in the Lipstick Red/True Blue 75/25 v/v mixture and the Lipstick Red/True Blue 50/50 v/v mixture at 1016, 1226, 3166  $\text{cm}^{-1}$ , and 3392  $\text{cm}^{-1}$  which are indicative of the presence of quinacridone pigments (Table 1.1) found in red inks. The Lipstick Red/True Blue 25/75 v/v mixture only has the band at 1016  $\text{cm}^{-1}$  present from the bands associated with quinacridones. Unlike in the XRF spectrum, the intensities of the peaks are not directly comparable without SNV normalization due to different areas of the sample being analyzed. These different areas of the sample contain different thicknesses of ink, changing the intensities of bands. However, the presence of these peaks allows for the association of the Lipstick Red/ True Blue mixed inks to be associated with Lipstick Red. Similarly, the presence of peaks at 1088, 781, and 756  $\text{cm}^{-1}$  allow for the association of the Lipstick Red/True Blue mixtures to be associated with the True Blue ink. In order to determine if differentiation of the Lipstick Red and True Blue ink mixtures from manufactured inks of similar color was possible using IR, the mixtures were compared to the IR spectrum of Dark Purple, the manufactured ink

that is visually closest in color to the 50/50 Lipstick Red/True Blue v/v mixtures. Although the Dark Purple IR spectrum has a peak at  $1030\text{ cm}^{-1}$  which overlaps the band at  $1016\text{ cm}^{-1}$ , it is not as intense as the peak at  $1016\text{ cm}^{-1}$  in the 50/50 Lipstick Red and True Blue ink IR spectrum (Figure 5.5B). The IR spectrum of Dark Purple also lacks any of the peaks associated with the quinacridones from the red inks or the copper phthalocyanines from the blue inks. This would allow for differentiation between the Dark Purple and the Lipstick Red and True Blue mixtures through the use of IR.

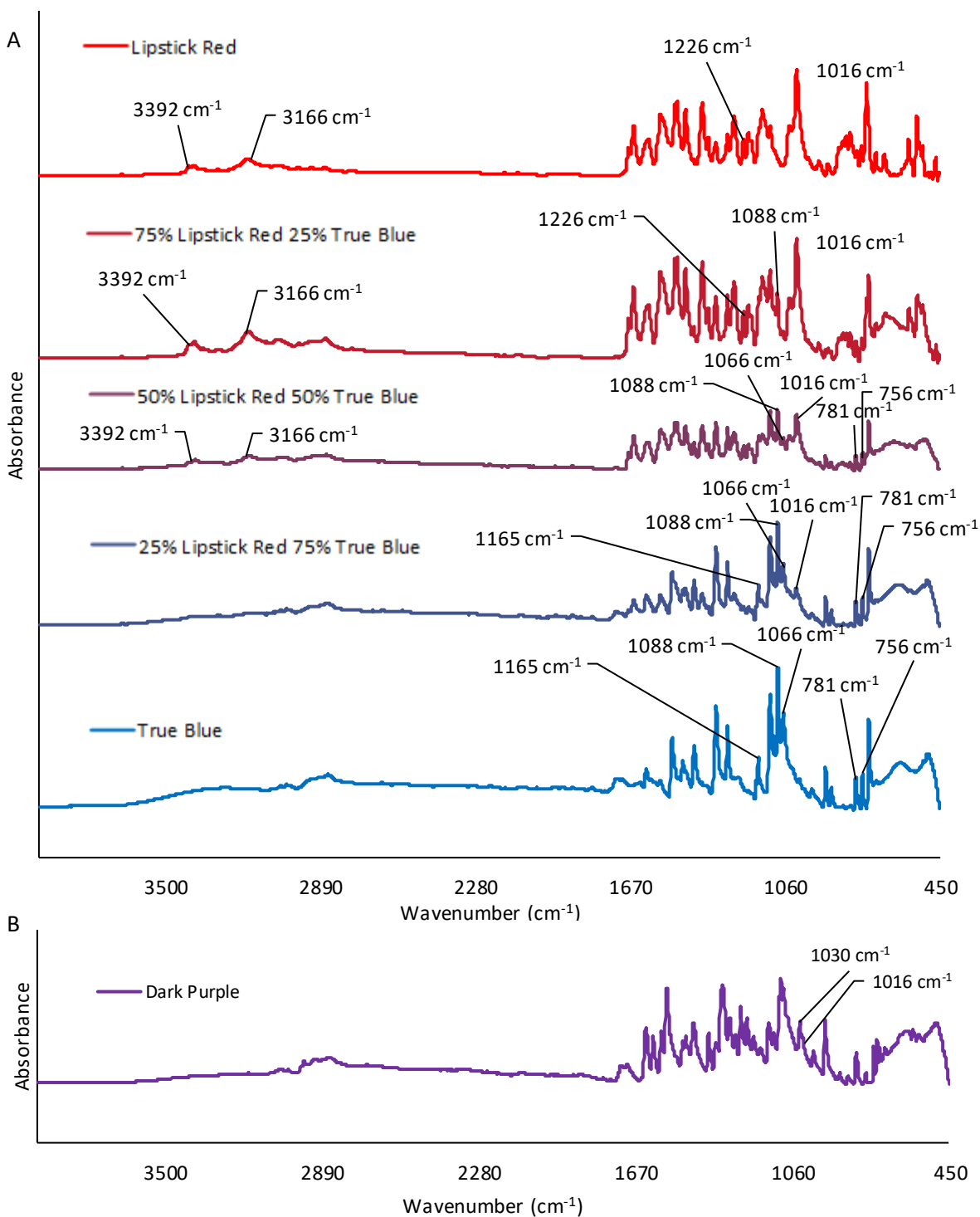


**Figure 5.5:** A) Representative IR spectra of Lipstick Red and True Blue as well as 25/75, 50/50 and 75/25 v/v mixtures of these inks and B) Representative IR spectrum of Dark Purple

The IR spectra of a series of mixtures between Lightning Yellow and True Blue are observed in Figure 5.6A. The first thing to note is that the Lightning Yellow and True Blue inks have many IR absorptions in common including, 756, 781, and  $1088\text{ cm}^{-1}$  which are associated with phthalocyanines. In section 4.3.2 it was suggested that this indicates the presence of an isoindole containing component in the Lightning Yellow ink. This makes direct comparisons of peak intensities difficult as the intensity of many of the peaks in the spectra of the Lightning Yellow and True Blue mixtures are dependent on both inks. However, general trends can be observed. For instance, in the True Blue ink, the  $1088\text{ cm}^{-1}$  band is the most intense peak in the spectrum. However, in the Lightning Yellow IR spectrum, a peak at  $1508\text{ cm}^{-1}$  is the most intense peak. A progression of the change in the intensities of these peaks can be observed in the Lightning Yellow and True Blue inks with the  $1088\text{ cm}^{-1}$  peak being the most intense peak in the 25/75 Lightning Yellow/True Blue v/v mixture, both the  $1088$  and  $1508\text{ cm}^{-1}$  peaks being almost the same intensity in the 50/50 Lightning Yellow/True Blue v/v mixture, and the  $1508\text{ cm}^{-1}$  peak being the most intense peak in the 75/25 Lightning Yellow/True Blue v/v mixture. This would be expected as the concentration of the True Blue ink decreases and the concentration of the Lightning Yellow ink increases among these ink mixtures. In addition to this, the XRF spectrum of Lightning Yellow and True Blue ink share no peaks in common, allowing for further association of the mixtures of these inks with their manufactured ink sources.

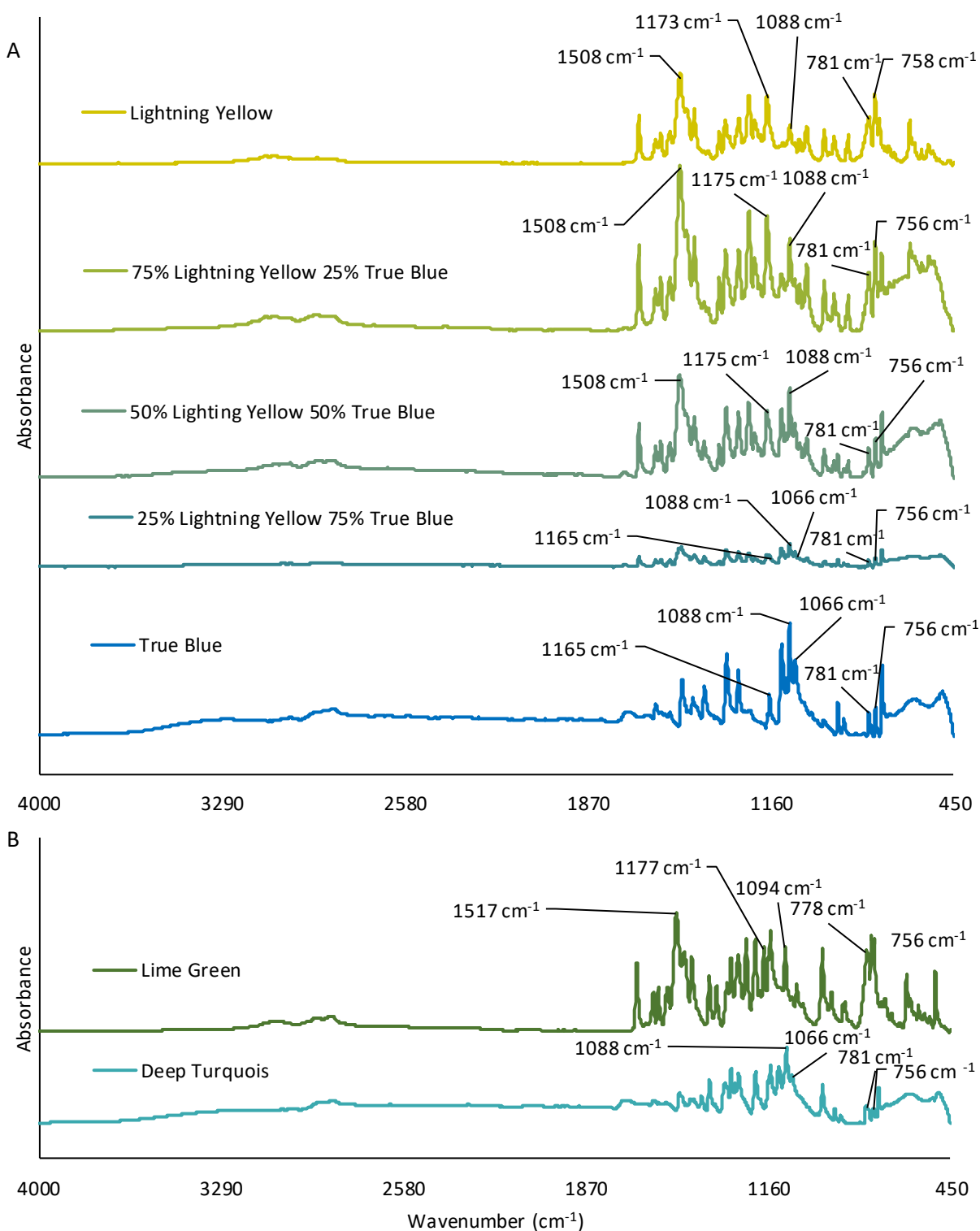


**Figure 5.6:** A) Representative IR spectra of Lightning Yellow and True Blue as well as 25/75, 50/50 and 75/25 mixtures of these inks and B) Representative IR spectra of Deep Turquoise and Lime Green

When the IR spectra of the True Blue and Lightning Yellow mixtures are compared to the IR spectra of Lime Green and Deep Turquoise, many of the same peaks are observed, however, they are shifted in wavenumber. In the Lime Green spectrum, the most intense peak is at  $1517\text{ cm}^{-1}$  which is close to the  $1508\text{ cm}^{-1}$  observed in the Lightning Yellow and True Blue mixtures. Peaks are also observed at  $1177$ ,  $1094$ ,  $778$  and  $756\text{ cm}^{-1}$  in the Lime Green spectrum. This causes the spectrum to look very similar to that of the 75/25 Lightning Yellow/True Blue v/v mixture; however, the Lime Green spectrum's peaks at  $778$  and  $756\text{ cm}^{-1}$  are more intense when compared to other peaks in the spectrum than the peaks at  $781$  and  $756\text{ cm}^{-1}$  in the 75/25 Lightning Yellow/True Blue v/v mixture. This could aid in differentiation. Further differentiation of these mixtures from Lime Green is possible through the presence of Ti in the mixed samples, mentioned in section 5.1. As for the spectrum for Deep Turquoise, it completely lacks peaks near  $1508\text{ cm}^{-1}$  allowing for it to be easily differentiated from the Lightning Yellow and True Blue ink mixtures.

As previously mentioned in section 4.3.1, the black inks have featureless IR spectra (Figure 4.5). When the featureless spectra are standard normal variate (SNV) normalized, peaks that are caused by drift in the IR background are accentuated (Figure 4.7) which cause artifacts. When the Lining Black ink is mixed with the True Blue ink in any proportion, all peaks in the IR spectrum become orders of magnitude less intense than peaks within the IR spectrum of True Blue. As the intensity of the peaks in the IR spectra of the Lining Black and True Blue ink have such a low intensity, SNV normalization causes artifacts to be accentuated as in the Lining Black inks. IR peaks associated with copper phthalocyanine, found in blue inks, such as  $1088\text{ cm}^{-1}$ , attributed to the  $\text{C}_\alpha\text{-N}_\alpha$  and  $\text{N}_\alpha\text{-Cu-N}_\alpha$  vibration, and  $1165\text{ cm}^{-1}$ , which is assigned to C-C bond

consistent with phthalocyanine (1), are still observable in the mixed Lining Black and True Blue IR spectrum which contain 50% or more True Blue ink (Figure 5.7). However, the intensity of the 1088 and 1165  $\text{cm}^{-1}$  peaks between the 50/50 and 25/75 Lining Black/True Blue mixtures which are similar. This does not allow differentiation between these ink mixtures. Also, the Lining Black and True Blue mixture which contains 75% Lining Black has a featureless IR spectrum like the Lining Black ink and therefore would not be able to be differentiated from Lining Black. Due to these issues, it would be necessary to observe the XRF spectra of these inks as well in order to differentiate them which is possible based on the intensity of the Ti and Cu peaks in their spectra.

Peaks associated with quinacridones, 1016, 1226, 3166  $\text{cm}^{-1}$ , and 3392  $\text{cm}^{-1}$ , are observed in mixtures of Lipstick Red and Lining Black which contain 50% or more Lipstick Red. Similar to the Lining Black and True Blue mixtures, a decrease in the intensity of all peaks associated with Lipstick Red is observed in the mixtures Lining Black and Lipstick Red, especially in the mixtures which contain 50% or more Lining Black where the peaks are orders of magnitude less intense (Figure 5.8A) than those observed in Lipstick Red. However, unlike in the mixtures of Lining Black and True Blue, the mixtures of Lipstick Red and Lining Black follow the pattern in which inks which contain more of one color have more intense peaks that are associated with that color. Unfortunately, in comparing the IR spectra of Lipstick Red and Lining Black mixtures to the IR spectra of Deep Red and Dark Red it is observed that the Lipstick Red and Lining Black mixtures which contain 50% or more Lipstick Red have the same peaks as Deep Red and Dark Red indicating no differentiation is possible based on the IR data alone. However, the XRF data would be able to differentiate these inks based on the presence of S.

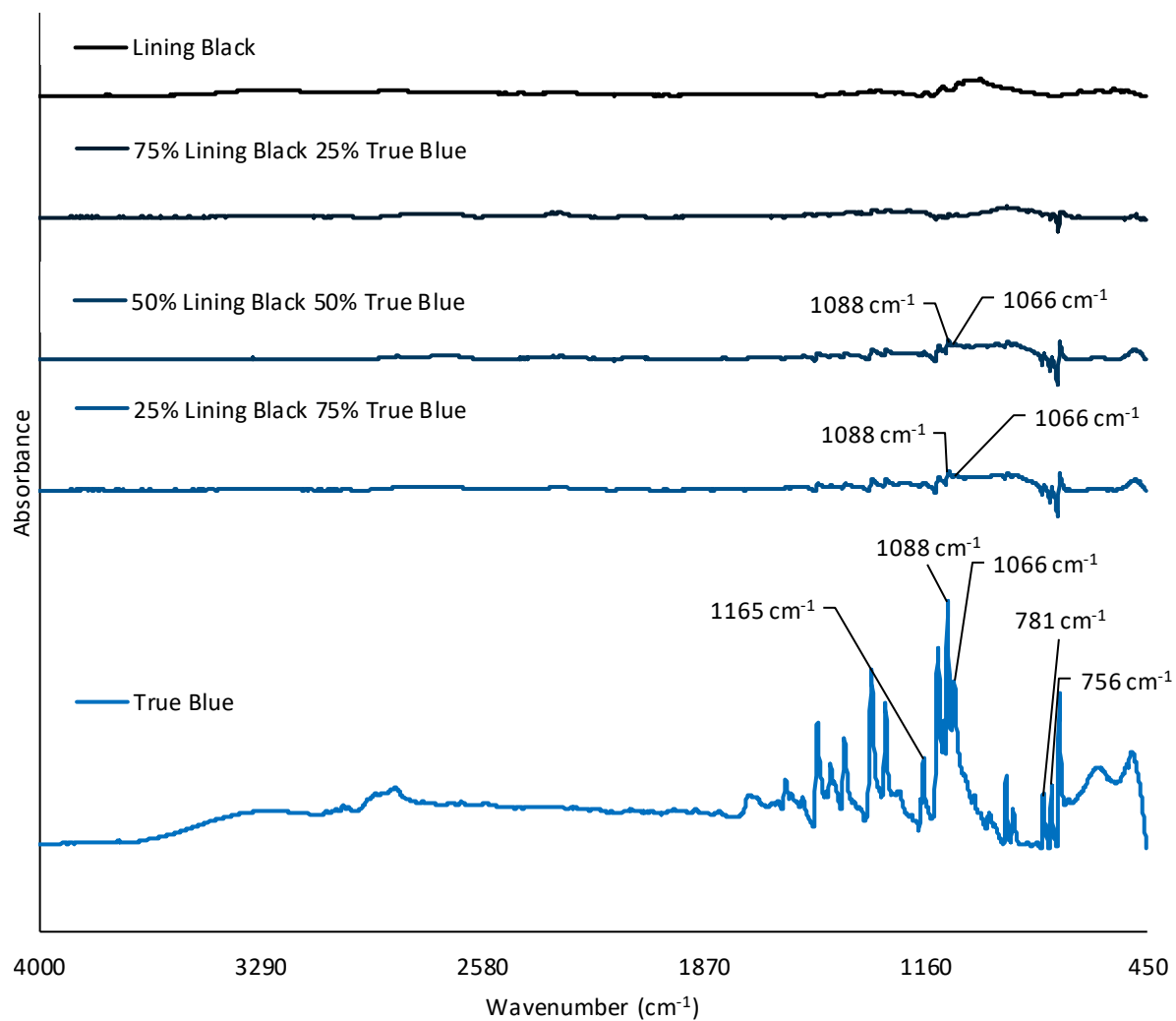


**Figure 5.7:** A) Representative IR spectra of Lining Black and True Blue as well as 25/75, 50/50 and 75/25 mixtures of these inks



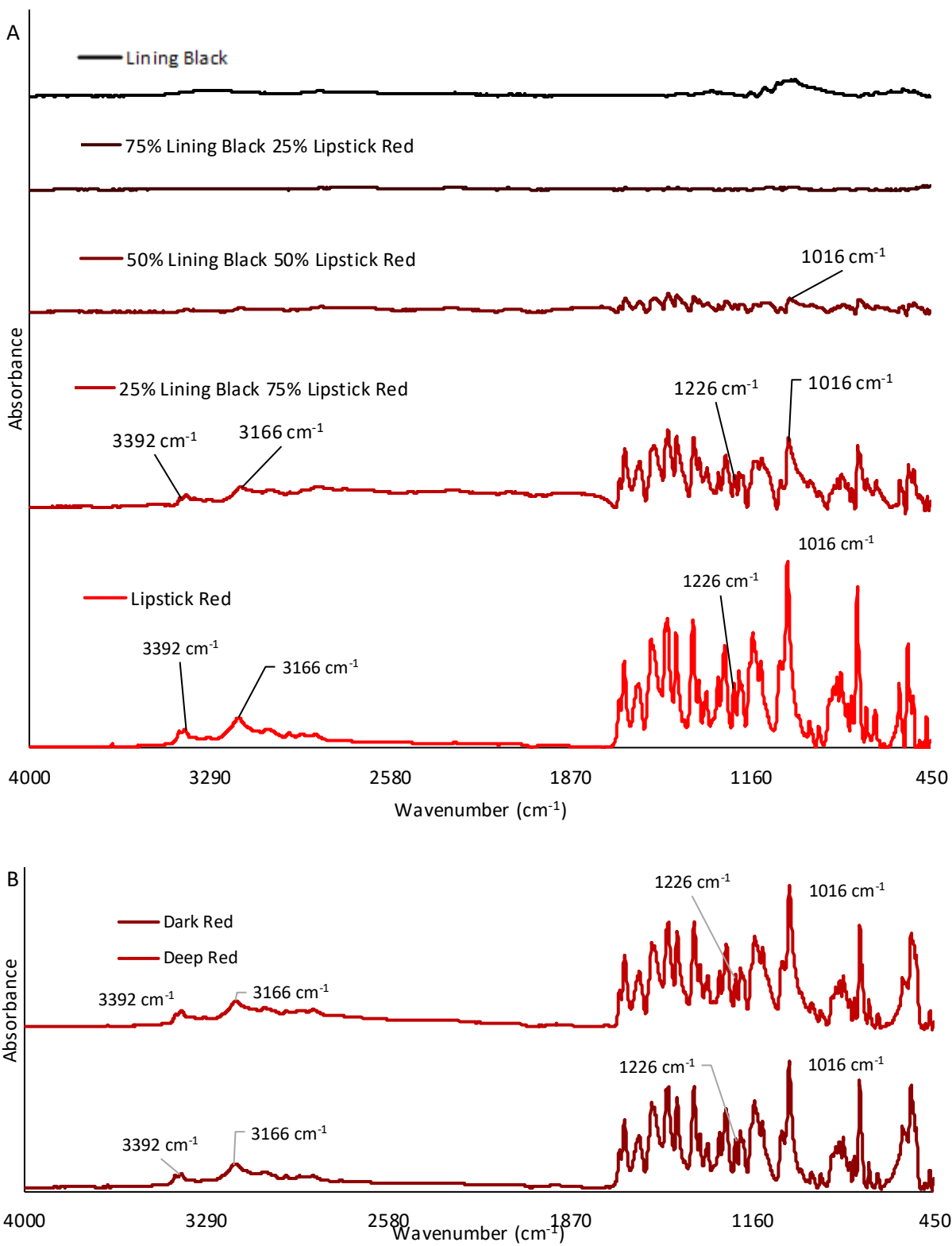


**Figure 5.8:** A) Representative IR spectra of Lining Black and Lipstick Red as well as 25/75, 50/50 and 75/25 mixtures of these inks and B) Representative IR spectrum of Dark Red and Deep Red

### 5.3 Multivariate Statistical Analysis of Reduced Variable Mixed Inks

#### 5.3.1 PCA analysis of Mixed Inks

The same feature selection that was performed on the manufacturers' inks (see section 4.3.1) was performed on the ink mixtures. The samples were then projected onto the PCA scores plots for PCs 1-4 which had been previously generated for the individual ink. In the scores plot for PC 1 vs PC 2, most of the mixed ink samples are positioned between the two original colors, with mixtures that contain a majority of one ink positioning closer to that ink (Figure 5.9). For instance, the mixture of 75/25 Lipstick Red/True Blue v/v positions closer to Lipstick Red than the 50/50 v/v mixture of the same inks which positions closer to Lipstick Red than the 25/75 mixture of the same inks. This would be expected due to the increase in concentration of the Lipstick Red ink. This also occurs for mixtures of Lightning Yellow and True Blue as well as most of the mixtures of Lining Black and Lipstick Red.

One of the 50/50 Lining Black/Lipstick Red v/v mixtures does not follow this trend and overlaps the 75/25 Lining Black/Lipstick Red mixtures on PC1. This is due to a fluctuation in the background of the IR spectrum for the 50/50 v/v mixture which was accentuated due to normalization. This fluctuation affected a peak near  $3330\text{ cm}^{-1}$ , associated with NH-O bonds. This bond is one of highest negative influences on PC1 (Figure 4.9) causing this 50/50 mixture to load much more negatively on PC1 than the other 50/50 mixtures. However, in PC 4 all Lining Black and Lipstick Red mixtures follow the pattern of positioning between the inks that they are comprised of with mixtures that contain a majority of one ink positioning closer to that majority ink (Figure 5.10). This is due to the IR spectral peaks having little to no influence on this PC while S, which is found in Lining Black, and Fe, which is in both Lining Black and Lipstick Red, are

the strongest negative influences on PC 4. Further, Si, which is found in Lipstick Red, is one of the strongest positive influences on PC 4. The intensities of these peaks change with the amount of the ink they are associated with in the mixture (Figure 5.4A), causing the differentiation.

In contrast to most of the other mixtures, some Lining Black and True Blue ink mixtures are not positioned between Lining Black and True Blue on the scores plot of PC 1 vs PC 2. In Figure 5.9A and C, the 25/75 v/v mixture is positioned between True Blue and Lining Black on PC 1; however, this mixture is positioned more negatively on PC 2 than True Blue while Lining Black is positioned positively. Also, the 50/50 and 75/25 v/v mixtures of these inks are positioned very closely on PCs 1 and 2 between the Lining Black and True Blue inks. These mixtures containing blue ink position negatively on PC 2 due to the presence of Ti which is weighted negatively on PC 2 (Figure 4.9). Many of the IR spectra peaks including the peaks associated with isoindole, C=O, amide, and azo bonds, which affect the positioning of True Blue, have a negative influence on PC 2. The SNV normalization of the Lining Black and True Blue mixtures caused peaks near these IR absorptions to be accentuated causing the mixed inks to position more negatively on PC 2 than would be expected. As the 25/75 v/v mixture contains a majority True Blue, this mixture contains higher amounts of Ti than the others. The combination of the Ti and accentuated peaks causes the 25/75 v/v mixture to position more negatively on PC 2 than the True Blue ink it originates from.

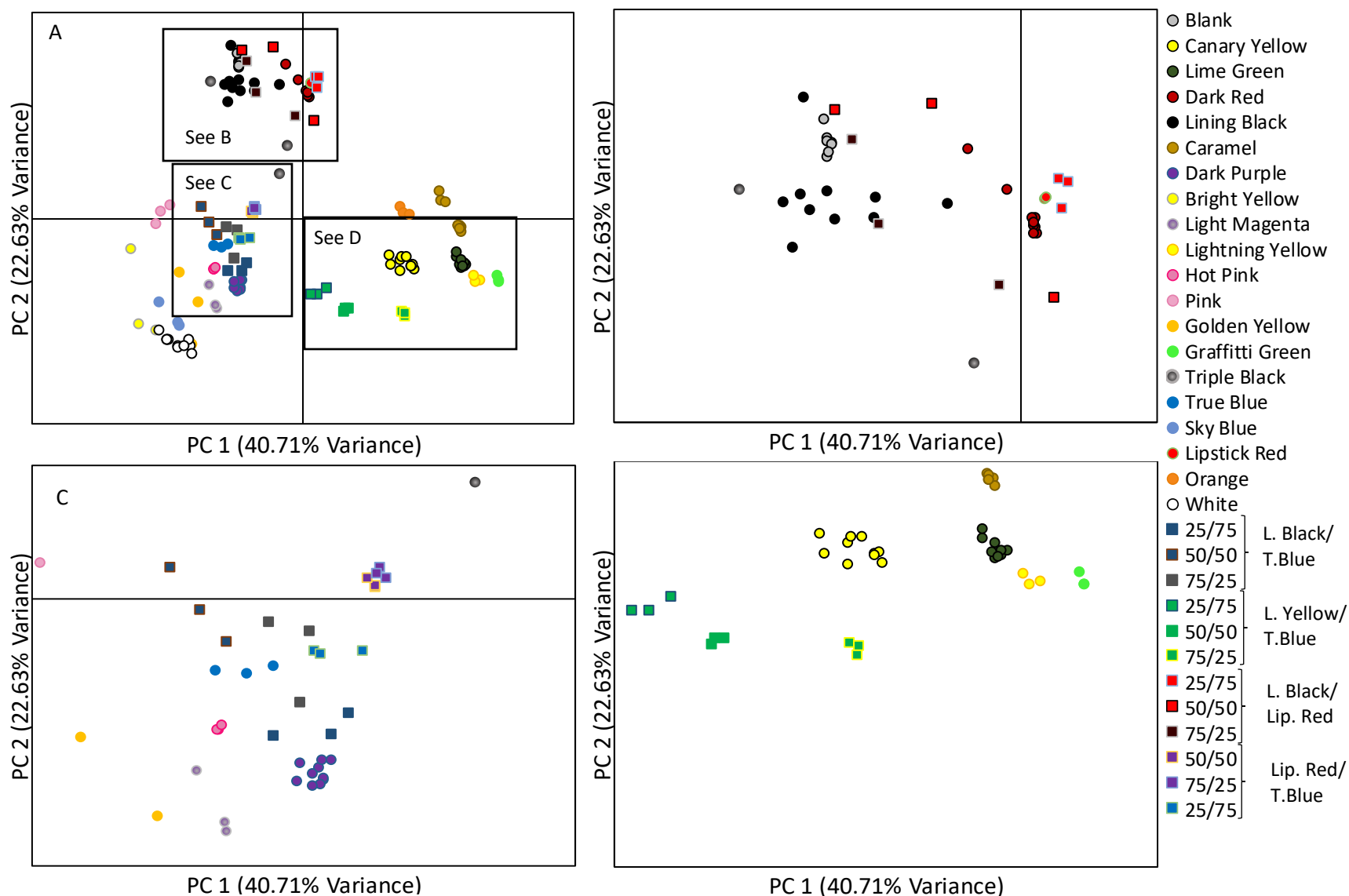


**Figure 5.9:** Projected PCA scores plots showing mixed inks for (A) PC 1 vs PC 2, (B) PC 1 vs PC 2 with the area near the red inks enlarged, (C) PC 1 vs PC 2 with the area near the blue inks enlarged and (D) PC 1 vs PC 2 with the area near the yellow inks enlarged of feature selected IR and XRF

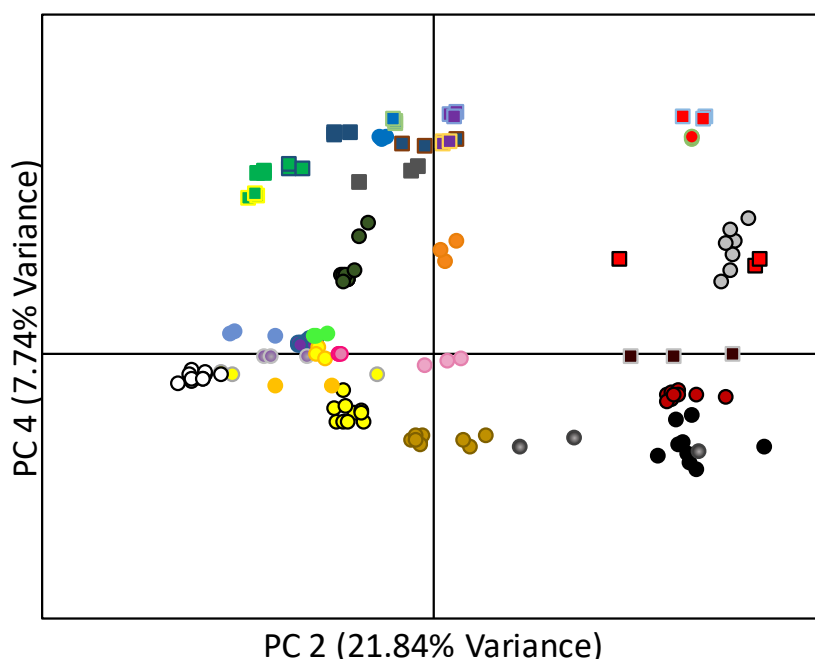


**Figure 5.10:** Scores plot of PC2 vs PC 4 of feature selected XRF and IR data with mixed inks projected.

The mixed inks and manufactured inks of the similar color are successfully distinguished on the first two PCs. For instance, Dark Purple is positioned negatively on both PC 1 and 2 while the mixture that is visually most similar in color to it, 50/50 Lipstick Red and True Blue, is positioned negatively on PC 1, close to Dark Purple, but more positively on PC 2. The difference in position on PC 2 is due to the XRF peak associated with Cl. In Figure 5.1B, the Cl peak is significantly less intense in the mixture than Dark Purple. The mixed 50/50 v/v mixture also contains Cu (Figure 5.1A) as well as an absorbance associated with C-polycyclic bonds ( $1016\text{ cm}^{-1}$ ) in the IR spectrum. Dark Purple does not have a peak associated with Cu in its XRF spectrum (Figure 5.1B) and, although Dark Purple has a peak at  $1030\text{ cm}^{-1}$  in its IR spectrum that overlaps with  $1016\text{ cm}^{-1}$ , the intensity of the peak at  $1016\text{ cm}^{-1}$  is not as intense as the peak observed in the 50/50 Lipstick Red and True Blue mixed ink spectrum (Figure 5.5: . Both the Cu in the XRF spectrum and the C-polycyclic band in the IR spectrum load positively on PC2 while the Cl peak

in the XRF spectrum loads negatively, causing the differentiation of Dark Purple and the 50/50 Lipstick Red/True Blue v/v mixture on PC 2.

The 50/50 v/v mixture of Lightning Yellow and True Blue is also distinguished from Lime Green on PC 1 and PC 2. The primary reason for this is that Ti is present in 50/50 mixture but not in Lime Green. Also, the Cl peak is twice as intense in Lime Green than in the 50/50 mixture. Titanium has the highest negative influence on PCs 1 and 2, while Cl has a strong positive influence on PC 1. This causes the separation between Lime Green and the 50/50 mixture on the first two PCs.

While most mixed inks are distinguished from manufactured inks on the first two PCs, the 50/50 mixture of Lining Black and Lipstick Red does overlay with Dark Red. This is due to each having the same peaks in the IR spectrum. Dark Red contains Fe that is orders of magnitude more intense than in the 50/50 mixture. However, the 50/50 mixture contains S while Dark Red does not. The 50/50 mixture also contains a Si peak that is orders of magnitude lower than in Dark Red. Sulfur, Fe and, Si have a negligible effect on PC 1 compared to the organic components and, although they do have a positive effect on PC 2, the organic components have an equal negative influence on this PC causing the mixture to overlap Dark Red. Further differentiation of the inks is possible in higher PCs. In PC 4, clear separation of all mixtures of Lining Black and Lipstick Red from Dark Red is observed (Figure 5.9B). Iron and S are the two peaks with the most negative influence on PC 4 while Si is the second most positive influence, causing the Dark Red to be positioned more negatively than the mixtures of Lining Black and Lipstick Red on PC 4.

Although the mixtures of Lining Black and True Blue do not have a corresponding color in the manufactured inks, one concern would be differentiation of the mixtures from True Blue since so few peaks are present in the XRF and IR spectra of the Lining Black ink. The mixtures are differentiated from True Blue on PC 1 and PC 2; however, these ink mixtures do not show a progression between their ink sources, True Blue and Lining Black, on PCs 1 and 2 as seen in other ink mixtures due to the accentuation of peaks through the SNV normalization mentioned earlier.

Through PCA, most of the mixed inks were able to be correctly differentiated from manufactured inks of similar colors. However, inks which contain Lining Black either required higher PCs in order to achieve differentiation or were variable in their positioning on the scores plots. To investigate further differentiation of the inks, hierarchical cluster analysis (HCA) was investigated.

### 5.3.2 HCA analysis of Mixed Inks

Hierarchical cluster analysis (HCA), was performed on the scores of each mixture on the first 4 PCs of the PCA (Figure 5.11). In the dendrogram, replicates of the mixed inks of the same mixture that do not contain lining black cluster with each other first at a similarity level of over 90%, while mixtures that contain Lining Black cluster to each other first but at a similarity ranging between 70% and 95%. This correlates with the large variation in mixtures containing Lining Black due to artifacts in the IR spectra as a result of normalization.

For Lipstick Red and True Blue, all of the 75/25 v/v mixtures cluster with each other at a similarity of 97%, all of the 50/50 v/v mixtures cluster at a similarity of 97%, and all of the 25/75 v/v mixtures cluster first at a similarity of 95%. The 75/25 v/v mixture then clusters to the 50/50

v/v mixture at a similarity of 92%. However, the 25/75 v/v mixture clusters to a cluster of True Blue and mixtures of Lining Black and True Blue first at a similarity of 88%. This trend is expected as the 75/25 and 50/50 v/v mixtures contain more components associated with red such as Si, Fe, and IR bonds associated with quinacridones than the 25/75 mixture. The cluster of the 50/50 and 75/25 mixture then clusters to a cluster containing True Blue, the 25/75 v/v mixture, as well as mixtures of Lining Black and True Blue at a similarity of 79%. This cluster does not contain any other manufactured inks and does not cluster to any other manufactured inks until a similarity level of less than 30% which implies that these inks are not associated with any manufactured ink other than True Blue, including Lipstick Red, Dark Red, and Deep Red.

For mixtures of Lightning Yellow and True Blue, the 75/25 v/v mixtures cluster with each other at a similarity of 98%, the 50/50 v/v mixtures cluster at a similarity of 94%, and the 25/75 v/v mixtures cluster to each other first at a similarity of 98%. The 75/25 mixture then clusters to the 50/50 mixture at a similarity of 87.3% and then to the 25/75 mixture at a similarity of 77%. This cluster then clusters to a cluster containing True Blue and other mixtures containing True Blue at a similarity level of 44%. As before, this cluster does not cluster to any other manufactured inks until a similarity level of less than 30%. More importantly, the Lightning Yellow and True Blue mixtures never cluster to any of the manufactured green inks. This would suggest that these mixtures could be associated with True Blue and differentiated from the green inks through HCA.

Mixtures of Lining Black and Lipstick Red do not initially cluster to each other. The 25/75 Lining Black/Lipstick Red v/v mixtures cluster to Lipstick Red at 91.4%, the 50/50 v/v mixtures cluster to Dark Red at 58.4%, and the 75/25 v/v mixtures cluster to the filter paper (blank)



samples at 67.1% without ever clustering to the other Lining Black/Lipstick Red mixtures. This also is expected since the 25/75 mixture is positioned next to Lipstick Red in PCs 1-4, the 50/50 mixture is positioned next to Dark Red in PCs 1-3, and the 75/25 mixture is positioned next to the filter paper samples in PCs 1, 2, and 4.

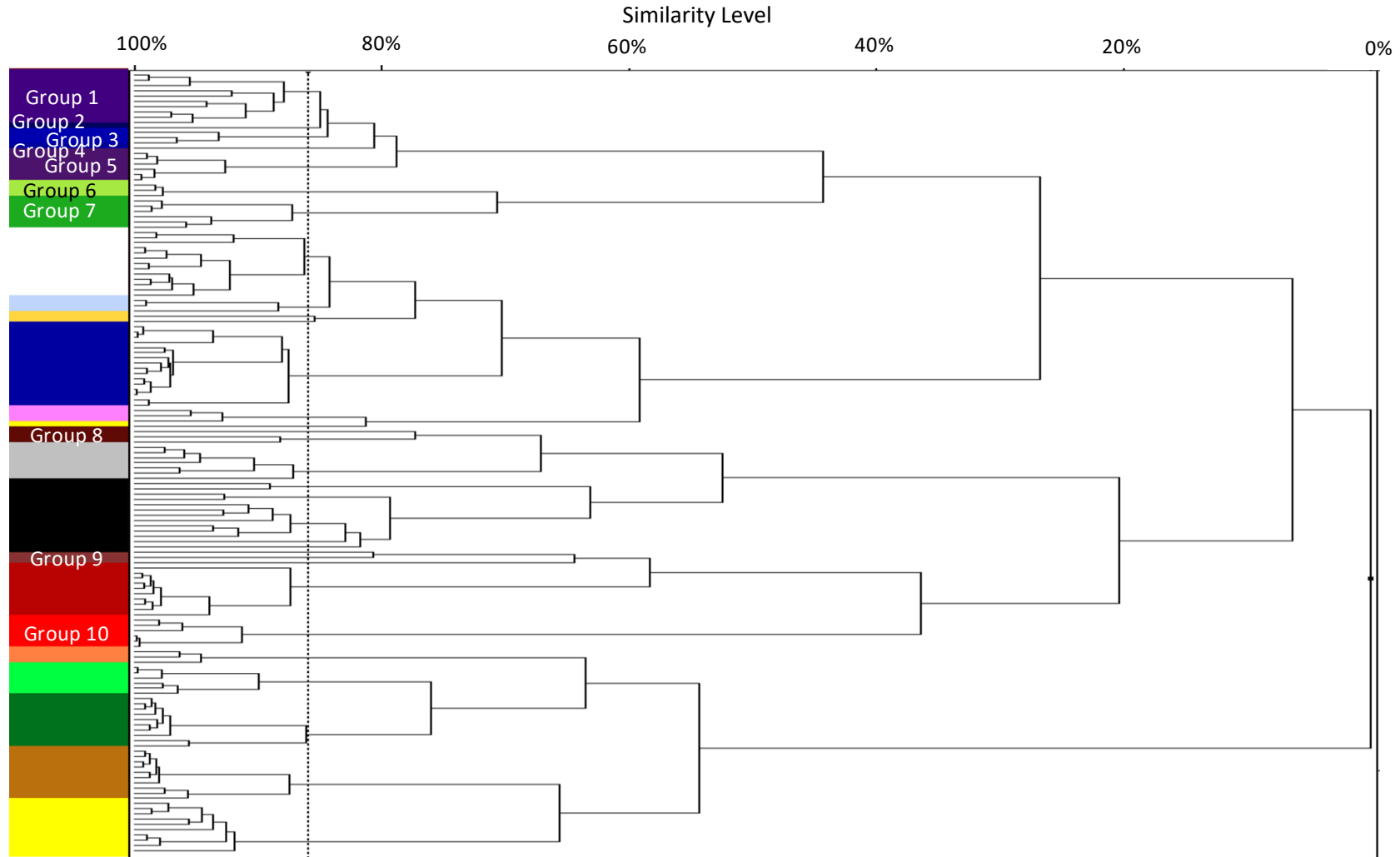


**Figure 5.11:** HCA dendrogram of ink mixtures. **Group 1:** 25/75 Lipstick Red/True Blue, two 75/25 and two 50/50 Lining Black/True Blue v/v mixtures, and all True Blue replicates, **Group 2:** one 75/25 Lining Black/True Blue v/v mixture, **Group 3:** all 25/75 Lining Black/True Blue v/v mixtures, **Group 4:** one 50/50 Lining Black/True Blue v/v mixture, **Group 5:** all 75/25 and 50/50 Lipstick Red/True Blue v/v mixtures, **Group 6:** all 75/25 Lightning Yellow/True Blue v/v mixtures, **Group 7:** all 50/50 and 25/75 Lightning Yellow/True Blue v/v mixtures, **Group 8:** all 75/25 Lining Black /Lipstick Red mixtures, **Group 9:** all 50/50 Lining Black/ Lipstick Red v/v mixtures, and **Group 10:** all 25/75 Lining Black/Lipstick Red mixtures

#### 5.4 Summary of Multivariate Statistical Analysis of Mixed Ink Samples

Through IR and XRF analysis, it was determined that inks that have been mixed together could be differentiated from manufactured inks based on their organic and inorganic composition. Although both PCA and HCA were able to differentiate most mixed inks from manufactured inks of similar colors, each had advantages. The HCA was able to provide information on one of the likely components which make up the mixed ink. For instance, the HCA was able to cluster the mixed Lightning Yellow and True Blue inks to True Blue which is not apparent in the PCA. However, the HCA is not able to provide accurate information on the second ink component. In the PCA scores plots, the ink mixtures were generally positioned between the two inks which comprise the ink mixture, giving complimentary information to HCA.

#### 5.5 SEM-EDS Analysis of Tattoo Inks

The use of scanning electron microscopy-energy dispersive spectrometry (SEM-EDS) was also explored for the detection of tattoo inks in decomposed tissue. SEM-EDS is more widely available in forensic labs than XRF and provides a similar elemental analysis as XRF as well as organic information similar to IR. SEM-EDS also has an advantage as the location of elements within a sample can be determined through various scan features, which was necessary for the analysis of tissue samples. Before analyzing inks in tissue samples, a subset of inks was analyzed by SEM-EDS in order to compare the functionality of the SEM-EDS to IR and XRF (Figure 5.12).

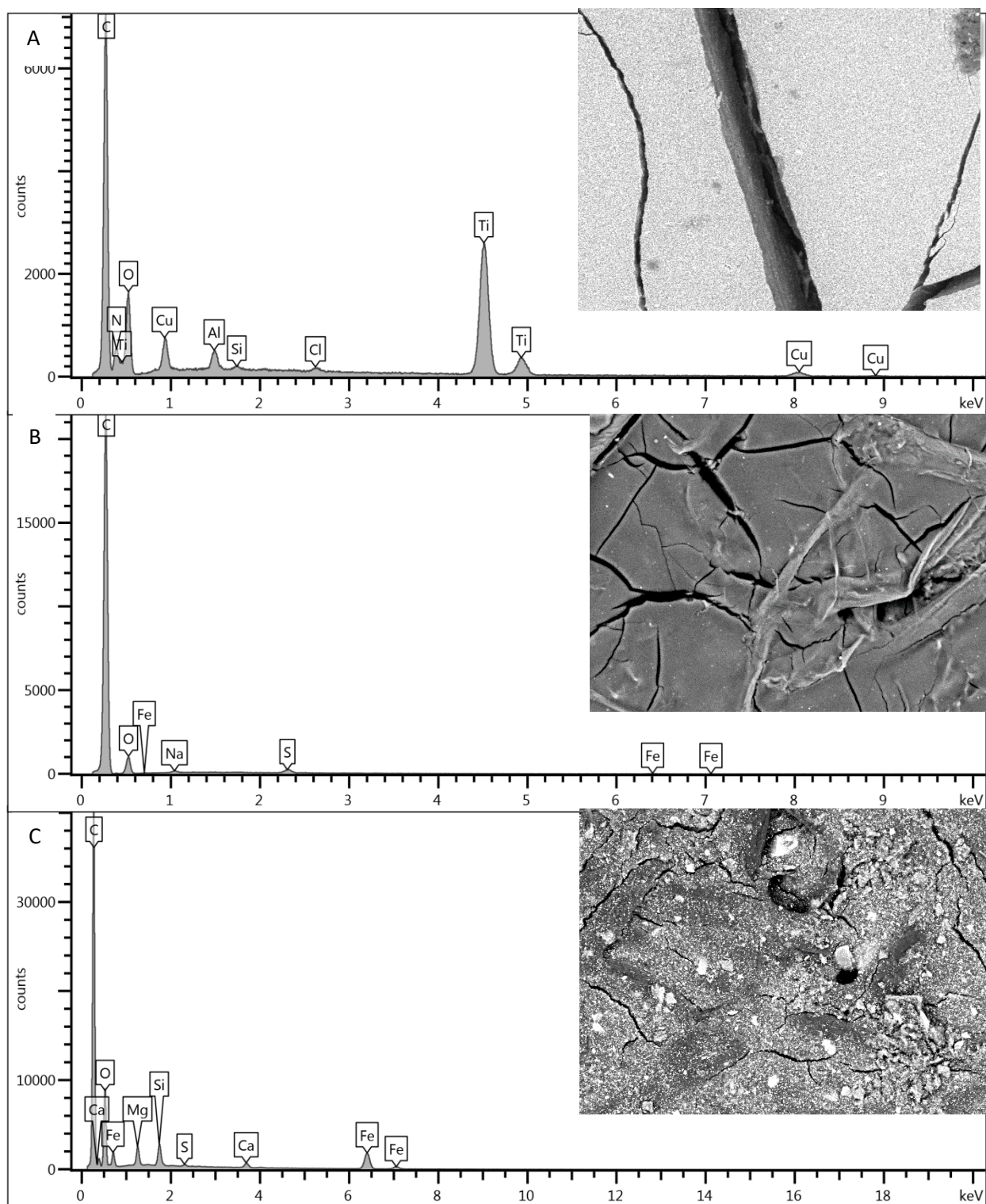


**Figure 5.12:** SEM images (500x magnification, Working Distance 10 mm, 15 keV) in backscatter mode with EDS spectra of (A) True Blue, (B) Lining Black, and (C) Lipstick Red tattoo inks

The EDS spectra give similar information on the ink composition as observed in the XRF and IR spectra of each ink. For example, peaks observed at 8.046 and 8.904 keV in the EDS spectra correspond to Cu, while a peak at 0.392 keV indicates N, and a peak at 0.277 keV indicates C. The presence of Cu, N, and C are expected due to the copper phthalocyanine pigment. Peaks at 4.512 and 4.933 keV indicate the presence of Ti while a peak at 0.525 keV indicates the presence of O. This is also expected due to the titanium dioxide pigment believed to be used as a whitening agent in this ink (2, 5). The detection of Cu, Ti, C, O, and N highlights the advantage of the SEM-EDS in that both organic and inorganic components could be detected whereas, previously, XRF and IR were both required for detection of the same elements.

Further, in the EDS spectrum of True Blue (Figure 5.12 A), there is a peak at 0.928 keV which is associated with the  $L_{\alpha}$  transition of Cu as well as peaks at 1.486 keV and 1.740 keV associated with the  $K_{\alpha}$  transitions of aluminum (Al) and Si. These elements were not previously observed in the XRF spectrum of the same ink. This is likely due to a difference in the amount of energy used to produce x-rays in each method. In EDS, 15 keV of energy was used while in the XRF analysis 20 keV was used. X-rays and electrons of higher energy penetrate deeper into the surface of the sample. The more material these x-rays/electrons pass through the more non-characteristic x-rays are produced. This causes an increase in the baseline of the EDS or XRF spectrum. The higher energy used in the XRF spectrum could likely have produced more non-characteristic x-rays, increasing the baseline, causing the peaks for Al and Si to be below the baseline. The observation of Al and Si in the sample could indicate the presence of an aluminum

silicate, a thixotropic agent (5), within the True Blue ink which had not been detected previously.

In Lining Black (Figure 5.12B), few elements are detected, with the peak at 0.277 keV associated with the  $K_{\alpha}$  transition for C, which is the most intense peak in the spectrum. This is to be expected as the main component of black ink is carbon black. As with the XRF spectrum (Figure 4.2), S is detected in the EDS spectrum with a peak at 2.309 keV that is the largest inorganic peak within the spectrum. Peaks associated with Fe are also observed at 6.409 keV and 7.059 keV which are less than one-fifth the intensity of the S peak, similar to that previously observed in the XRF spectrum.

Iron is also observed in the Deep Red ink with peaks in the EDS spectrum at 6.409 keV and 7.059 keV associated with the  $K_{\alpha}$  and  $K_{\beta}$  transitions for Fe, respectively, as well as a peak at 1.740 keV associated with the  $K_{\alpha}$  transition for Si, and a peak 0.525 keV associated with the  $K_{\alpha}$  transition for O. These elements were previously indicated by both XRF and IR. Magnesium was also observed by SEM-EDS with a peak at 1.254 keV associated with the  $K_{\alpha}$  transition. The intensities of the Mg and Si peaks are approximately the same intensity as the peak associated with  $K_{\alpha}$  transition for Fe in the EDS spectrum. This differs from the relative intensities of the peaks seen in the XRF spectrum (Figure 4.2) in which the Si and Mg peaks are less than one-fifth the intensity of the peak associated with the Fe  $K_{\alpha}$  transition. This can again be explained by the difference in energies used to produce x-ray fluorescence in each instrument.

Observing the SEM backscatter images, the difference in composition among True Blue, Lining Black, and Dark Red is apparent. The backscatter SEM image for True Blue (Figure 5.12A) is primarily white, indicative of the heavy elements within the ink, such as Ti and Cu. The large

black line down the middle of the image is a crack in the surface of the ink on the filter paper. The backscatter image for Lining Black (Figure 5.12B) is primarily grey which is due to the presence of heavier elements such as Fe being orders of magnitude lower than in inks such as Dark Red which contains inclusions of heavy elements like Si, Mg, and Fe mixed among lighter elements. These inclusions of heavy elements cause the SEM image of Dark Red to look speckled as the heavier elements like Si, Mg, and Fe have a lighter color than the surrounding elements which mainly consist of C. This contrasts with the uniformity of elements observed in the True Blue and Lining Black inks. The heavy elements such as Cu are incorporated into the pigment of the True Blue ink, copper phthalocyanine, as is the C in the Lining Black ink and would, therefore, be expected to be found throughout the sample in order to provide the ink a uniform color. However, the Si, Mg, and Fe are added to the Dark Red ink as thixotropic and shading agents and wouldn't necessarily need to have a homogeneous spread throughout the Dark Red ink sample, leading to the pockets of white pixels in the SEM backscatter image of the Dark Red ink.

Through the observation of the SEM images and EDS spectra of True Blue, Lining Black, and Dark Red, these inks can be differentiated by SEM-EDS based on concentrations of inorganic elements such as Fe, Ti, S, Mg, Si, and Al. To further investigate the use of the composition of tattoo inks to aid in the identification of highly decomposed remains, tattoo ink in decomposed tissue was analyzed by SEM-EDS.

## 5.6 Analysis of Tattoo Ink within Decomposed Tissue via SEM-EDS

The tattooed pig had been allowed to decompose for 19 days in order to achieve decomposition which obscured the tattoos. Decomposition had occurred from the 14<sup>th</sup> to the

31<sup>st</sup> of August, 2015. During this time the temperature ranged from 12 °C to 29 °C with most days being sunny. This allowed for the decomposition to progress quickly. After the first day of decomposition, the tattoo ink was still visible on the skin (Figure 5.13A). The tattoo ink was still visible through the decomposition until the 19<sup>th</sup> day of collection. For this reason, the 1<sup>st</sup> and 19<sup>th</sup> days of collection will be discussed. The other days of collection are shown as supplemental Figure A 5.1 to Figure A 5.3.

As can be seen in Figure 5.13A, the tattooed side of the pig was facing up during decomposition. This caused the pig's blood to pool at the bottom of the carcass. As blood is the primary source of iron within porcine tissue, there was no detectable iron present in the tissue surrounding the tattooed area (Figure 5.13B). Iron, Mg, and Si were used for the detection of the Dark Red ink within the porcine tissue since there would be no interference from these elements within the tissue. Figure 5.13B and C show the SEM-EDS layered map scan for the blank tissue sample and the tattooed tissue sample after one day of decomposition. In these views, the instrument scans across an area of sample. As the instrument scans across a sample it overlays colored pixels corresponding to the concentration of elements over the backscattered image collected. In this collection, the map function was set to show Mg, Si, and Fe which had green, orange, and pink pixels, respectively. The Aztec program (vers. 3.1, Oxford Instruments, Abingdon, UK) displays pixels for Mg, Si, and Fe whenever X-ray corresponding to these elements are detected. This includes non-characteristic X-rays from the background which happen to overlap the keV of the characteristic fluorescence of Mg, Si, and Fe. Due to this, pixels associated with Fe, Mg, and Si can be observed in the map of the blank sample (Figure 5.13B) although no Fe, Mg, or Si was present. However, this is represented by the even



distribution of these pixels throughout the map as well as how dispersed they are compared to a map which contains these elements. The lack of these elements can be observed in the corresponding EDS spectrum. The backscatter image of the blank tissue collected after one day of decomposition also shows areas of the tissue in which there are elements that have higher atomic weight than the surrounding tissue, indicated by the white areas. This was found to be osmium (Os) from the osmium tetroxide fixation which had been performed on the tissue samples.

Iron, Mg, and Si were all detected in the tattooed tissue which had decomposed for 1 day. The backscatter image of the tattooed area of skin contains a speckle-like pattern in which there are heavy elements surrounded by lighter elements (Figure 5.13C). This, combined with the presence of Fe, Mg, and Si, indicates the possible presence of Dark Red ink. It was also observed that areas of tissue containing Mg corresponded with areas of tissue containing Si. This is possibly due to the presence of magnesium silicates within the tattoo ink. This association of elements is not observed within tissue samples and further proves the possible presence of Dark Red ink within the tissue.

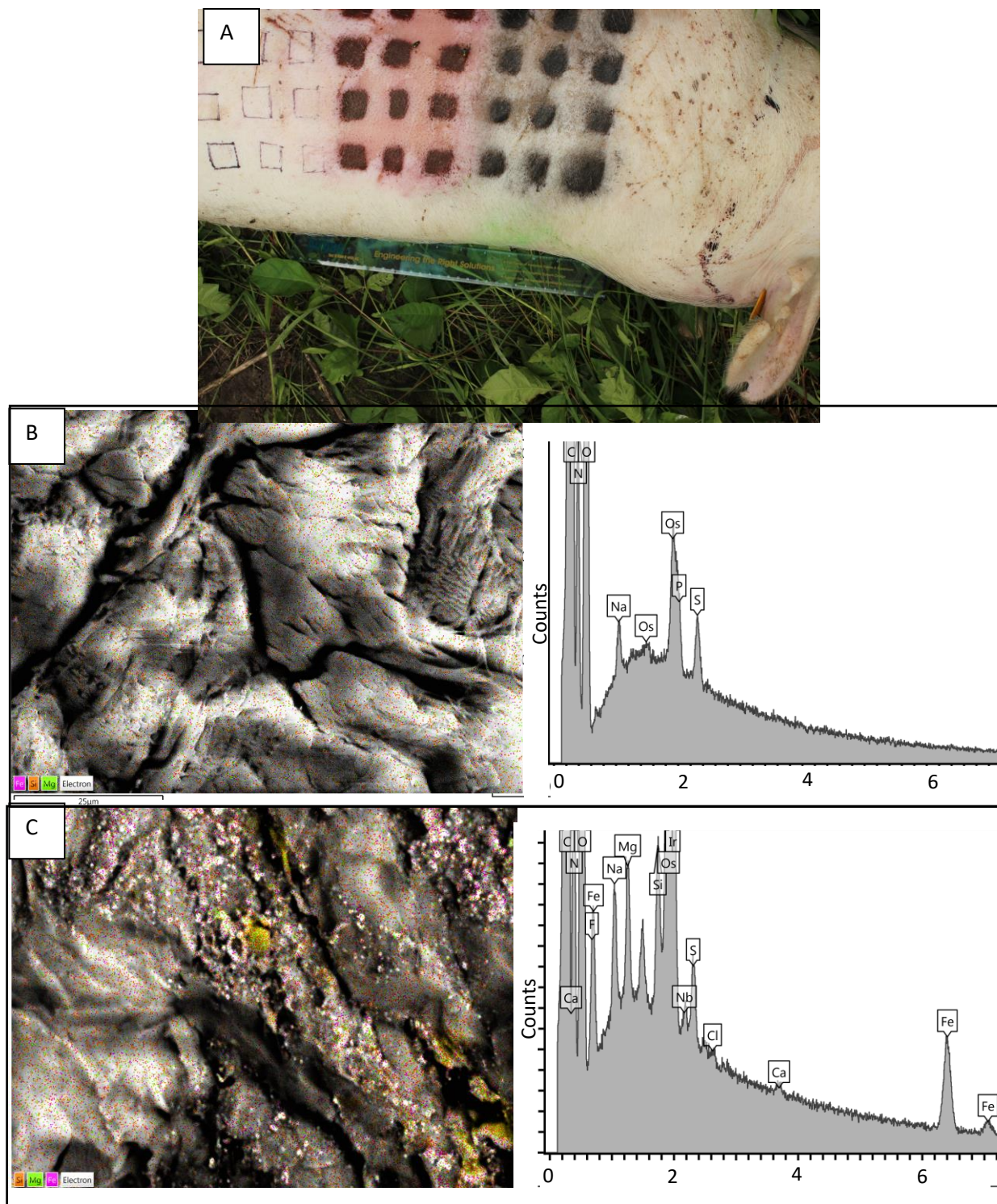


**Figure 5.13:** (A) Picture of Pig after 1 day of decomposition (B) SEM-EDS layered map image of pig skin without ink 1500x with corresponding EDS spectrum (C) SEM-EDS layered map image of porcine tissue with Dark Red ink 1500X with corresponding EDS spectrum.

After 19 days of decomposition, the pig had entered the dry tissue stage in which the tissue becomes dry and leathery almost like the skin found on a mummy. Advanced stages of decomposition were apparent throughout the carcass. Parts of the carcass had started to skeletonize. The rib cage, from which previous tissue had been excised for analysis, had become exposed and the snout and other facial features had become skeletonized. This is important as a body missing facial features would require secondary identifiers such as tattoos for identification. Brown discoloration of the skin completely concealed the tattoos (Figure 5.14A). The blank sample after 19 days of decomposition did not contain any Fe, Mg, or Si and the white areas seen in the backscatter image can be attributed to Os (Figure 5.14B).



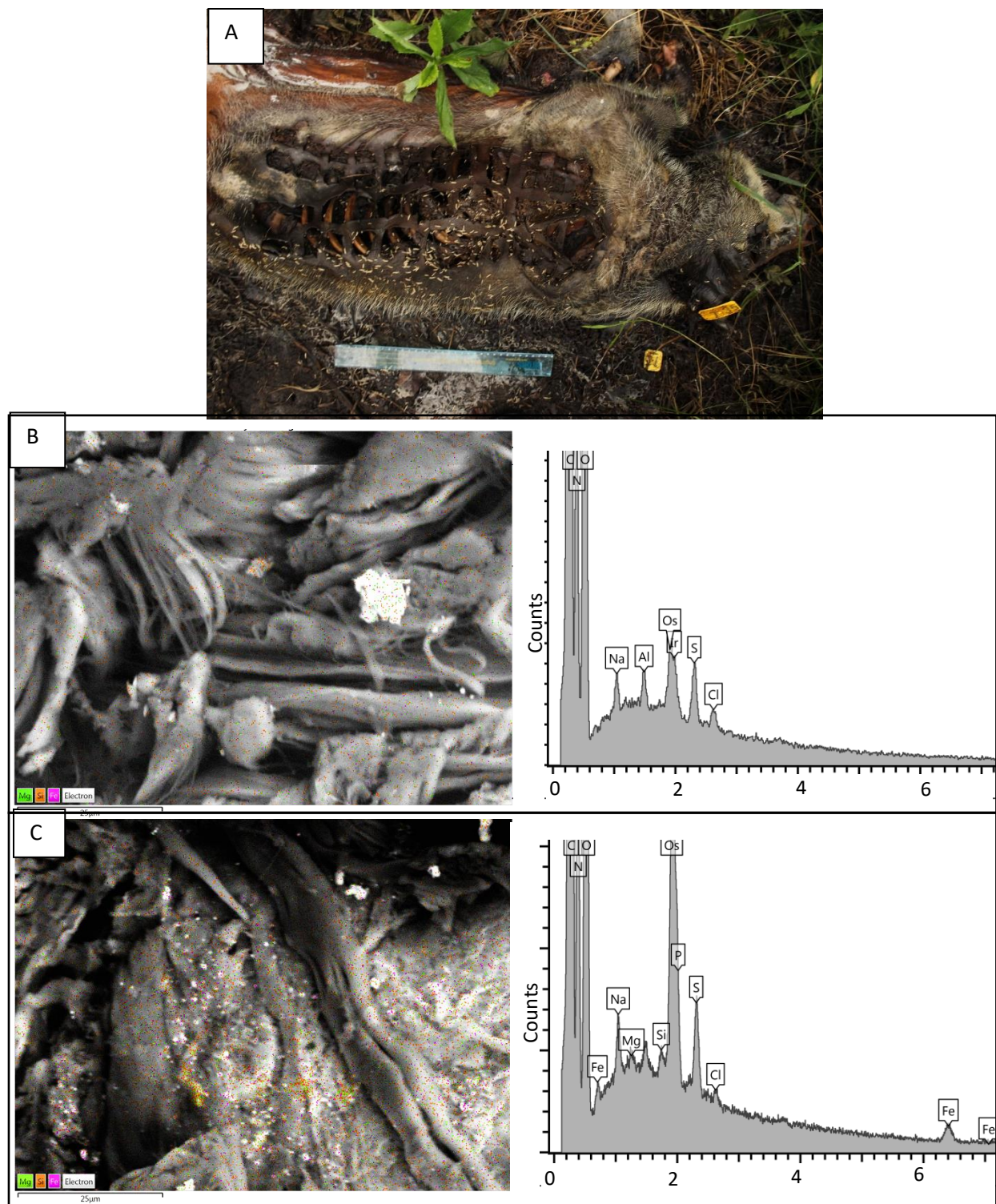


**Figure 5.14:** (A) Picture of Pig after 19 days of decomposition (B) SEM-EDS layered map image of pig skin without ink 1500X with corresponding EDS spectrum (C) SEM-EDS layered map image of porcine tissue with Dark Red ink 1500X with corresponding EDS spectrum.

In the tattooed tissue sample, levels Fe, Mg, and Si were detected that were the same intensity as those seen in the tattooed samples which had decomposed for only one day (Figure 5.14). The same speckled pattern is observed in the backscatter image and Mg and Si are also associated with each other, indicating the possible presence of Dark Red ink.

However, if this sample were presented in a forensic lab, it would have to be noted that one of the elements used for detection of the ink, Fe, can also be found in the body in high concentrations. If the body were positioned where the blood had pooled into the area that held the tattoo, Fe would not be able to be used as an identifier. The concentration of S in the tissue also increased as the decomposition process proceeded. This would make the detection of black inks containing carbon black especially difficult as the other element found in black ink, C, is also found in high abundance in tissue. This would suggest that this technique is more applicable to inks which contain elements that do not occur in high abundance in the body such as blue inks which contain Cu and Ti and inks which contain thixotropic agents which have Al, Si, and Mg. Discrimination of the inks from the tissue could be improved with IR analysis which would be able to determine functional groups present that do not naturally occur in the body. The use of IR may also be able to detect the presence of black ink due to the affect the ink has on the absorption of substances it is mixed with.

## 5.7 SEM-EDS Analysis of Tattoo Inks

Through the use of SEM-EDS, it was observed that red, black, and blue tattoo inks could be differentiated based on the concentration of Fe, Si, Mg, Cu, Ti, S, and Al present. Dark Red tattoo ink was also detected in decomposed tissue based on the presence of Mg, Si, and Fe

even when the tattoo had been concealed due to the advanced state of the decomposition.

These elements and many of the inorganic elements found in tattoo inks are either thixotropic agents or components used for shading. As many of these elements do not occur in high abundance in the tissues of the body, these elements could be used to screen for the presence of a tattoo.

## APPENDIX

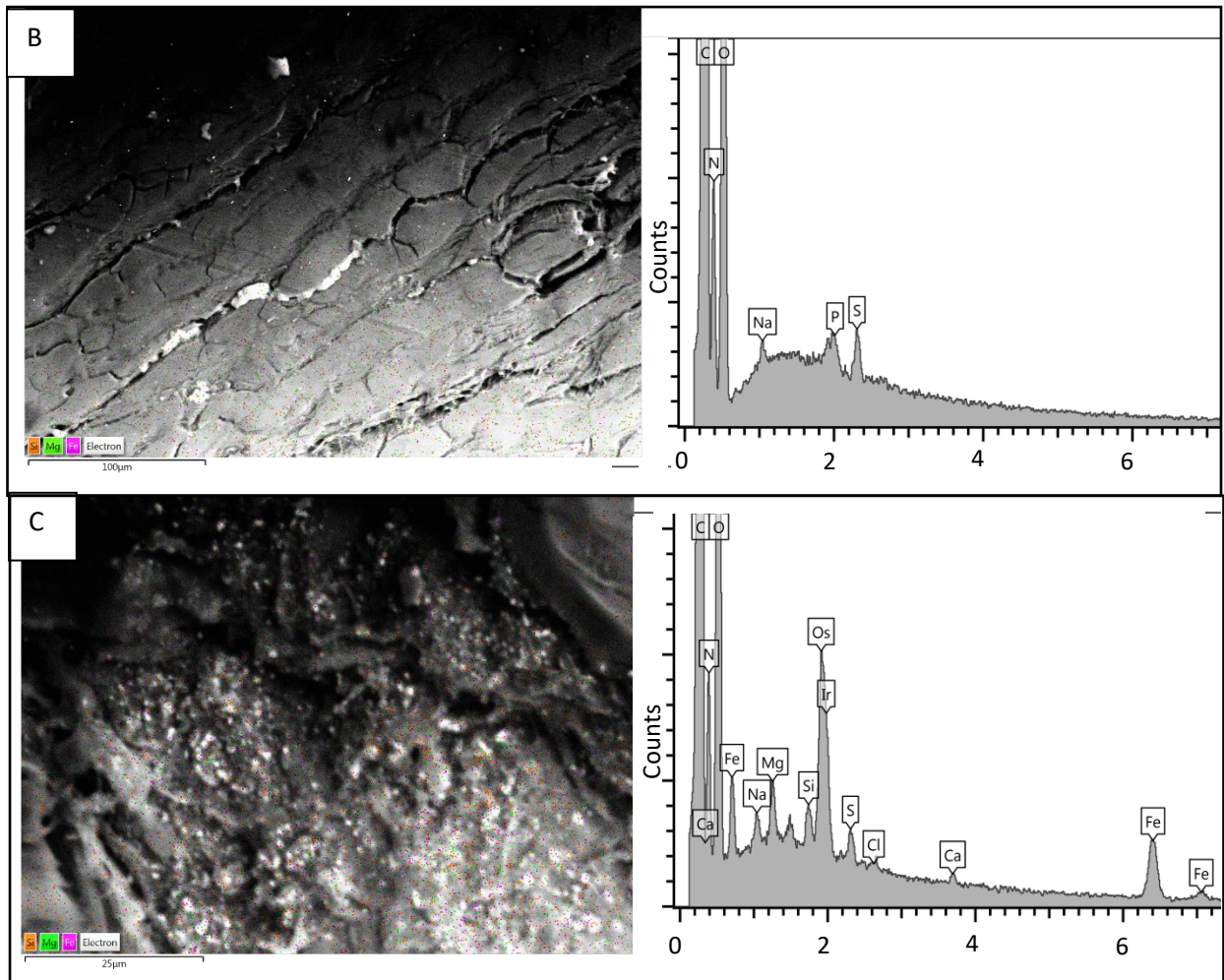


**Figure A 5.1:** A) Picture of Pig after 3 days of decomposition (B) SEM-EDS layered map image of pig skin without ink 1500X with corresponding EDS spectrum (C) SEM-EDS layered map image of porcine tissue with Dark Red ink 1500X with corresponding EDS spectrum.



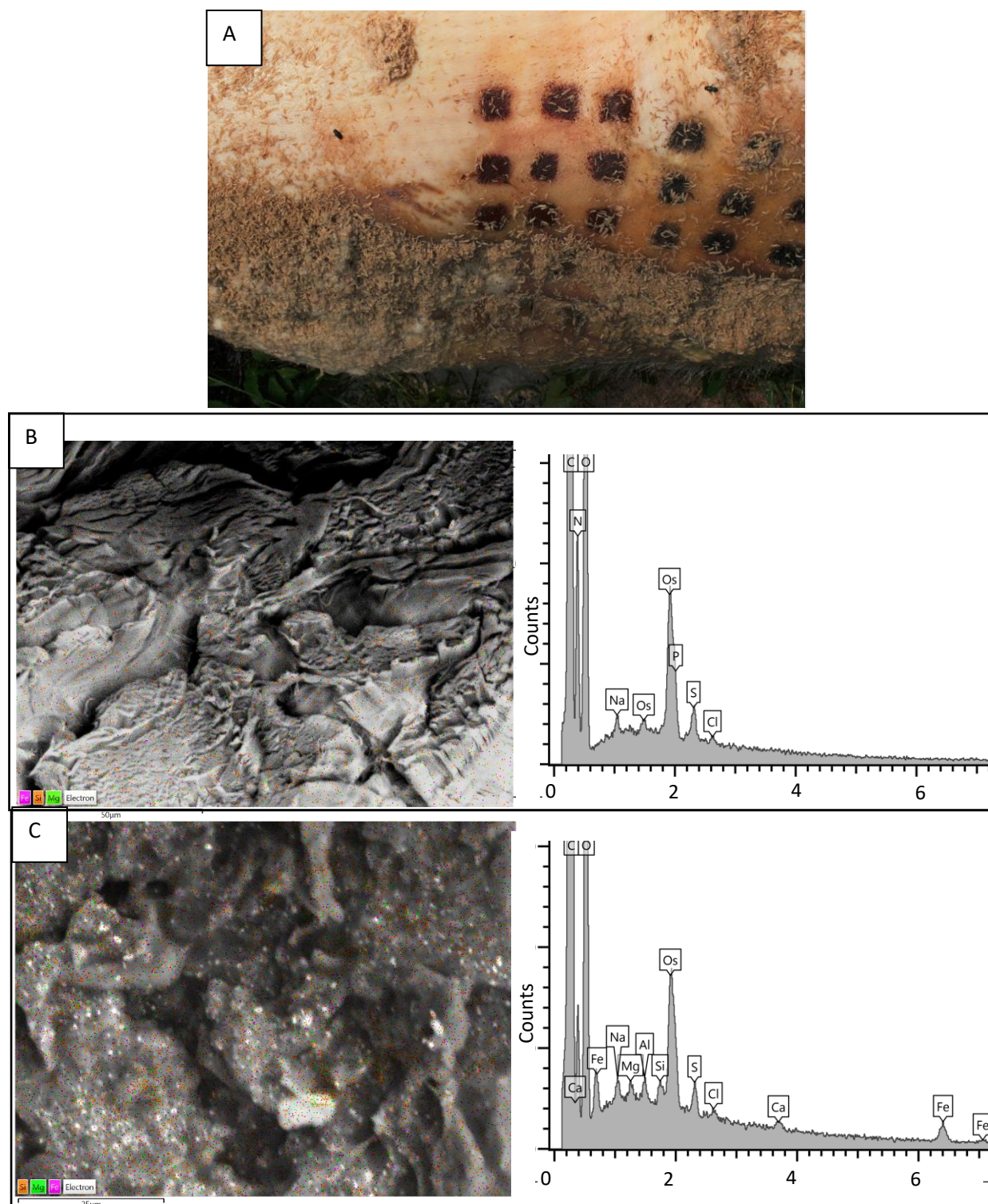


**Figure A 5.2:** A) Picture of Pig after 6 days of decomposition (B) SEM-EDS layered map image of pig skin without ink 1500X with corresponding EDS spectrum (C) SEM-EDS layered map image of porcine tissue with Dark Red ink 1500X with corresponding EDS spectrum.

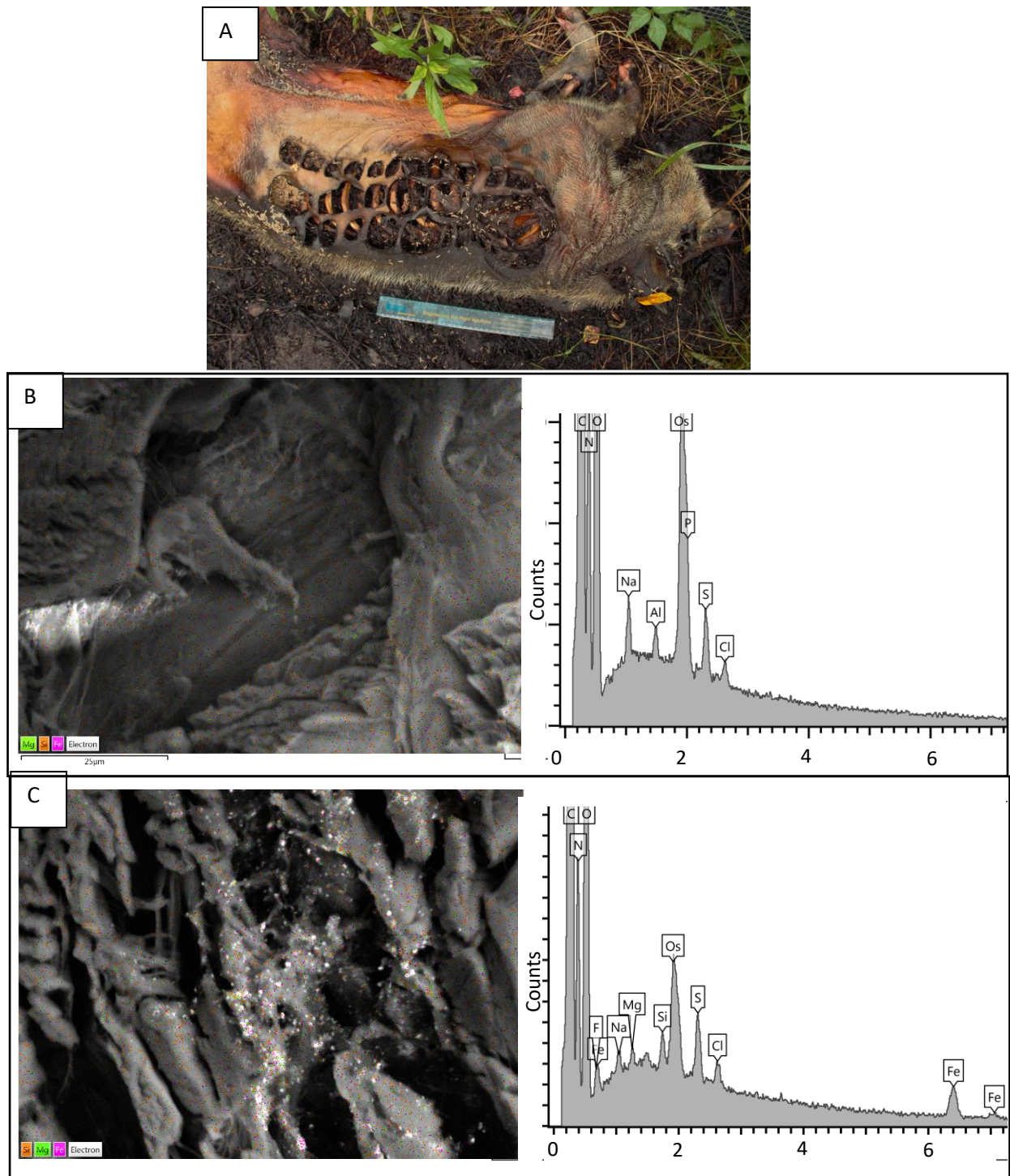


**Figure A 5.3:** A) Picture of Pig after 13 days of decomposition (B) SEM-EDS layered map image of pig skin without ink 1500X with corresponding EDS spectrum (C) SEM-EDS layered map image of porcine tissue with Dark Red ink 1500X with corresponding EDS spectrum.

## REFERENCES

## REFERENCES

1. Basova T, Kiselev V, Schuster B-E, Peisert H, Chasse T. Experimental and theoretical investigation of vibrational spectra of copper phthalocyanine: polarized single-crystal Raman spectra, isotope effect and DFT calculations. *J Raman Spectrosc.* 2009;40:2080-7.
2. Miranda MD. *Forensic Analysis of Tattoos and Tattoo Inks.* 1 ed. Boca Rotan, Fl: CRC Press, 2016.
3. del Puerto E, Domingo C, Garcia J, Ramos G, Sanchez-Cortes S. Adsorption Study and Detection of the High Performance Organic Pigments Quinacridone and 2,9-Dimethylquinacridone on Ag Nanoparticles By Surface-Enhanced Optical Spectroscopy *Langmuir.* 2014;50:753-61.
4. Taafe A, Knight AG, Marks R. Lichenoid tattoo hypersensitivity. *British Medical Journal.* 1978;1:616-8.
5. Chemical Substances in Tattoo Ink Survey of chemical substances in consumer products Copenhagen, DK: Miljøstyrelsen; 2012;155.

## Chapter 6      Conclusions and Future Directions

### 6.1 Conclusions

The recent surge in popularity of tattoos in the recent decade has caused an increased potential for the use of tattoos to aid in the identification of highly decomposed remains. The current techniques employed by forensic pathologists to visualize tattoos can be impeded by modifications to the surface of the skin such as discoloration during decomposition. Further, more advanced visualization techniques are not able to detect all tattoo inks, with x-ray radiographs only able to detect inks containing metallic components and infrared spectroscopy not able to detect some colors of ink such as red. However, chemical analysis of lymph nodes which contain ink from tattoo sites has the potential to be used to determine color and position of tattoos on highly decomposed remains.

This study investigated the use of organic and inorganic tattoo ink components to determine the presence and color of tattoo ink within highly decomposed remains. X-ray fluorescence (XRF) spectroscopy and attenuated total reflectance-Fourier transform infrared (ATR-FTIR) spectroscopy were used to determine the inorganic and the organic composition of 30 tattoo inks respectively. An initial model for PCA was developed based on a subset of the 30 inks which was able to show separation of tattoo inks into three main quadrants on the PCA. The first consisted of red and black inks, the second consisted of orange, green, and yellow inks, and the third consisted of inks in which Ti was the main contributor to the XRF spectrum.

When the model was tested using a separate subset of tattoo inks, many of the projected inks were positioned in areas of the PCA that were consistent with the inks used to produce the model. However, differences were observed with some inks including Light Red and Scarlet Red

which each positioned lower on PC2 than the red inks used to make the model. This was due to the presence of Cl in these inks which was not observed in the reds used in the training set. This would suggest that, although many of the inks were separated, there are ink components which were not observed in the training set, implying that further studies would require a larger training set to have a more comprehensive model.

Hierarchical cluster analysis (HCA) had also been applied to the PCA scores for both the training set and test set. Using a similarity level of 0.863, it was observed that further differentiation of the inks within the three groups observed by PCA was possible. For instance, the red inks were separated from the black inks as well as the True Blue, the purple inks, and white inks all being separated from each other. However, some of the lighter shaded tattoo inks, like Sky Blue and Bright Yellow, which contained primarily Ti in their XRF spectra could not be separated. In a scenario in which a light color other than white is observed within decomposed tissue, the color would have to be referred to as a light color with the current information available.

If this type of identification method were to be implemented in a forensic case, one of the first obstacles to overcome is that tattoos do not always consist of one color. If an analyst were to analyze a lymph node which had obtained ink from a tattoo containing multiple inks, it is important to be able to differentiate between inks which had been combined within the lymph node from manufactured inks. Due to this, a study was done applying the same techniques and PCA model to a series of ink mixtures. Through this study, it was determined that mixtures of inks were able to be differentiated from manufactured inks. For instance, a 50/50 v/v mixture of True Blue and Lipstick Red was able to be differentiated from dark purple



through the PCA due to the mixture containing Cu causing it to position higher than Dark Purple on the PC2.

Further investigation of the use of tattoo inks in the identification of highly decomposed remains was pursued through the analysis of decomposed tattooed porcine tissue. Tattooed and untattooed tissue which had been collected during five periods over 18 days of decomposition. This tissue was then analyzed by SEM-EDS for inorganic composition. Dark Red tattoo ink was detected in decomposed tissue based on the presence of Mg, Si, and Fe even when the tattoo had been concealed due to the advanced state of the decomposition.

The analyses performed provide a proof of concept of the use of tattoo ink components in the identification of highly decomposed remains. Tattoo inks can be separated by color as well as differentiated from surrounding tissue based on chemical composition of the tattoo ink. Once further developed, the techniques described in this study could be used to provide an additional identifier when examining unknown highly decomposed remains.

## 6.2 Future Directions

One difficulty found throughout this study was the identification of black inks. The differentiation of black ink relied heavily on the lack of significant peaks in either the XRF or IR spectrum, not the presence. This could be a problem when black ink is analyzed in tissue as the organic composition of the tissue may mask the tattoo ink. When black ink had been combined with other ink colors in the mixed ink study, the effect of black ink on the IR spectrum could be observed when the ink comprised 50% or more of the mixture. This caused the spectrum of the mixture to become more flat with a high absorbing baseline like in the pure black ink sample.

This effect on the IR spectrum has the potential to be used as an indicator of black ink in tissue and warrants further investigation.

To determine if black ink is detectable, an experiment could be done in which both untattooed and tattooed porcine tissue are analyzed by ATR-FTIR. A method to process the tattooed tissue would have to be developed to minimize the interference of the surrounding tissue. To do this, a formalin fixation could be tested to start as Miranda has used this fixation method, reporting that it had reduced the interferences of the surrounding tissue (1).

Additionally, the misclassification of tattoo inks in the test set suggests that a larger training set is required for a more accurate representation of tattoo ink composition. Therefore an expansion of the training set would be required. This expansion should take into account more tattoo ink manufacturers as only two manufacturers were represented in this study. Other color palettes may also need to be investigated. For instance, no fluorescent colors have been reported in this study. Due to their fluorescent color, it would be expected that these inks would consist of large, aromatic ring structures which may not appear in the current dataset.

Lastly, for this technique to be of use to forensic scientists, it would need to be applicable to lymph node samples as this is how the scientist would be able to determine the location of tattoos on the body. One of the first studies to be done would be to determine if tattoo ink can be detected within lymph nodes using the previously described techniques. As the absorption of tattoo ink into lymph nodes takes time, a study such as this would most likely need to be performed on lymph nodes recovered from subjects which have had tattoos for a certain amount of time. However, information on the rate of absorption of tattoo ink into lymph nodes



is not currently available, nor is how the amount of ink in a lymph node relates to the size or age of a tattoo; many further studies are possible to investigate these phenomena.

## REFERENCES

## REFERENCES

1. Miranda MD. Forensic Analysis of Tattoos and Tattoo Inks. 1 ed. Boca Rotan, Fl: CRC Press, 2016.